LA-2465

C.1

LOS ALAMOS SCIENTIFIC LABORATORY

OF THE UNIVERSITY OF CALIFORNIA ○ LOS ALAMOS NEW MEXICO

LOS ALAMOS POWER REACTOR EXPERIMENT NO. II

LAPRE II

LOS ALAMOS NATL. LAB. LIBS.
3 9338 00320 9763

FOR REFERENCE

NOT TO BE TAKEN FROM THIS ROOM

CAT. NO. 1935 LIBRARY BUREAU

LEGAL NOTICE

This report was prepared as an account of Government sponsored work. Neither the United States, nor the Commission, nor any person acting on behalf of the Commission:

A. Makes any warranty or representation, expressed or implied, with respect to the accuracy, completeness, or usefulness of the information contained in this report, or that the use of any information, apparatus, method, or process disclosed in this report may not infringe privately owned rights; or

B. Assumes any liabilities with respect to the use of, or for damages resulting from the use of any information, apparatus, method, or process disclosed in this report.

As used in the above, "person acting on behalf of the Commission" includes any employee or contractor of the Commission, or employee of such contractor, to the extent that such employee or contractor of the Commission, or employee of such contractor prepares, disseminates, or provides access to, any information pursuant to his employment or contract with the Commission, or his employment with such contractor.

Printed in USA. Price $ 2.50. Available from the

Office of Technical Services
U. S. Department of Commerce
Washington 25, D. C.

LA-2465
REACTORS--POWER
TID-4500, 15th Edition

LOS ALAMOS SCIENTIFIC LABORATORY
OF THE UNIVERSITY OF CALIFORNIA LOS ALAMOS NEW MEXICO

REPORT WRITTEN: April 1960

REPORT DISTRIBUTED: October 28, 1960

LOS ALAMOS POWER REACTOR EXPERIMENT NO. II
LAPRE II

Report compiled by
R. A. Clark

Contributors

M. E. Battat
H. I. Bowers
R. A. Clark
L. D. P. King
B. J. Melton
B. J. Thamer
L. A. Whinery
W. R. Wykoff

This report expresses the opinions of the author or authors and does not necessarily reflect the opinions or views of the Los Alamos Scientific Laboratory.

Contract W-7405-ENG. 36 with the U. S. Atomic Energy Commission

LOS ALAMOS NATIONAL LABORATORY
3 9338 00320 9763

ABSTRACT

Design features and operating characteristics of the Los Alamos Power Reactor Experiment No. II are discussed in this report. Results of performance tests and of an examination conducted after disassembly of the reactor are presented. Recommendations for work on uranium phosphate-fueled reactors are made.

CONTENTS

		Page
ABSTRACT		3
CHAPTER 1	REACTOR CHARACTERISTICS AND LOCATION	11
	1.1 Introduction	11
	1.2 Reactor Characteristics	13
	1.3 Reactor Location	16
CHAPTER 2	CONCLUSIONS AND RECOMMENDATIONS FOR FUTURE WORK	19
	2.1 Conclusions	19
	2.2 Recommendations	20
	2.3 Advanced Concepts	21
CHAPTER 3	THE REACTOR SYSTEM	23
	3.1 Reactor Vessel	23
	3.1.1 Design	23
	3.1.2 Stress Analysis and Hydrostatic Test	26
	3.1.3 Vessel Cladding	30
	3.2 Feedwater Manifold	37
	3.2.1 Description of Feedwater Manifold	37
	3.2.2 Description of Seal	37
	3.2.3 Description of Seal Test	37
	3.2.4 Test Results	44
	3.3 Steam Generator	46
	3.3.1 Design Criteria	46
	3.3.2 Construction	47
	3.3.3 Testing	47
	3.4 Fuel Line	51
	3.5 Safety Enclosure	52
	3.6 Reflector	58
CHAPTER 4	FUEL AND GAS SYSTEM	61
	4.1 Fuel System	61
	4.2 Gas System	67
	4.3 Emergency Fuel Recovery System	70
CHAPTER 5	HEAT REMOVAL SYSTEM	72
	5.1 Primary Loop	72
	5.2 Secondary Loop	75
	5.3 Equipment Design Data	75
	5.4 Vent Drain System	81
	5.5 Operating Experience	84
CHAPTER 6	INSTRUMENTATION	85
	6.1 Control Point	85
	6.2 Operational Instruments and Controls	85

Page

		6.2.1 Fuel System	85
		6.2.2 Heat Removal System	90
		6.2.3 Fuel Reservoir Cooling System	91
	6.3	Radiation Detection	91
	6.4	Neutronics	91
		6.4.1 Startup Counters	91
		6.4.2 Neutron Level	92
		6.4.3 Reactor Period	92
		6.4.4 Reactor Fuel Level Detector	92
CHAPTER 7	FUEL SOLUTION		93
	7.1	Chemical Properties	93
	7.2	Fuel Preparation	93
	7.3	Effects of Reactor Operation on the Fuel	94
		7.3.1 Radiolytic Gas	94
		7.3.2 Analysis of Fuel After Operation	94
CHAPTER 8	REACTOR PHYSICS		97
	8.1	Calculational Method	97
	8.2	System Geometry	97
	8.3	Fuel Solution Data	98
	8.4	Calculations	99
	8.5	Cold Critical Experimental Data	103
	8.6	Hot Critical Experimental Data	106
	8.7	Nuclear Behavior of the System	109
CHAPTER 9	REACTOR OPERATION		118
	9.1	Fuel Volume	118
	9.2	Shutdown	119
	9.3	Radiation	120
	9.4	Full Power Operation	120
	9.5	Power Demand Experiment	121
		9.5.1 Recombination	121
		9.5.2 Fuel Solution Temperature	122
		9.5.3 Reactor Pressure	122
		9.5.4 Rapid Power Changes	125
		9.5.5 Steam Temperature	127
CHAPTER 10	POST MORTEM		130
	10.1	Fuel Solution	130
	10.2	Vessel and Steam Generator	131
APPENDIX			134
REFERENCES			137

Page

TABLES

CHAPTER 3 THE REACTOR SYSTEM
3.1 Stresses Determined from Strain Gage Data and Comparison with Calculated Stresses 30
3.2 Feedwater Manifold Seal Test 45

CHAPTER 7 FUEL SOLUTION
7.1 Expansion Coefficients and Vapor Pressures of the Fuel 95
7.2 Fuel Analyses 95

CHAPTER 8 REACTOR PHYSICS
8.1 Calculated and Experimental Data for Cylindrical Assemblies 101
8.2 Calculated Total Extrapolation Lengths 101
8.3 Calculated Critical Core Volumes for Cylindrical Reactor 102
8.4 Calculated Critical Core Volume and k_{eff} for Cylindrical Reactor 103

CHAPTER 10 POST MORTEM
10.1 Fuel Analysis 130

APPENDIX A.1 Temperature-Pressure Identification 134
A.2 Reactor Operation Data 136

ILLUSTRATIONS

CHAPTER 1 REACTOR CHARACTERISTICS AND LOCATION
1.1 LAPRE II, Showing Basic Components 12
1.2 Plan View of LAPRE II Installation 17
1.3 Elevation of LAPRE II Installation 18

CHAPTER 3 THE REACTOR SYSTEM
3.1 Elevation of Reactor Assembly 24
3.2 Location of Strain Gages During Hydrostatic Test of Reactor Vessel 27
3.3 Reactor Vessel with Strain Gages Attached 28
3.4 Strain vs Internal Pressure in Reactor Vessel 29
3.5 Reactor Vessel Showing Internal Gold Cladding 32
3.6 Reactor Vessel Lid (Derby) Showing Gold Cladding 33
3.7 Gold Clad Feedwater Tube Sheet with Tube Hole Liner in Position for Welding 34
3.8 Gold Clad Feedwater Tube Sheet after First Welding Pass on Tube Hole Liner 35
3.9 Gold Clad Feedwater Tube Sheet after Final Welding Pass on Tube Hole Liner 36

Page

3.10 Reactor Vessel Lid Showing Feedwater and Steam Tube Sheets 38
3.11 Feedwater Manifold Gold Gasket 39
3.12 Details of Feedwater Manifold Seal 40
3.13 Metallographic Section of Feedwater Manifold Seal 41
3.14 Details of Feedwater Manifold Seal Mockup 42
3.15 Schematic Diagram of Feedwater Manifold Seal Test 43
3.16 Reactor Vessel Lid with Heat Exchanger and Flow Baffle Attached 48
3.17 Bottom View of Heat Exchanger Showing Graphite Spacers and Flow Baffle Supports 49
3.18 Top View of Heat Exchanger 50
3.19 Details of Reactor Fuel Line Connections 53
3.20 Fuel Line Port in Safety Enclosure 55
3.21 Details of Steam and Feedwater Port in Safety Enclosure 56
3.22 Neutron Source Tube 57
3.23 Movable Reflector or Shim 59

CHAPTER 4 FUEL AND GAS SYSTEM
4.1 Schematic Diagram of Fuel and Gas System 62
4.2 Fuel Line Connections to Fuel Reservoir Tank 64
4.3 Fuel Reservoir Tank Flange Details 66
4.4 Reactor Vessel Vent Line 69
4.5 Schematic Diagram of Emergency Fuel Recovery System 71

CHAPTER 5 HEAT REMOVAL SYSTEM
5.1 Schematic of Heat Removal System 73
5.2 Primary Pumps No. 1 and No. 2 Flow vs Head 79
5.3 Primary Pumps No. 3 and No. 4 Flow vs Head 80
5.4 Control Valve Flow vs Head 82
5.5 Control Valve Loading Pressure vs Valve Lift 83

CHAPTER 6 INSTRUMENTATION
6.1 Plan of Control Point 86
6.2 Control Point Instrument Panels 87
6.3 Control Point Instrument Panels 88
6.4 Control Point Instrument Panels 89

CHAPTER 8 REACTOR PHYSICS
8.1 Shim Position vs Fuel Temperature 108
8.2 Reactor Startup - Neutron Level and Reactor Temperature vs Time - Phase 1 110
8.3 Reactor Startup - Neutron Level and Reactor Temperature vs Time - Phase 2 111
8.4 Reactor Startup - Neutron Level and Reactor Temperature vs Time - Phase 3 112
8.5 Neutron Level vs Time - Pulse Operation 116

			Page
CHAPTER 9	REACTOR OPERATION		
	9.1	Fuel Temperature vs Reactor Power	123
	9.2	Reactor Pressure vs Reactor Power	124
	9.3	Neutron Level and Reactor System Temperatures vs Time	126
	9.4	Steam Discharge Temperature from the Top Heat Exchanger Coil vs Reactor Power	128
	9.5	Steam Temperature vs Reactor Power	129
CHAPTER 10	POST MORTEM		
	10.1	Reactor Assembly in Safety Enclosure at Start of Post Mortem	132
	10.2	Reactor Heat Exchanger, Derby, and Flow Baffle Before Installation in Reactor Vessel Reactor Heat Exchanger, Derby, and Flow Baffle After Reactor Operation	133
APPENDIX	A.1	Schematic Diagram of LAPRE II Heat Disposal System	135

Chapter 1

REACTOR CHARACTERISTICS AND LOCATION

1.1 Introduction

The Los Alamos Power Reactor Experiment No. II, LAPRE II,[1,2,3] was a test of a compact homogeneous reactor using a fuel solution composed of UO_2 (93.5% U^{235}) dissolved in 95% H_3PO_4. Reactor design was started early in 1955 with the intention of capitalizing on the inherent advantages of this reactor type as well as on the most recent information on materials and chemistry available at that time. Much of the information used in the design of LAPRE II was obtained from research on problems encountered in the design and construction of LAPRE I.[4,5] Many of the design features were slanted toward portable power reactor specifications existing at the time. Standard items (pumps, heat exchangers, etc.) were used wherever possible. The design did not include generating equipment, but the heat dump could simulate turbine-generator operation. A schematic view of the reactor is shown in Fig. 1.1.

Construction of LAPRE II was begun in February 1956. This report describes the reactor, the fuel solution, reactor components and auxiliaries, reactor physics, and reactor operation.

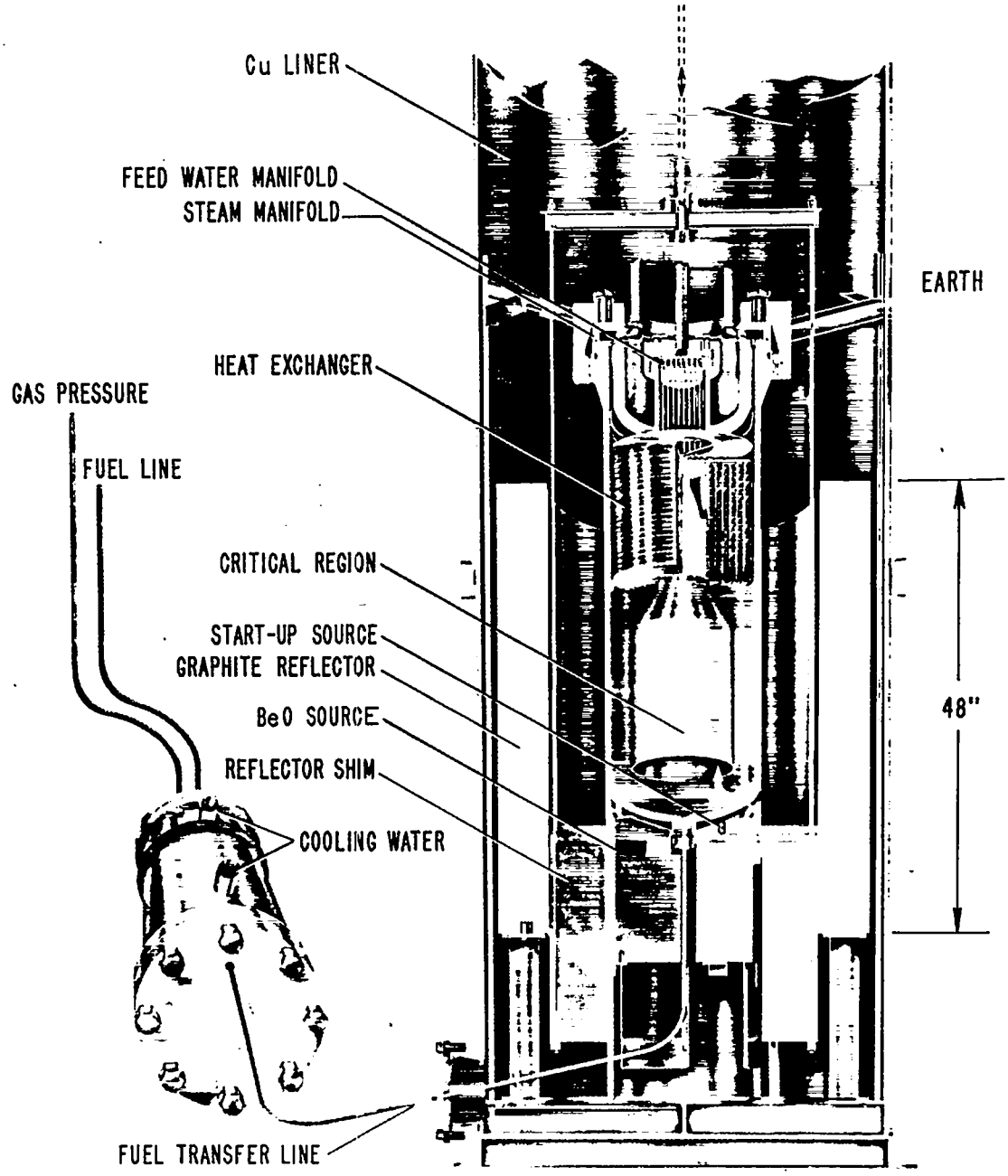

LOS ALAMOS POWER REACTOR
EXPERIMENT NUMBER 2

Fig. 1.1 LAPRE II, Showing Basic Components

1.2 Reactor Characteristics

General

Name	LAPRE II
Location	TA-35 - LASL, Los Alamos, N. M.
Purpose	Test of phosphate fuel containment; demonstration of homogeneous convection-cooled power reactor
Type	Homogeneous
Neutron energy	Thermal
Status	Test completed; post mortem in progress
Power	800 kw thermal
Fuel	UO_2 (93.5% U^{235}) dissolved in H_3PO_4, operated with hydrogen overpressure
Moderator	Water and H_3PO_4
Reflector (fixed and movable)	BeO (3 in.), Graphite (8 in.)

Reactor Vessel

Over-all volume	101 liters
Steam generator region	31.2 liters
Core region	61.8 liters
Over-all length, bottom of vessel to top of flange	54-3/4 in.
Inside diameter of vessel	14.750 in.
Wall thickness of vessel	0.625 in.
Height of core region	24.8 in.
Height of heat exchanger region	14.0 in.
Vessel material	Type 316 stainless steel
Cladding	0.015 in. Au (99.95%)
Vessel seal	Au crush ring plus seal weld
Working pressure limit for vessel at 900°F (ASME allowable)	1130 psi

Fuel Solution

Composition	0.35 M UO_2 in 17.5 M (95%) H_3PO_4
Fuel solution volume at 800°F	95 liters
Fuel solution volume at 70°F	83 liters
Power density (based on core volume)	12.9 kw/liter
Fissionable material inventory	6.73 kg U^{235}
Vapor pressure of solution at operating temperature (800°F)	~ 720 psi
Density of fuel solution at 70°F	1.88 g/cc
Density of fuel solution at 800°F	1.62 g/cc
$H:U^{235}$ in fuel solution	177
Radiolytic gas evolved	Adequately recombined by back reaction above 700°F.

Steam Generator

Heat exchanger area	41.2 ft^2
Construction	44 spirally wound coils, each with 18 ft of 3/16 in. o.d. x 1/8 in. i.d. stainless steel, Au-clad (0.006 in.) tubing. Vertical pitch 0.300 in., horizontal pitch 0.492 in.
Coolant	Water (H_2O)
Coolant flow rate	2370 lb/hr (4.75 gpm)
Coolant temperature	435°F inlet, 744°F outlet
Coolant pressure	650 psi
Coolant pressure drop through heat exchanger and feedwater heater	150 psi - at 750 kw extracted
Over-all heat transfer coefficient	310 $\frac{Btu}{hr\ ft^2\ °F}$ (calculated)
	450 $\frac{Btu}{hr\ ft^2\ °F}$ (measured at No. 1 coil)
Method of fuel circulation	Natural convection
Fuel solution velocity	1/2 ft/sec in heat exchanger region (calculated)
Heat disposal	Reactor coolant to secondary heat exchanger to air radiator

Reactor Control

Temperature	Movable 6 in. thick annular sleeve, or shim (3 in. graphite, $\rho = 1.67$, + 3 in. BeO, $\rho = 2.7$). Total reactivity effect of 13.9% $\Delta k/k$. Temperature increase of ~ 20°F/in. of shim travel in mid-range of 23 in. total travel.
	Maximum insertion rate, shim travel, 0.02 in./sec, or $\Delta k/\Delta t$, < 5¢/sec.
Power	Determined by heat leak and demand of heat dump. Power changes made by regulating flow in primary loop.
Safety	Negative temperature coefficient of reactivity and no available excess reactivity. Also, any pressure rise in reactor vessel returned fuel to non-critical reservoir of 110 liter capacity. If pressure became greater than 1250 psi, a rupture disc in series with a relief valve would vent reservoir to waste disposal to maintain pressure at 1200 psi; a parallel rupture disc would vent system if pressure reached 1350 psi. A manually controlled vent valve could also be used to transfer fuel from reactor into reservoir. Fuel input rate controlled by (1) a flow-limiting orifice on pressurizing gas line, (2) preset pressure and volume on injection line to reactor, and (3) the diameter of the fuel line. Fuel input rate limited to $\Delta k/\Delta t$ = 10¢/sec.
Shielding	Earth fill (rhyolitic tuff, $\rho = 1.4$, and sand). Exclusion area to insure 25 ft of earth between reactor and personnel. Primary loop and reservoir tank also below ground level. Gamma and neutron dose rates below tolerance outside exclusion area with reactor at full power.

Reactor Physics

Critical Mass - 70°F	
Shim out	2.8 kg
Shim in	2.4 kg
Shim worth	13.9% k_{eff} (calculated)
Temperature coefficient	-6×10^{-4} $\Delta k/k$ °C (Prompt temperature coefficient associated with fuel expansion)

1.3 Reactor Location

LAPRE II was located in an exclusion area on the south side of the main laboratory building at TA-35, LASL. A schematic view of the installation is shown in Fig. 1.2. The location and the underground arrangement of the reactor were chosen as an economical means of obtaining the necessary personnel protection without the expense of biological shielding construction. An incidental feature was the simulation of a portable reactor installation. Figure 1.3 shows a schematic elevation of the reactor and its auxiliaries.

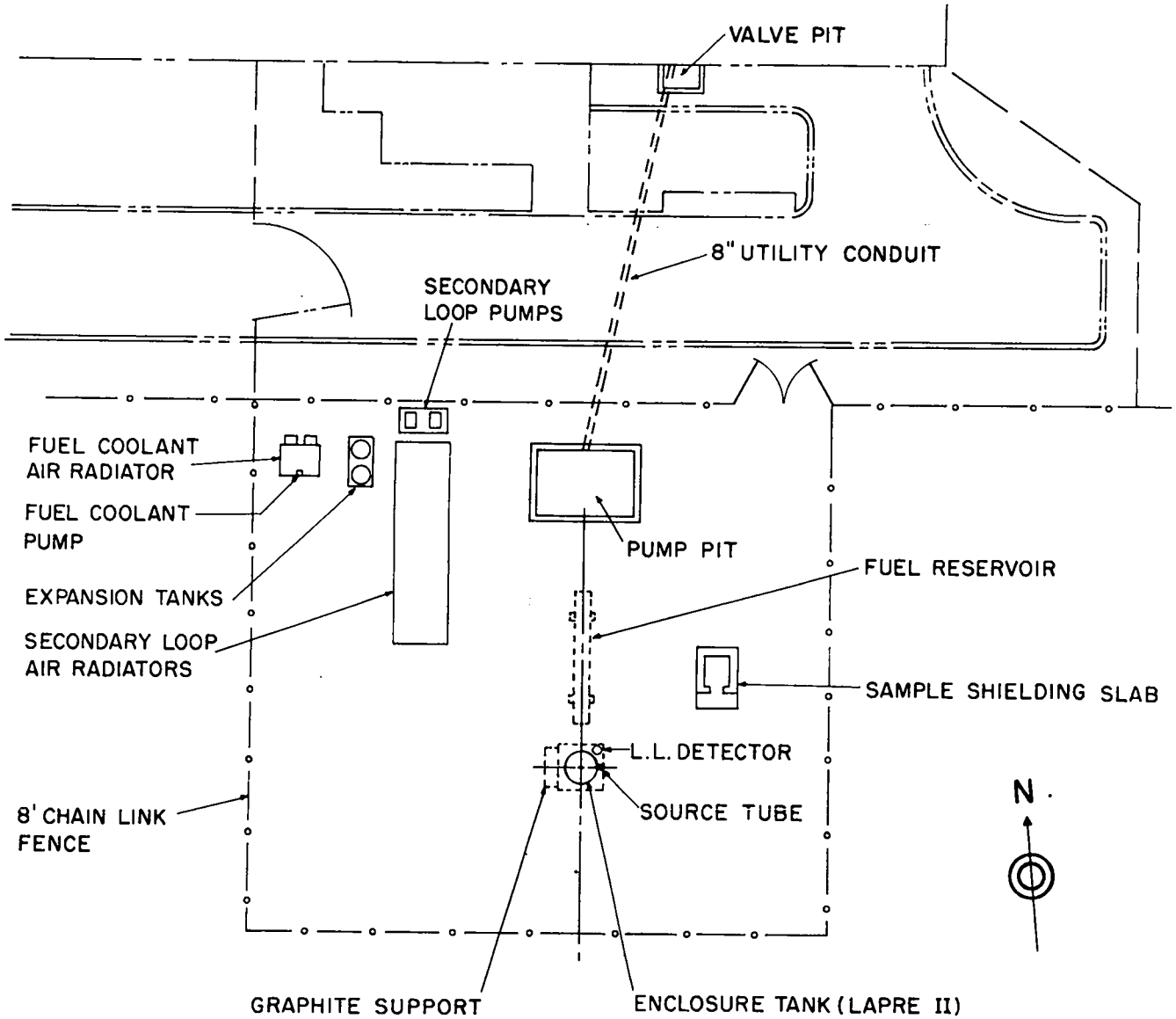

Fig. 1.2 Plan View of LAPRE II Installation

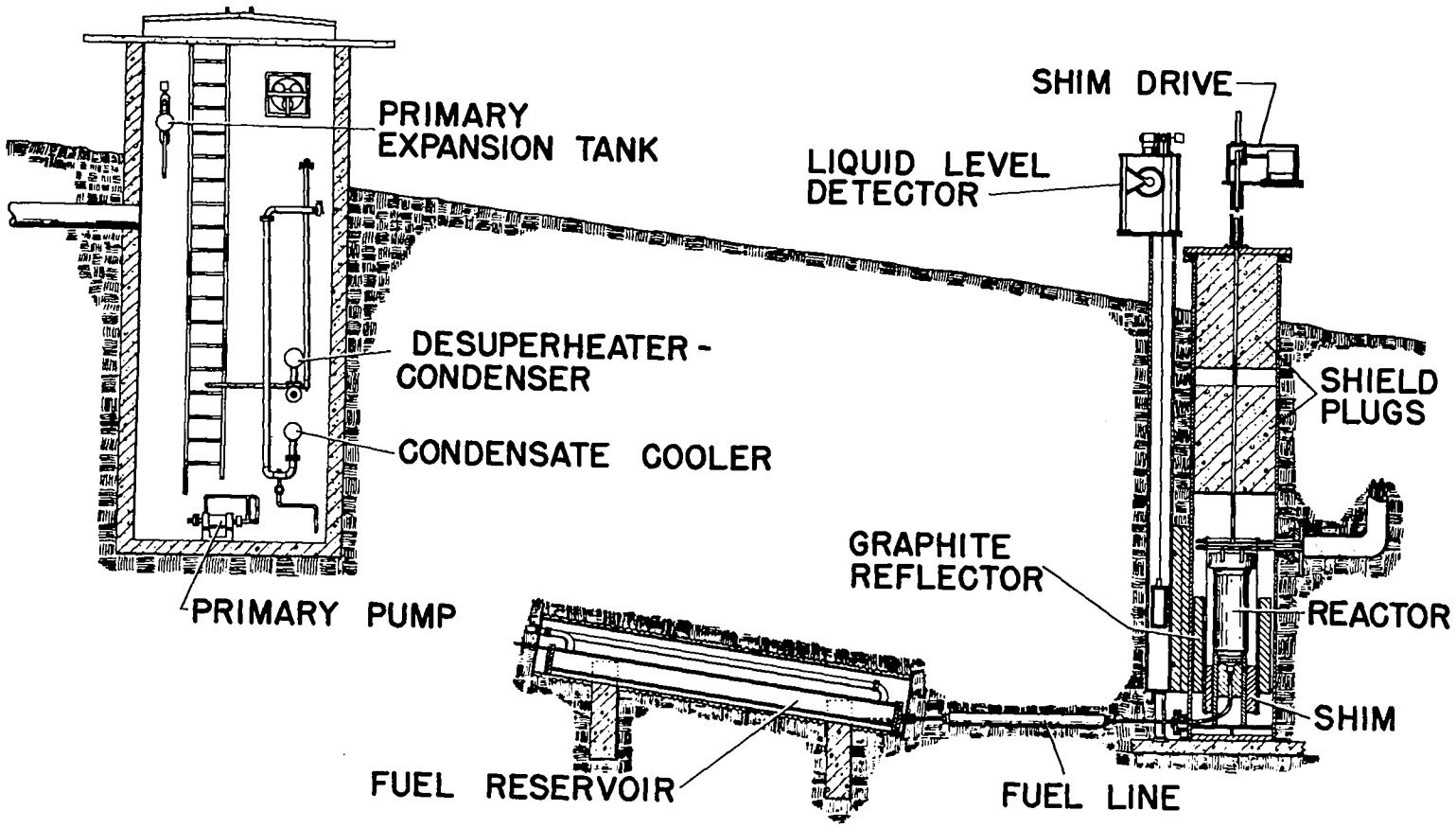

Fig. 1.3 Elevation of LAPRE II Installation

Chapter 2

CONCLUSIONS AND RECOMMENDATIONS FOR FUTURE WORK

2.1 Conclusions

The experimental operation of LAPRE II demonstrated some desirable properties of the UO_2-H_3PO_4 fuel system and indicated other areas where additional development of reactor fabrication techniques might be desirable in order to exploit the system to full advantage with confidence. A summary of the experiment can be stated as follows:

1. The reactor system demonstrated excellent nuclear behavior, operating as a constant-temperature energy source whose output was determined only by external load demand. The temperature of the fuel solution and of the superheated steam output was set by the uranium concentration in the fuel and by the position of the adjustable shim.

2. The internal recombination of all radiolytically produced gases was adequate for the peak power density achieved (13 kw/liter). Substantially higher power densities are undoubtedly possible since it was found that adequate recombination occurred whenever the fuel temperature was above 700 °F, which was about 100 °F below the normal operating temperature of the reactor. The rate of recombination is known to be a sensitive function of the temperature.

3. Superheated steam was produced in a simple once-through internal heat exchanger using two-phase flow.

4. The instrumentation of the reactor vessel was intentionally limited in an attempt to minimize fabrication difficulties. The detailed interpretation of

the reactor behavior was, therefore, more difficult since many features, e.g., fuel level, temperature gradients, fuel flow, etc., had to be inferred from a few internal temperature measurements.

5. The location of the fuel vapor interface in a region having small fluctuations in fuel surface temperature was found to be a necessary operating condition. In the LAPRE II design this condition was met by filling the vessel with fuel to a level high on the surface of the top closure plug. The fuel surface temperature was then determined primarily by the surrounding wall and heat exchanger tube temperatures rather than by the fuel circulating out of the core. Under these conditions changes in power demand had little effect on the reactor pressure and hence on fuel movement between core and reservoir.

The principal problem encountered in the construction of the reactor was the providing of satisfactory fuel containment. The complete gold cladding, with absolute integrity, of all surfaces exposed to the fuel, although not excessively expensive, proved to be difficult in the LAPRE II design. Satisfactory techniques and procedures were devised as fabrication proceeded.

2.2 Recommendations

The numerous advantageous properties of the fuel and of the internal heat exchanger design used in this reactor warrant further investigation. The phosphate fuel appears to combine the desirable properties of the aqueous homogeneous fuels with those of molten salt systems while avoiding most of their faults.[6]

The well-known advantages of fluid or mobile fuels over solid elements apply to the phosphate type fuel. These are:

1. Good neutron economy with a simple fuel cycle
2. Large negative temperature coefficient for inherent safety
3. No fuel radiation damage to limit fuel burnup
4. No expensive fabrication or handling requirements as for solid fuel elements
5. Continuous or batchwise removal or addition of fuel for reprocessing[7,8,9] without reactor shutdown

The following disadvantages associated with aqueous homogeneous and molten fuel reactors[6] appear to be eliminated by the LAPRE II type reactor with internal heat exchanger and phosphate fuel.

1. Aqueous homogeneous reactors:
   (a) Radiation-induced corrosion
   (b) External circulation of fuel
   (c) Explosive decomposition products
   (d) High operating pressure
   (e) Thermal instabilities and precipitation
2. Molten salt fueled reactors:
   (a) High melting point of fuel
   (b) Large critical mass due to poor moderation of the salts
   (c) Parasitic neutron capture in salts

The long-term containment of the fuel, necessary for any successful reactor, is a problem common to fluid fuel reactors. The use of gold cladding has been shown to be possible for phosphate fuels but improvements in fabrication techniques and in cladding materials are still desirable. This type of containment is best suited for relatively small size power requirements where breeding is unimportant.[10] The Sandia Corporation[11] is studying the feasibility of making an engineering model of such a gold clad reactor for small portable power station use.

2.3 Advanced Concepts

A small effort on improved methods of containment for phosphate fuels is being carried out at Los Alamos. Recent results in England and the United States on the production of impervious graphite have made its use for reactor containment look promising. Corrosion tests at LASL using high density graphite indicate a negligible attack by either phosphate fuel or steam at 840°F. This resistance to attack was also demonstrated by the graphite sleeves used in the LAPRE II heat exchanger described in Section 3.3.2.

The excellent nuclear and physical properties of graphite in combination with phosphate fuel make these materials of interest for potential liquid fuel reactors with good neutron economy. A proposed reactor design would use impervious graphite as the common container and primary heat exchanger material. An in-pile experiment to test this concept is planned in which the phosphate fuel is contained in a sealed impervious graphite capsule surrounded by a steam jacket. Both coolant and fuel are to operate at 840°F and 800 psi. This experiment may also serve to demonstrate the long-term radiation stability of phosphate fuel.

Other reactor concepts using phosphate fuels may be of interest. A reactor in which the phosphate fuel is cooled by circulating an immiscible coolant in direct contact with the fuel might have some potential advantages. Water contamination in an organic coolant and a hydrogen environment due to decomposition of the organic coolant, which have been found troublesome in OMRE-type reactors, are not detrimental with phosphate fuel. The poor heat transfer properties of organic coolants would be greatly improved by direct contact lift or jet pumping of the fuel by the coolant.

Phosphate fuels may lend themselves to direct boiling reactors in which the heat transfer is accomplished in the vapor region of the reactor, thus reducing pumping and corrosion problems in the primary heat exchanger circuit. Low oxygen concentration problems encountered in previous boiling water reactor designs[6] would not be detrimental.

Further work on reactor designs and containment of the phosphate fuel seems warranted in view of the present information on LAPRE reactors.

Chapter 3

THE REACTOR SYSTEM

3.1 Reactor Vessel

3.1.1 Design

Reactor Vessel. The general design of the reactor vessel is shown in Fig. 3.1. The vessel itself was basically a 16 in. o.d. tube 49 in. long with a 2:1 ASME elliptical bottom. The wall thickness was 5/8 in. throughout. The upper end of the vessel was flanged out to a 19-1/2 in. diam Acme thread. On the bottom of the vessel a 3-1/2 in. o.d. boss was welded,which served to fasten the fuel line to the vessel. The reactor was supported by a short 16 in. diam skirt tack welded to the base of the vessel.

Reactor Cover. The reactor cover, or derby, as it is referred to throughout this report, consisted of a 13-7/8 in. o.d. cylinder, 11 in. long and closed with 2:1 ASME elliptical head. The derby slipped inside the upper end of the vessel, and was flanged to match the vessel closure flange. Since the derby was subjected to compressional stresses, the thickness was 1-1/8 in. throughout.

A 5-5/8 in. o.d. tube, 9-1/2 in. long, was welded into the center of the derby to serve as part of the feedwater inlet header. Thermal gradients resulting from the 400°F difference in temperature between the feedwater and the reactor existed along the length of this tube.

Closure. The gasket used was a 1/4 in. diam annealed solid gold ring which was compressed between the gold liners of the vessel and the derby. A groove, 0.145 in. deep, was used to locate the ring in the vessel. Bolting force

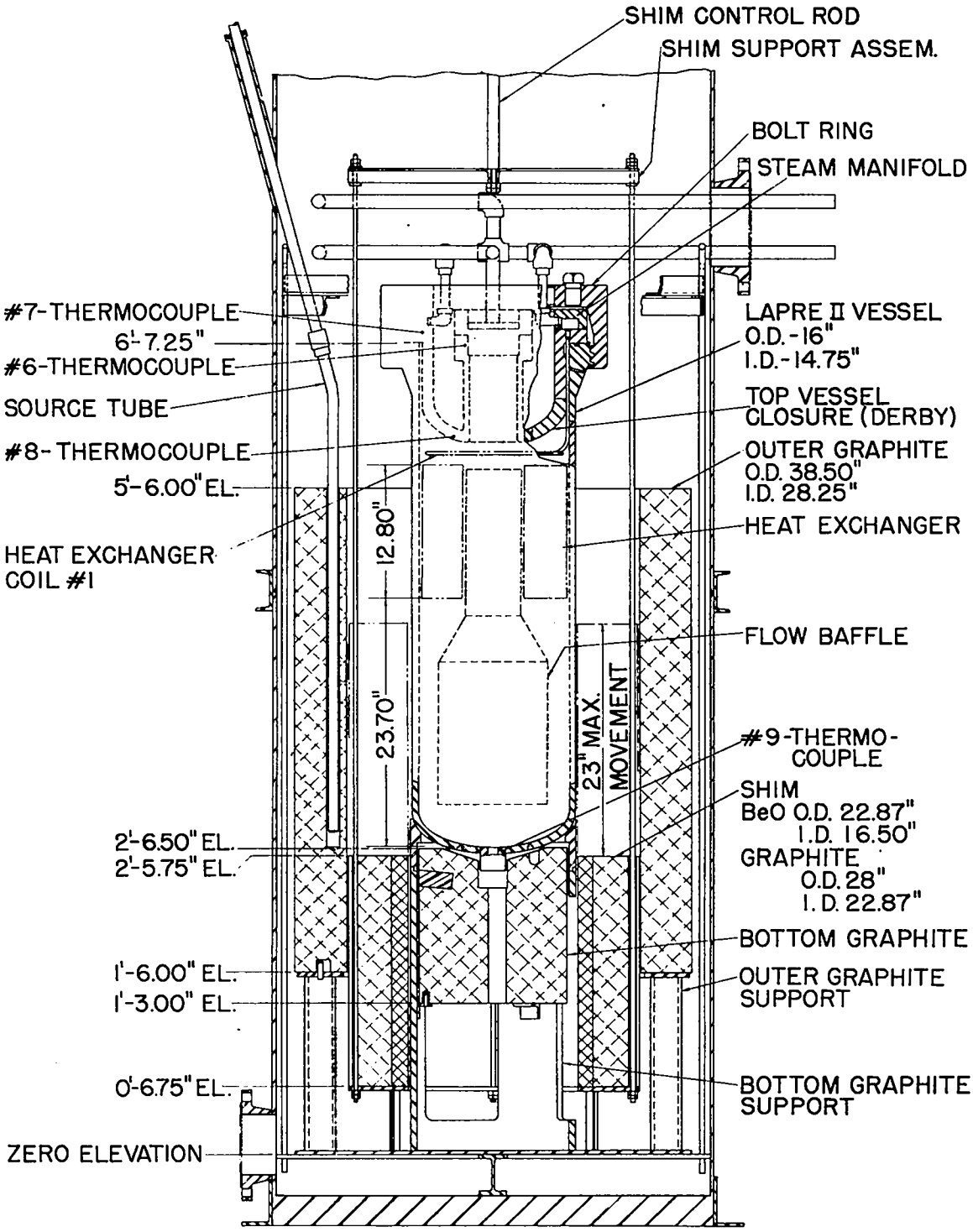

Fig. 3.1 Elevation of Reactor Assembly

was obtained from a large bolt ring which was fastened to the vessel by the 19-1/2 in. Acme thread. Sixteen 1-1/2 in. bolts transmitted the closing force from the bolt ring through the steam manifold to the reactor cover. Set up torque used on the bolts was 750 ft-lb.

As an added precaution the derby and the vessel were seal welded. The space between the seal weld and the gold ring was attached to a vacuum system during operation and monitored for fission product leakage. The steam manifold was also seal welded to the upper surface of the derby.

Fabrication. The vessel was fabricated from rolled plate and forgings welded together and then machined. The pieces were stress relieved prior to final machining. All material was Type 316 stainless steel.

The welds were given a 100% x-ray inspection with a 30 mil resolution. After repair of one defective weld on the bottom of the vessel, all weld radiographs were negative.

Fabrication of the major vessel components was done by the Nooter Corporation, St. Louis, Missouri.

Surface Preparation. All surfaces of the vessel and derby which were to be covered with gold cladding were carefully machined to approximately a 125 microinch turned finish using sharp tools. In addition, six equally spaced scratches about 10 mils deep were placed axially along the cylindrical surfaces. The purpose of this finish was to provide pump-out paths to all areas of the interface between the gold cladding and the vessel and derby walls.

Four 40 mil diam "weep holes" were drilled through the vessel wall and one through the derby (Fig. 3.1). After installation of the gold liner the weep holes were connected to a helium mass spectrometer used to test the integrity of the liner. During operation of the reactor, the weep holes were connected to a vacuum system which removed mercury formed by neutron capture in the gold. Evacuation of the space between the vessel wall and cladding also prevented any pressure build-up behind the cladding which might damage the gold liner.

3.1.2 Stress Analysis and Hydrostatic Test

Insofar as was practical, the reactor vessel was designed for service at 800 psi and 800°F according to ASME Code.[12] The closure flanges were calculated according to the Taylor Forge method[13] using allowable stresses from the ASME Code.

A hydrostatic test of the vessel assembly was made using SR-4 bonded wire strain gages (both single gages and 45° rosettes). Figure 3.2 shows the locations of the strain gages. Figure 3.3 is a photograph of the vessel assembly with the strain gages attached.

The vessel was pressurized twice with water, the first time to a pressure of 2800 psi and the second time to a pressure of 2945 psi. Data from the gages at Sections D and E are plotted in Fig. 3.4. Gage D shows that the 0.2% yield point of the metal would have been reached at a pressure of 3060 psi. Using the data from Gage E on the cylindrical section of the vessel, a yield strength for the Type 316 stainless steel of 36,700 psi was calculated. This figure is about what would be expected.[14]

Stresses as obtained from the hydrostatic test data are summarized in Table 3.1. These are only the stresses due to pressure and do not show the bolting stresses produced in the flange.

The maximum pressure stress is seen to occur at Section D, the junction of the vessel wall with the hub of the flange. Using the measured stresses at Section D and applying the distortion-energy theory of failure as advocated by Faupel,[15] the working limits of the vessel assembly were calculated. For this calculation, vapor pressure data for the fuel solution were taken from LA-2043[16]. A summary of the results is given below for the condition of no permanent gas overpressure.

	Fuel Temperature, °F	Vapor Pressure, psi
Maximum working stress	870	1170
0.2% yield point	965	1800
Vessel fracture	1095	3100

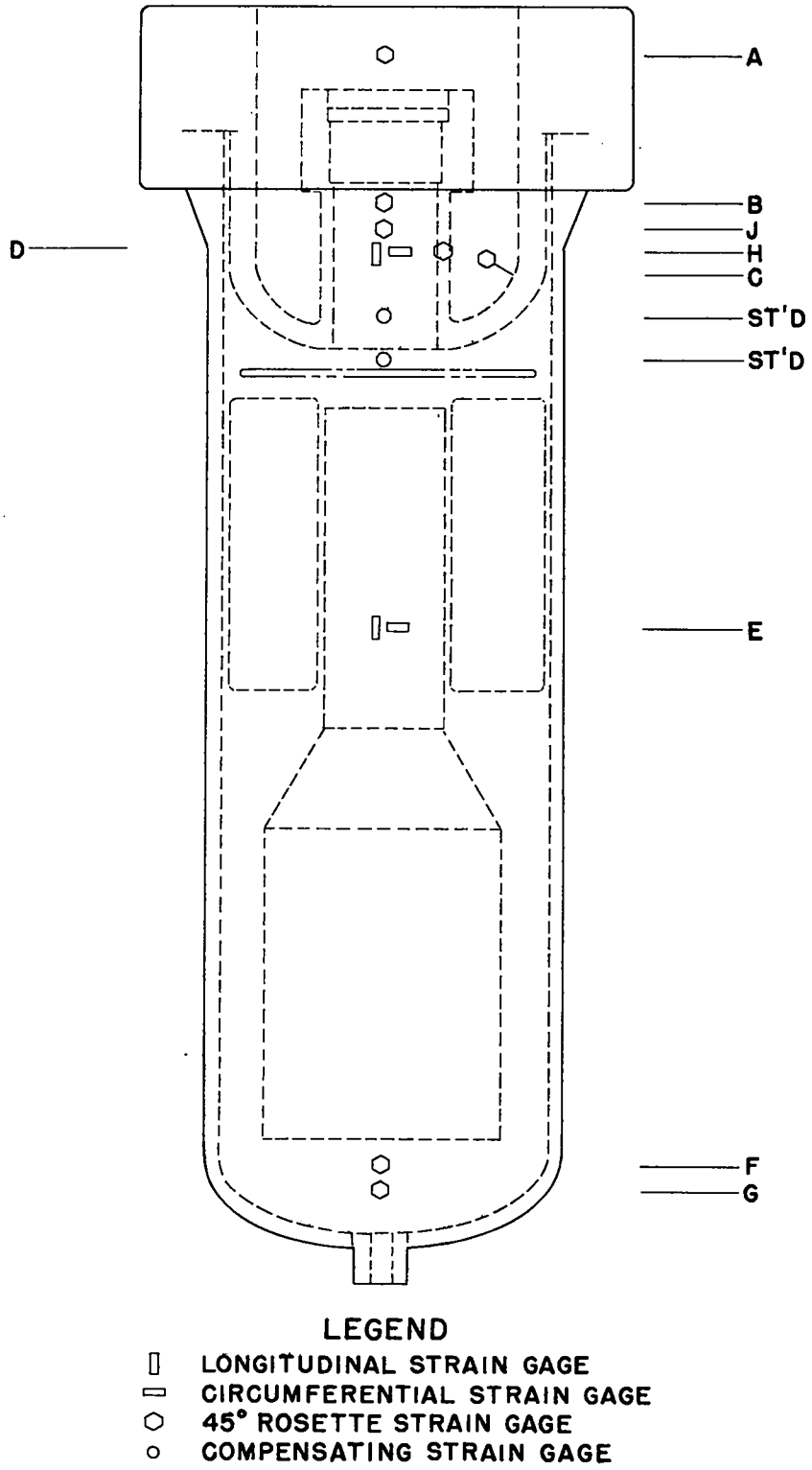

Fig. 3.2 Location of Strain Gages During Hydrostatic Test of Reactor Vessel

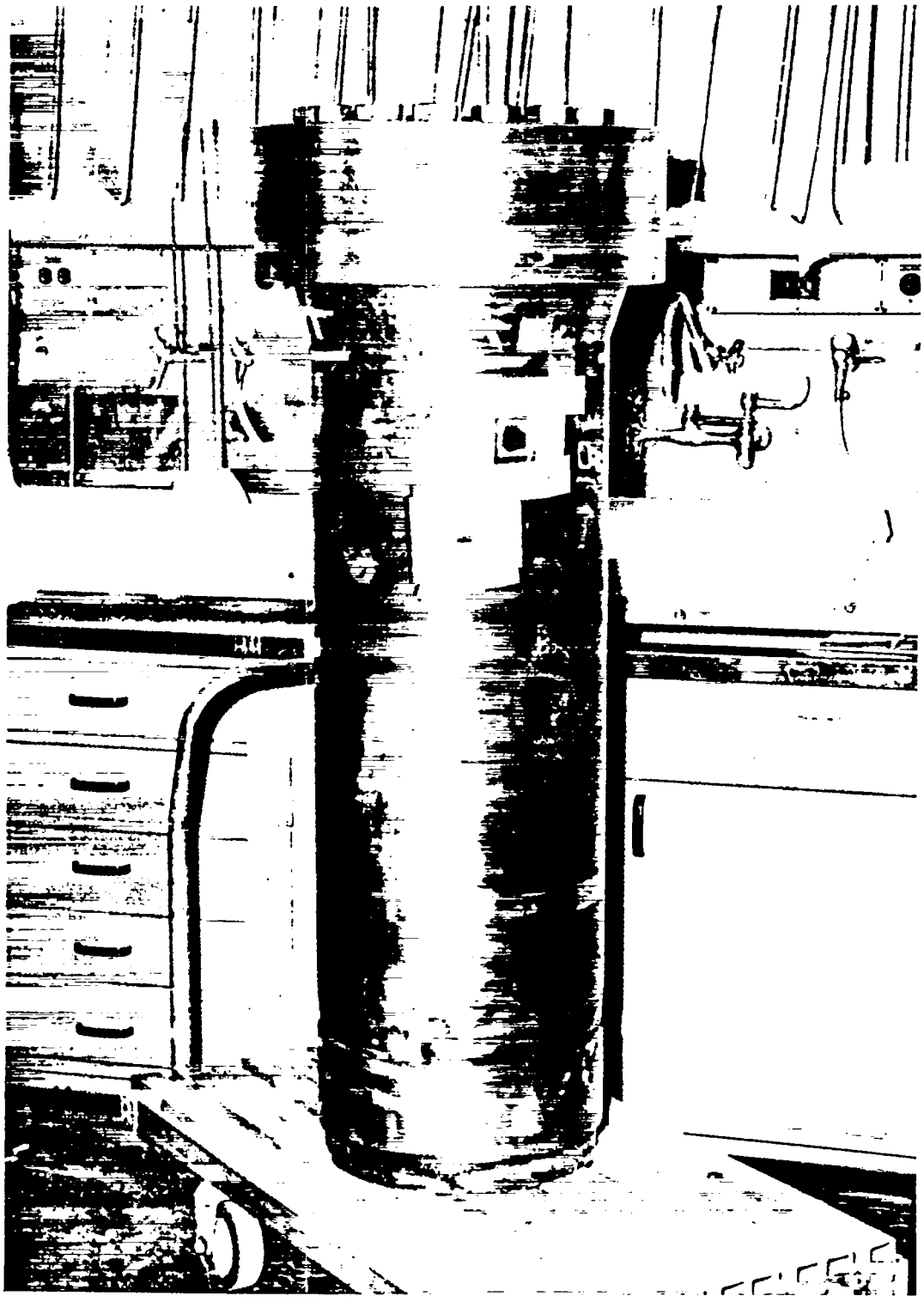

Fig. 3.3 Reactor Vessel with Strain Gages Attached

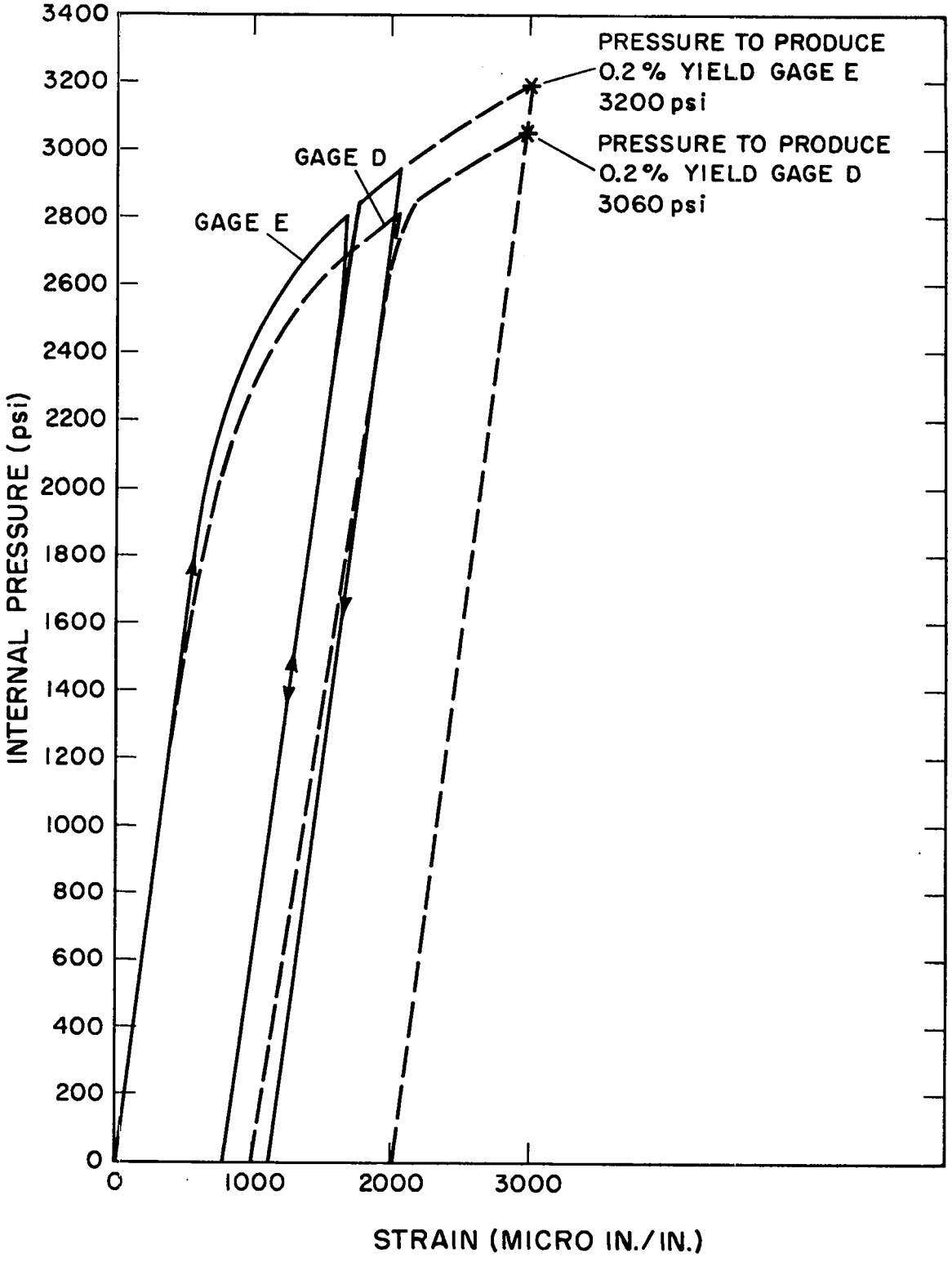

Fig. 3.4 Strain vs Internal Pressure in Reactor Vessel

TABLE 3.1

STRESSES DETERMINED FROM STRAIN GAGE DATA AND COMPARISON WITH CALCULATED STRESSES

(P = Internal Pressure)

Gage	Experimental Hoop	Experimental Longitudinal	Calculated Hoop	Calculated Longitudinal
A	0	1.4 P		
B	6.1 P	4.1 P		
C	-11.6 P	-3.6 P		
D	13.2 P	10.1 P	11.35 P	< 12.4 P
E	11.1 P	5.93 P	11.35 P	6.4 P
F	9.85 P	9.1 P		
G	6.1 P	5.6 P		
H	12.9 P	9.3 P		
J	10.0 P	5.5 P		

3.1.3 Vessel Cladding

In order to protect the vessel from contact with the corrosive fuel solution, all exposed stainless steel surfaces were protected with gold cladding. The initial cladding was purchased from the vessel fabricator, and although this liner had been inspected by dye penetrant methods and had successfully passed a helium leak test, acid (6NHCl) leaching of this liner revealed several hundred metallic inclusions. An attempt was made to repair the holes created by the dissolution of the inclusions, but it soon became apparent that a new cladding would have to be fabricated.

In preparation for fabricating a new cladding, samples of pure gold sheet obtained from various suppliers were inspected and tested but none of the sheet was found to be free from impurities. The predominant impurity in the sheet was iron, which apparently was imbedded in the sheet during the rolling operation. As a result of the above experience it was decided to fabricate the gold sheet at the Los Alamos Scientific Laboratory under carefully controlled conditions.

A complete description of the procedures, techniques, quality controls, and equipment used in the production of the sheet may be found in LAMS-2268.[17] The finished annealed sheet was radiographed and tested for continuity with a helium leak test prior to manufacture of the vessel liner. Fabricating procedures included welding (inert arc and oxyacetylene), spinning, and forging. Preliminary inspection of the liner was made with dye penetrant and in the final inspection the cladding was tested with a helium mass-spectrograph leak detector. The minimum detectable leak rate was $\sim 1.5 \times 10^{-7}$ cc He/sec, and any leakage in excess of this rate was deemed unacceptable.

The vessel cladding is shown in Fig. 3.5 with the clad derby being shown in Fig. 3.6. An illustration of technique is shown in Figs. 3.7, 3.8, and 3.9, where a sleeve is being welded to the feedwater tube sheet cladding.

The completed vessel cladding and derby cladding were tested for leakage at 50 psi He (70°F), 1500 psi He (70°F), and 680 psi He (800°F). In these tests no leakage in the vessel liner was observed until the final 680 psi, 800°F test. Three discontinuities were discovered in previously welded areas and were repaired. The derby cladding exhibited leaks in the flange tube sheet regions during all three tests, and although repairs were made, this area remained suspect since some leakage was observed after final repairs. The decision to proceed with a known leak was based upon the region in question being exposed only to the vapors from the fuel solution and not to the solution itself.

The transformation of the gold to mercury by neutron capture was a source of concern because of the effect which the presence of mercury might have on the physical properties of the gold cladding. Several studies were made which indicated that the diffusion rate at operating temperature ($\sim$ 800°F) of mercury from the solution or through the gold cladding was sufficiently large that the mercury could be removed by pumping on the space between the gold cladding and stainless walls. Additional tests indicated that gold sheet with 10% mercury added had sufficient strength to prevent deformation or rupture through a 0.040 in. hole.

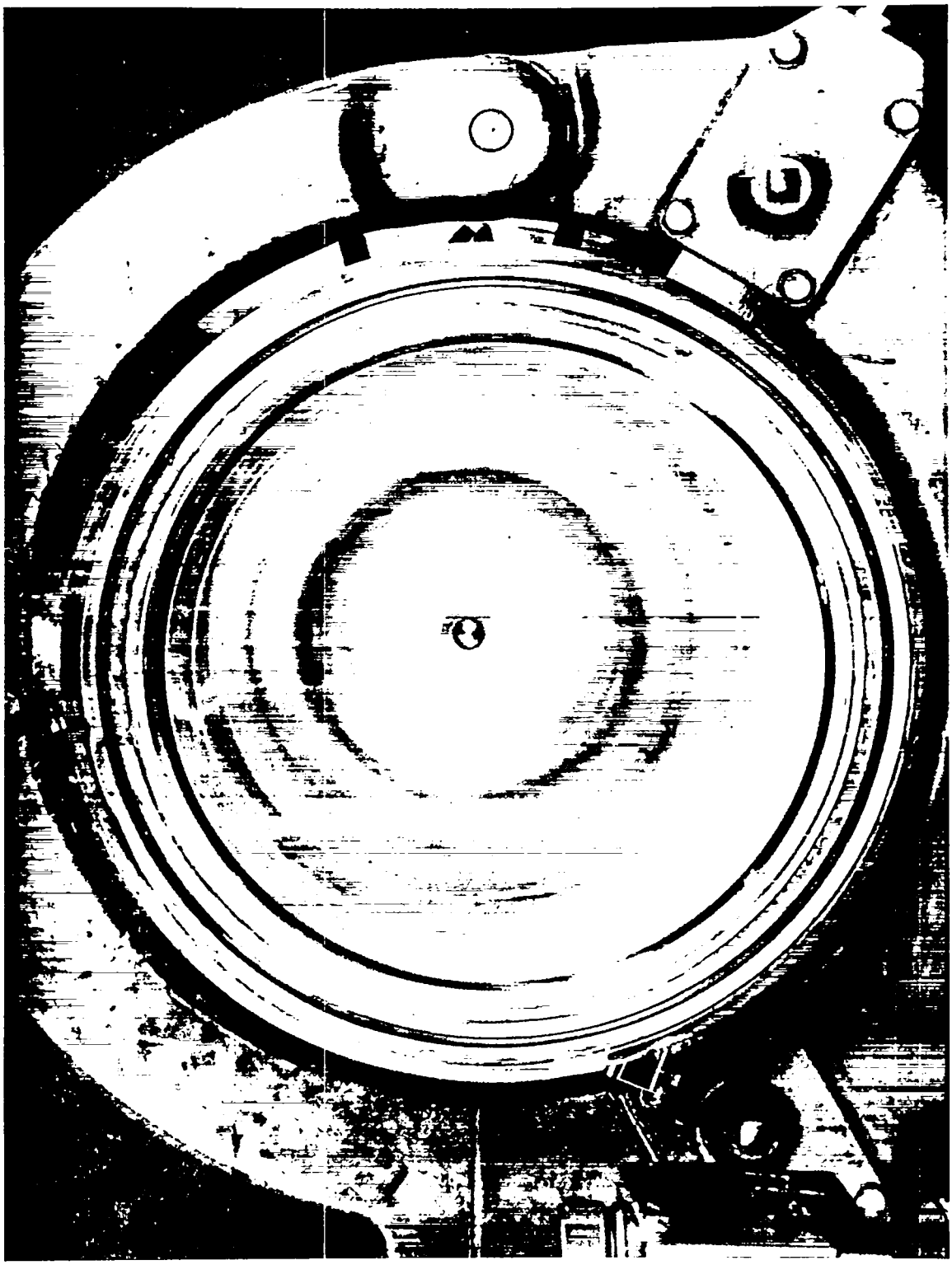

Fig. 3.5 Reactor Vessel Showing Internal Gold Cladding

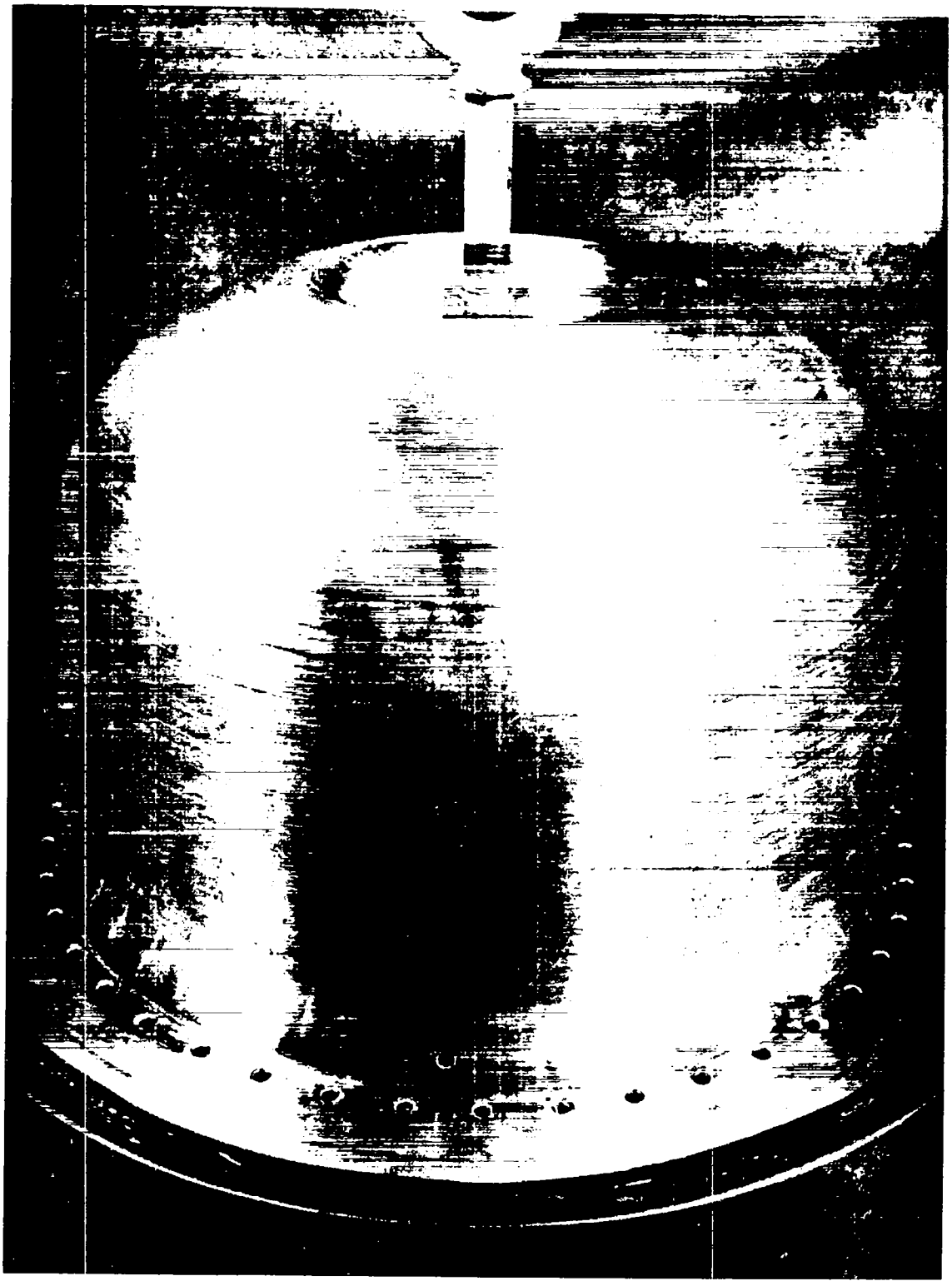

Fig. 3.6 Reactor Vessel Lid(Derby) Showing Gold Cladding

Fig. 3.7 Gold Clad Feedwater Tube Sheet with Tube Hole Liner in Position for Welding.

Fig. 3.8 Gold Clad Feedwater Tube Sheet after First Welding Pass on Tube Hole Liner.

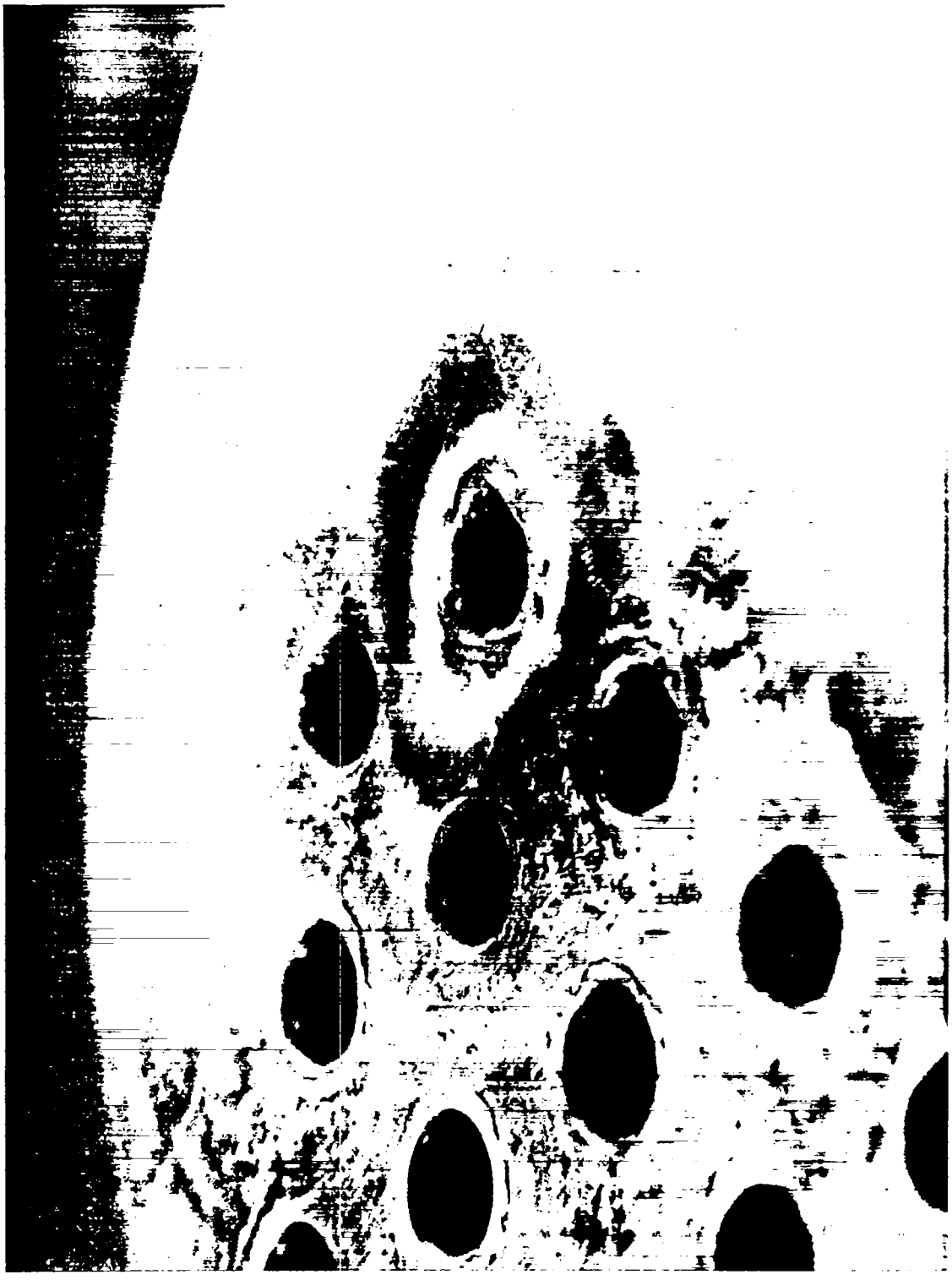

Fig. 3.9 Gold Clad Feedwater Tube Sheet after Final Welding Pass on Tube Hole Liner

3.2 Feedwater Manifold

3.2.1 Description of Feedwater Manifold

The feedwater manifold for the reactor steam generator was located in the 4-5/8 in. nozzle of the derby (Fig. 3.1). This location provided a long heat leak path between the reactor fuel and the feedwater tube sheet, thereby reducing thermal stresses. The feedwater manifold assembly consisted of the following components: gold clad tube sheet, manifold seal, and upper and lower bolt rings. The partially clad tube sheet is shown in Fig. 3.9 and the assembly in Fig. 3.10.

3.2.2 Description of Seal

The reactor vessel closure at the feedwater inlet was sealed by tightening the pull-up bolts and deforming a gold gasket (Figs. 3.11 and 3.12) to completely fill the gasket space between the nozzle of the derby and the feedwater tube sheet. (Figure 3.13 is a metallographic section of the gold gasket removed from the cold header mockup which shows how the gasket deforms and cold-welds to the gold cladding on the adjacent parts.) The sixteen 3/8 in. bolts were torqued to 25 ft-lb each which resulted in a pressure of 44,600 psi on the flat horizontal surface of the gold gasket. An internal reactor vessel pressure of 1000 psig increases the seating pressure by 12,500 psi. Examination of the cold header mockup after testing showed that the gold gasket continued to flow and, eventually, the pull-up bolts exerted no force. At this time the only seating force was that due to internal reactor vessel pressure.

3.2.3 Description of Seal Test

A full scale mockup of the cold header (Fig. 3.14) was constructed to test the feedwater manifold seal design and its behavior under conditions of rapid temperature changes. The tube sheet contained a cooling channel to facilitate thermal cycling the seal. Thermocouples were provided to measure the temperature difference across the seal. Two leak detector connections were provided: No. 1 to determine leakage through the gold cladding, and No. 2 to determine leakage past the gold gasket. A schematic diagram of the test setup is shown on Fig. 3.15.

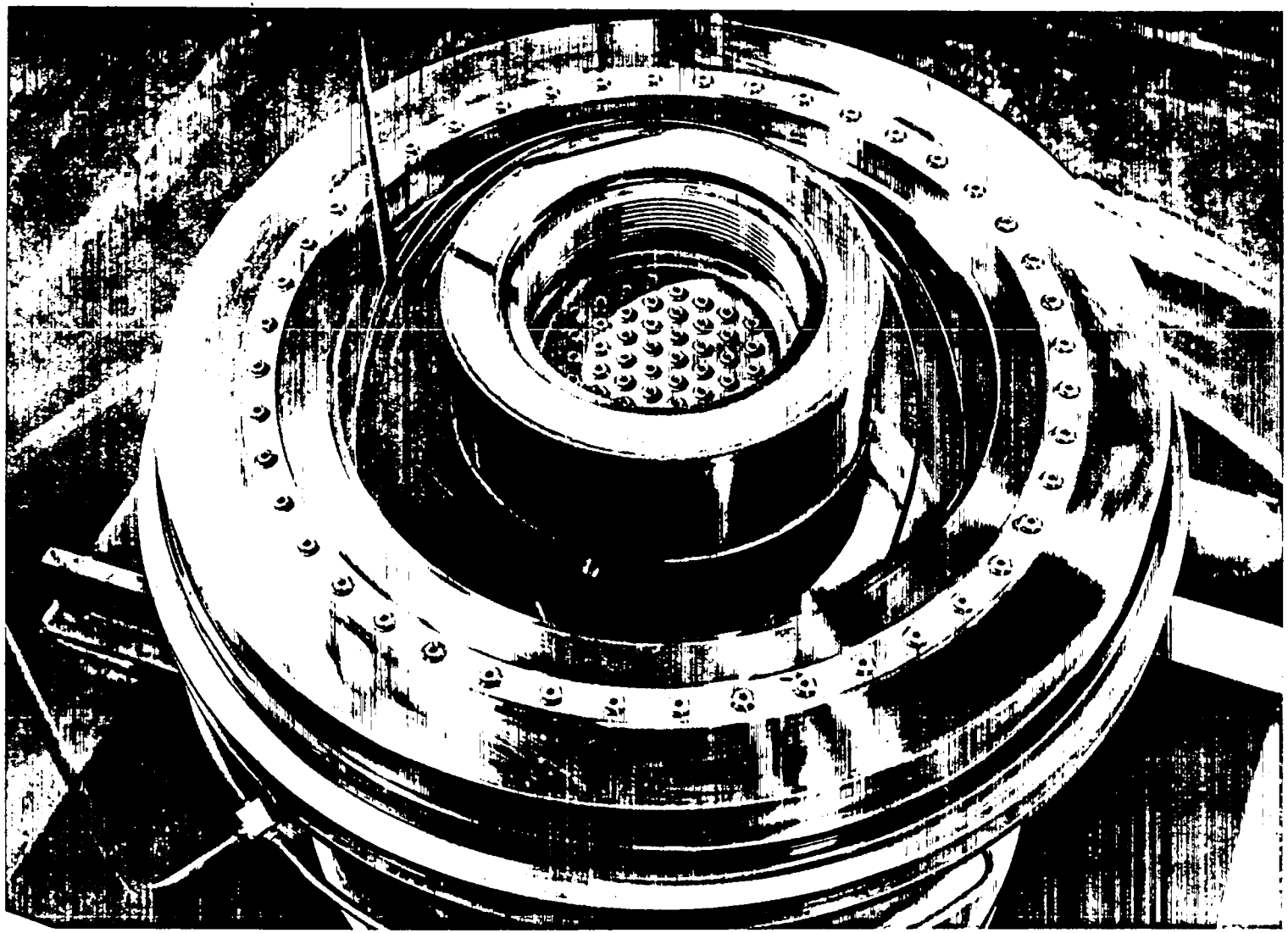

Fig. 3.10 Reactor Vessel Lid Showing Feedwater and Steam Tube Sheets

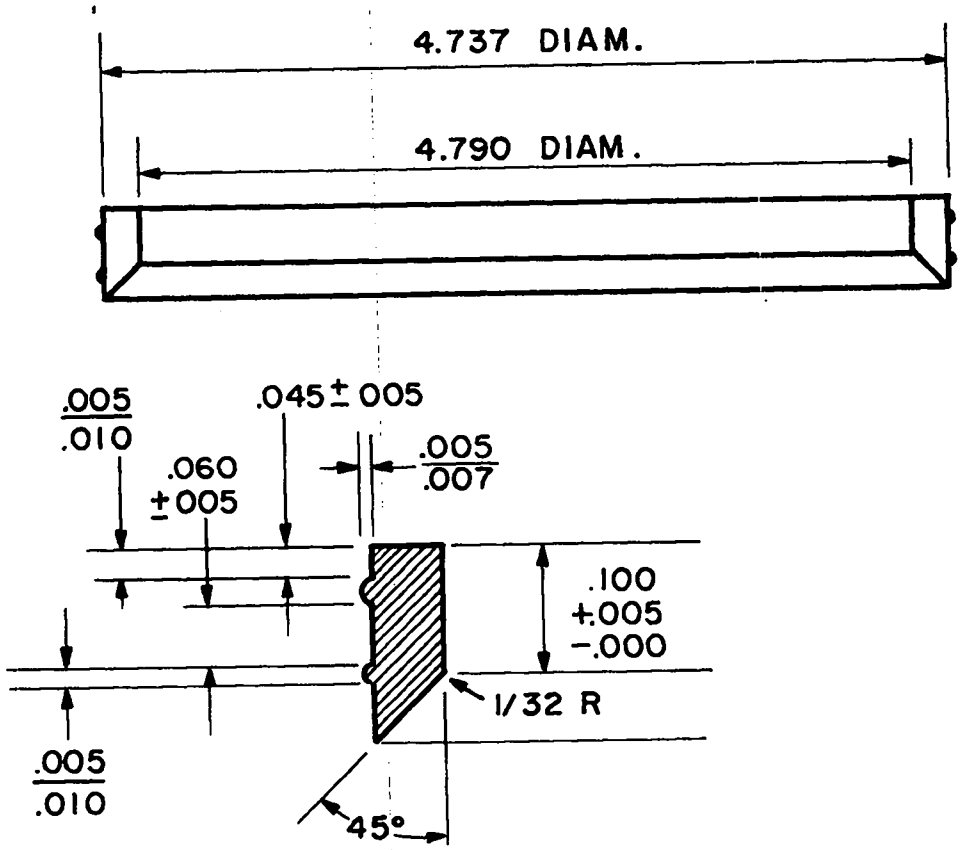

Fig. 3.11 Feedwater Manifold Gold Gasket

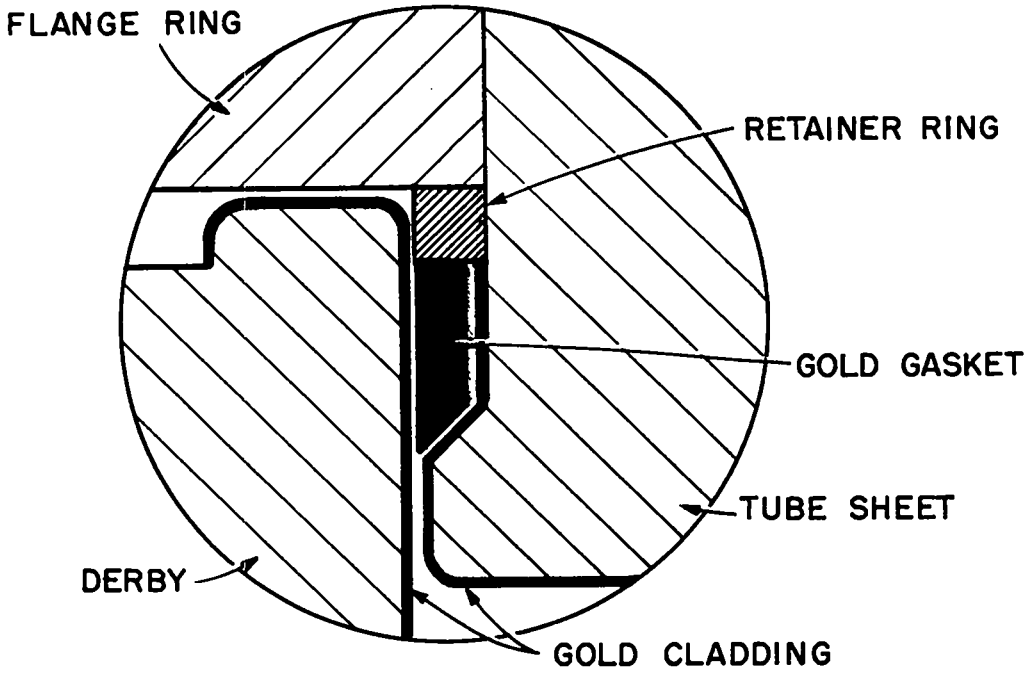

Fig. 3.12 Details of Feedwater Manifold Seal

Fig. 3.13 Metallographic Section of Feedwater Manifold Seal

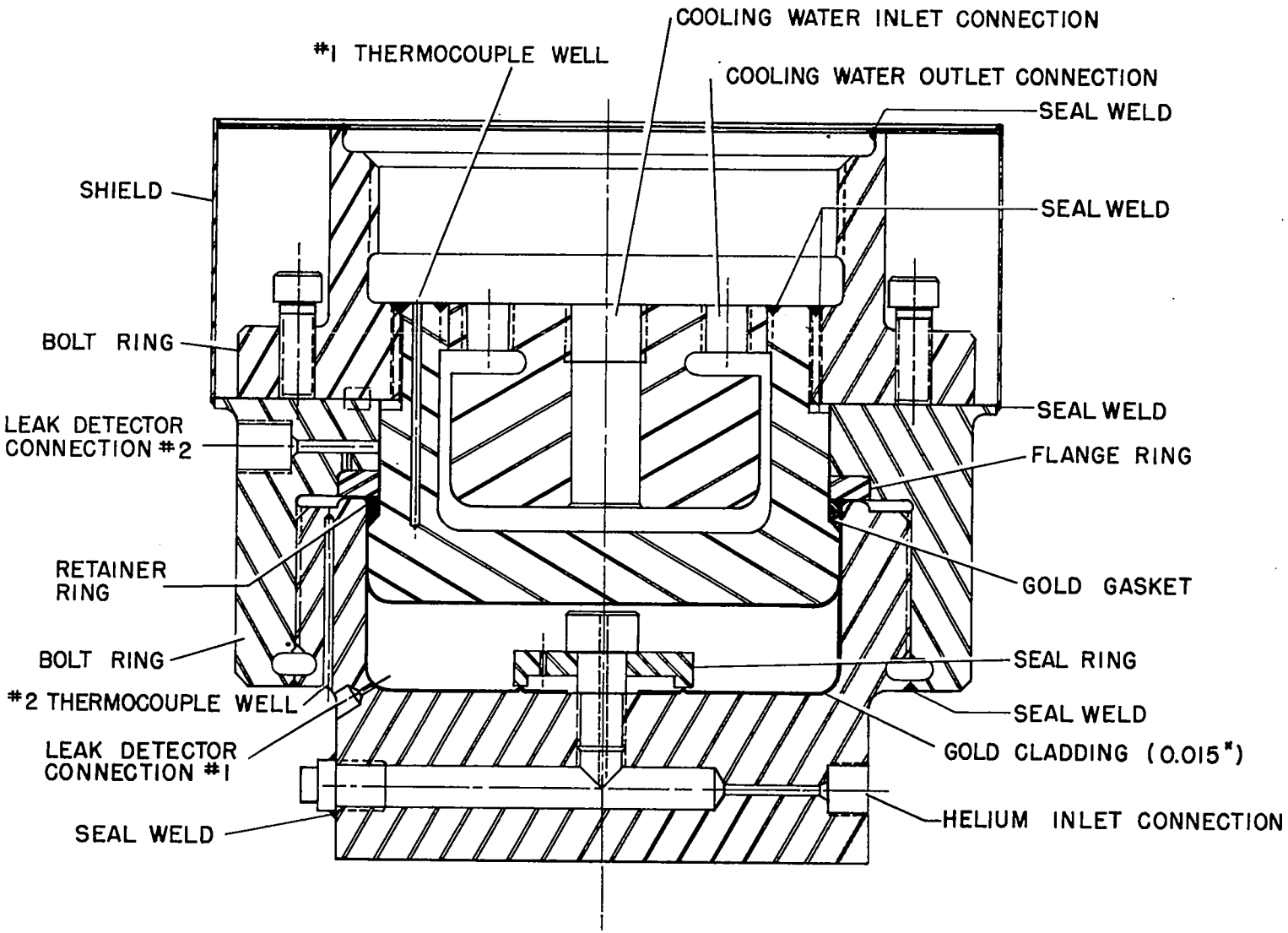

Fig. 3.14 Details of Feedwater Manifold Seal Mockup

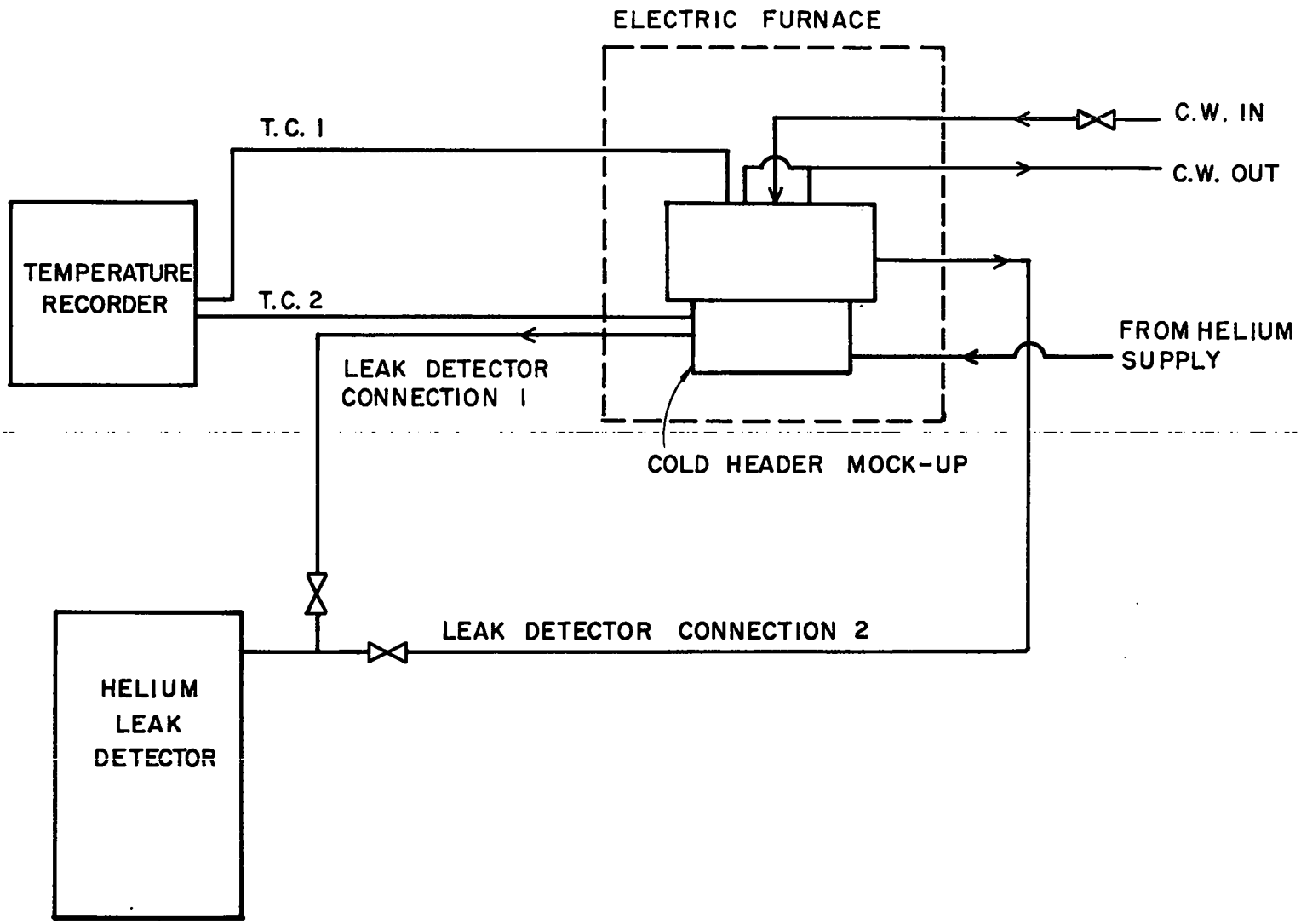

Fig. 3.15 Schematic Diagram of Feedwater Manifold Seal Test

3.2.4 Test Results

Several preliminary gasket designs were tested before the final design was selected. The final gasket design was tested as follows:

a. All structural parts of the cold header mockup were radiographically inspected.

b. The mockup was assembled. Each of the pull-up bolts was torqued and retorqued to 25 ft-lb until there was no more "give" in the gold gasket.

c. The mockup was hydrostatically pressure tested at 1500 psia with no indication of leakage. After hydrostatic testing, the unit was dried in a 150 °C oven for 24 hr.

d. The seal was helium leak checked at 1000 psig helium pressure and room temperature. No helium leak signals were obtained.

e. The unit was placed in a furnace and heated to 800 °F. Water, helium, and vacuum connections to the mockup were made as shown on Fig. 3.15.

f. The power to the electric furnace was turned off and cooling water admitted to the test unit by a manually operated valve in the water supply line. Cooling water flow was controlled so the difference in temperature between thermocouples No. 1 and No. 2 varied between 50 °F and 150 °F. Approximately 2 hr was required before the temperature indicated by thermocouple No. 1 returned to room temperature. The water was shut off and the test unit was reheated to 800 °F. The cooling cycle was then repeated.

During the first cooling cycle, a leak in the vacuum system appeared. During the second cooling cycle, helium was detected in the vacuum system, which indicated a leak in either the vacuum system, the gold seal, or the gold cladding. By the end of the sixth cooling cycle, it was definitely determined that the leak was in the vacuum system. The furnace was allowed to cool to room temperature, and the test mockup was then removed to repair the vacuum leak. During this operation the pull-up bolts were retorqued to 25 ft-lb each.

g. The test unit was next helium leak checked at room temperature. No vacuum leaks and no helium leaks past the gold gasket were detected during a 2 hr test at 850 psig helium pressure. An absolute pressure of $< 0.01\ \mu$ was obtained in the vacuum system.

h. The cold header mockup was put back into the furnace and twenty heating and cooling cycles performed as described in (f) above. Results observed are shown in Table 3.2.

TABLE 3.2

FEEDWATER MANIFOLD SEAL TEST

Cycle No.	At start of cycle He, psig	At start of cycle Temp, °F	Max. instantaneous leak rate, cc/yr	Comments
1 - 12	1030	815	0	
13	1030	820	220	Leak from leak detector connection No. 2.
14	1035	820	70	Leak from connection No. 2. Hint of leak from connection No. 1.
15	1025	820	> 8350	Leak from connection No. 2.
16	1020	800	170	do
17	1030	820	> 8350	Leak from both connections. 100 cc/yr leak from connection No. 1 after connection No. 2 leak disappeared.
18	1030	820	> 8350	Connection No. 1 valved off for entire cycle. Leak from connection No. 1 at start and end of cycle.
19	1035	835	50	do
20	1030	825	> 8350	do

During each cycle that leakage occured, the leak appeared shortly after the start of the cooling cycle. In each case the leak rate fluctuated, increasing and decreasing, before reaching a maximum. After maximum leak rate was reached, the helium signal then slowly dropped until it disappeared entirely except for the leak signal at connection No. 1 for cycles 17, 18, 19 and 20. The readings approximately 60 hr after completion of cycle 20 were:

He, psig	Temp. °F	Connection No. 2	Connection No. 1	Total
1020	810	6 cc/yr	14 cc/yr	20 cc/yr

The pressure in the vacuum system was maintained at 0.05 μ absolute or less throughout the entire 20 cycles.

The design and construction of the feedwater manifold seal were based on these test results. Reactor operational procedure was restricted so that a Δt of 100°F between feedwater inlet temperature and feedwater manifold temperature would not be exceeded, thereby assuring operating conditions for the seal far less severe than those imposed on the test mockup.

3.3 Steam Generator

A once-through heat exchanger or steam generator was located inside the reactor vessel submerged in the fuel solution. Crossflow of the fuel solution past the heat exchanger coils was produced by natural convection in the reactor vessel. The steam generator produced superheated steam from ~ 400°F inlet water.

3.3.1 Design Criteria

The design of the steam generator heat exchanger was based on a preselected outlet steam condition of 600°F and 600 psi. (Another fixed parameter was the size of gold clad tubing available. Drawing techniques limited the inside diameter and outside diameter, leaving the length as the only variable.) A fuel velocity of 0.5 ft/sec over the outside of the tubes, a reasonable value that might be achieved with natural convection flow, was used in the design calculations. Only the surface area of the spiral portion of the coils was considered as heat transfer surface. An average over-all heat transfer coefficient of $\frac{310 \text{ Btu}}{\text{hr ft}^2\ °\text{F}}$ was calculated and was used in establishing the heat transfer area (43 ft^2) necessary for extracting 800 kw of heat from the reactor. The as-constructed surface area in the spiral portion of the heat exchanger was 41.2 ft^2. The pressure drop for the steam side of the heat exchanger was calculated to be ~ 105 psi at 800 kw.

Complete data for a typical run are shown in the Appendix which indicate the satisfactory performance of the steam generator. The data are not sufficient to completely analyze the heat transfer characteristics of the heat exchanger, but by making several simplifying assumptions the over-all heat transfer coefficient for the top heat exchanger coil was estimated to be $\frac{\sim 450 \text{ Btu}}{\text{hr ft}^2\ °\text{F}}$, slightly larger than the average calculated coefficient of $\frac{310 \text{ Btu}}{\text{hr ft}^2\ °\text{F}}$.

3.3.2 Construction

The steam generator was fabricated from Type 347 stainless steel seamless tubes 25 ft long, with a 0.188 in. o.d. x 0.031 in. wall. To protect the stainless steel tubing from corrosion by the fuel solution, the tubes were externally clad with 0.006 in. thick gold (99.97% minimum purity). In order to obtain satisfactory gold cladding, careful inspection and a high degree of cleanliness were required during all steps of fabrication. Seamless gold tubes 0.260 in. o.d. x 0.010 in. wall x 12 ft long were obtained by a series of cupping and drawing operations starting with 3/16 in. sheet. All dyes used in the drawing operation were carefully cleaned before and after each draw. The gold was also cleaned, degreased, pickled, and inspected by dye penetrant after each drawing operation. In the final operation the 12 ft long seamless gold shell was threaded over the stainless tube and was passed through the final drawing die. During this last drawing operation the gold was elongated, decreased in wall thickness, and drawn tightly over the stainless steel tube, which acted only as a mandrel. The final diameter of the clad tube was 0.201 in.

The steam generator contained 44 spirally wound tubes. The spiral portion of each heat exchanger tube was wound on a pitch of 0.492 in., and the tube length in the spiral varied from 18 ft in the top coil to 20.5 ft in the bottom coil. The average length of tubing, per coil, including the straight inlet and outlet end portions, was 22.7 ft. The tubes were assembled as shown in Figs. 3.16, 3.17, and 3.18 on a vertical pitch of 0.3 in. Graphite spacers, used in the assembly to prevent gold-to-gold contact, were machined from Graph-i-tite "G" and from graphite extrusions. The assembly was bound together with gold alloy bands (92.5% Au, 7.5% Pt) 0.188 in. x 0.020 in. The tube ends were sealed into the feedwater and steam tube sheets with a compression type fitting using a gold swage ring to effect the seal between the tube sheet cladding and clad tube end. These connections have been fully described in LA-2292.[5]

3.3.3 Testing

Quality control procedures for the clad tubing used in the fabrication of the steam generator included the following tests:

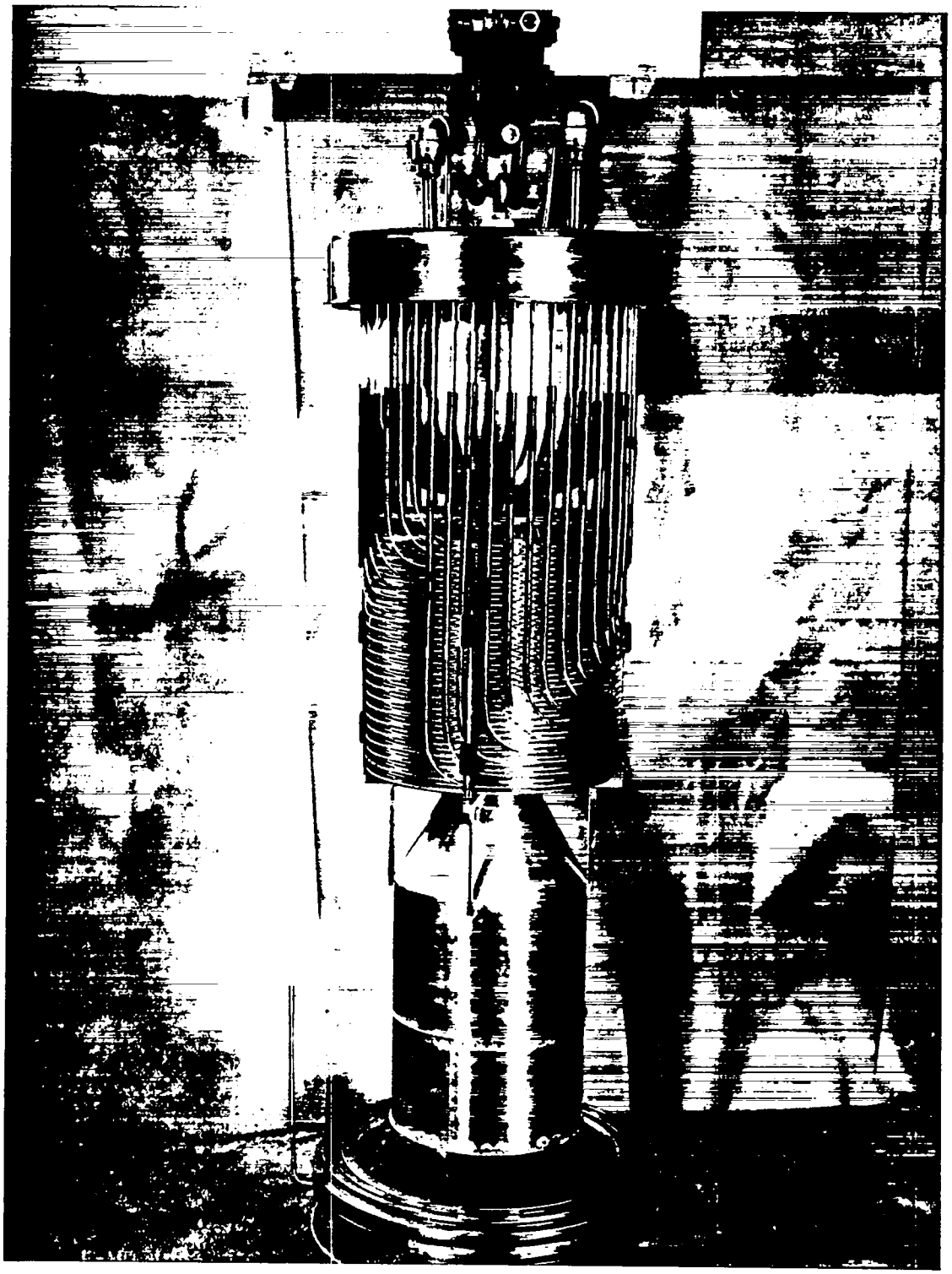

Fig. 3.16 Reactor Vessel Lid with Heat Exchanger and Flow Baffle Attached

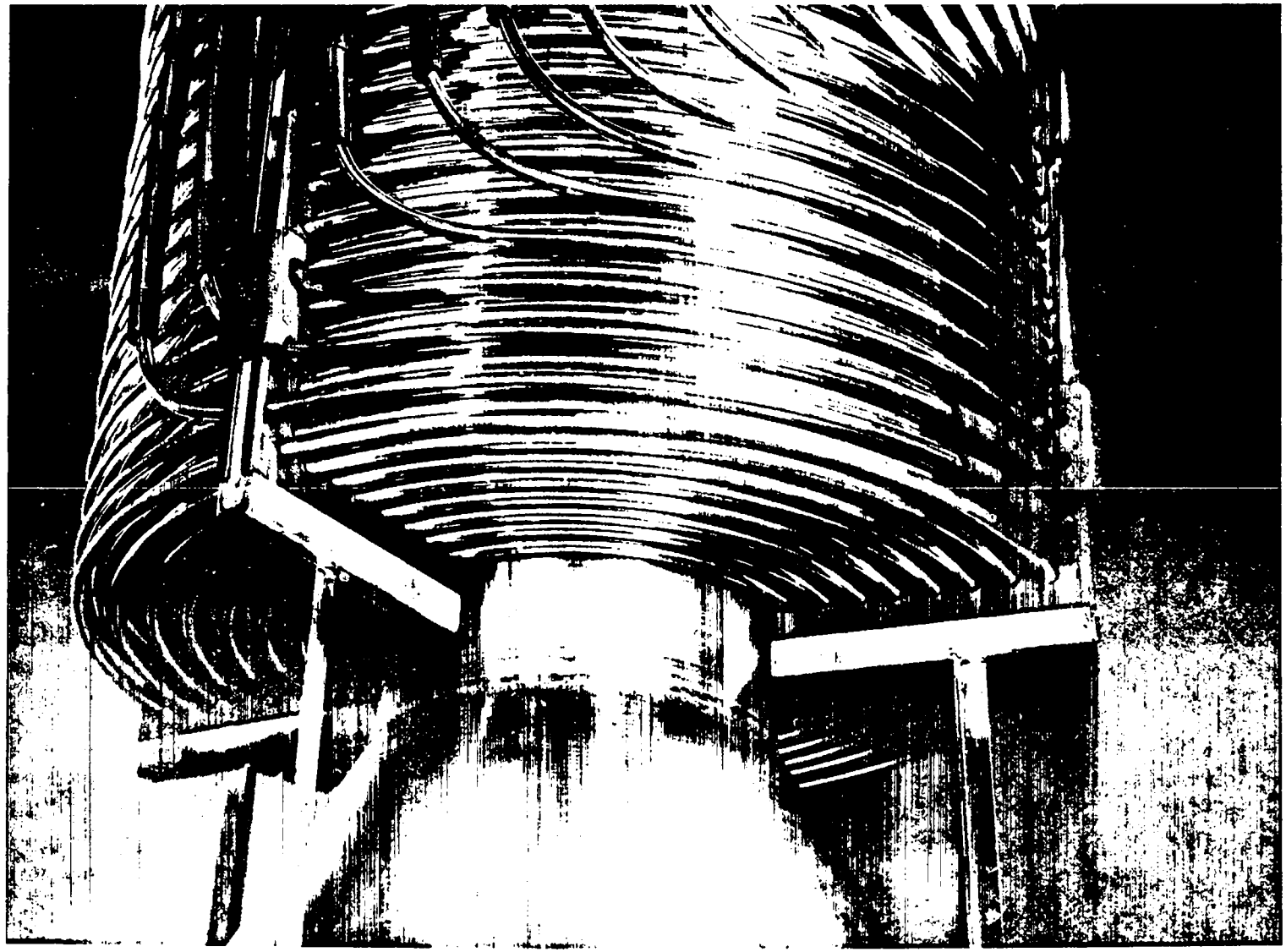

Fig. 3.17 Bottom View of Heat Exchanger Showing Graphite Spacers and Flow Baffle Supports

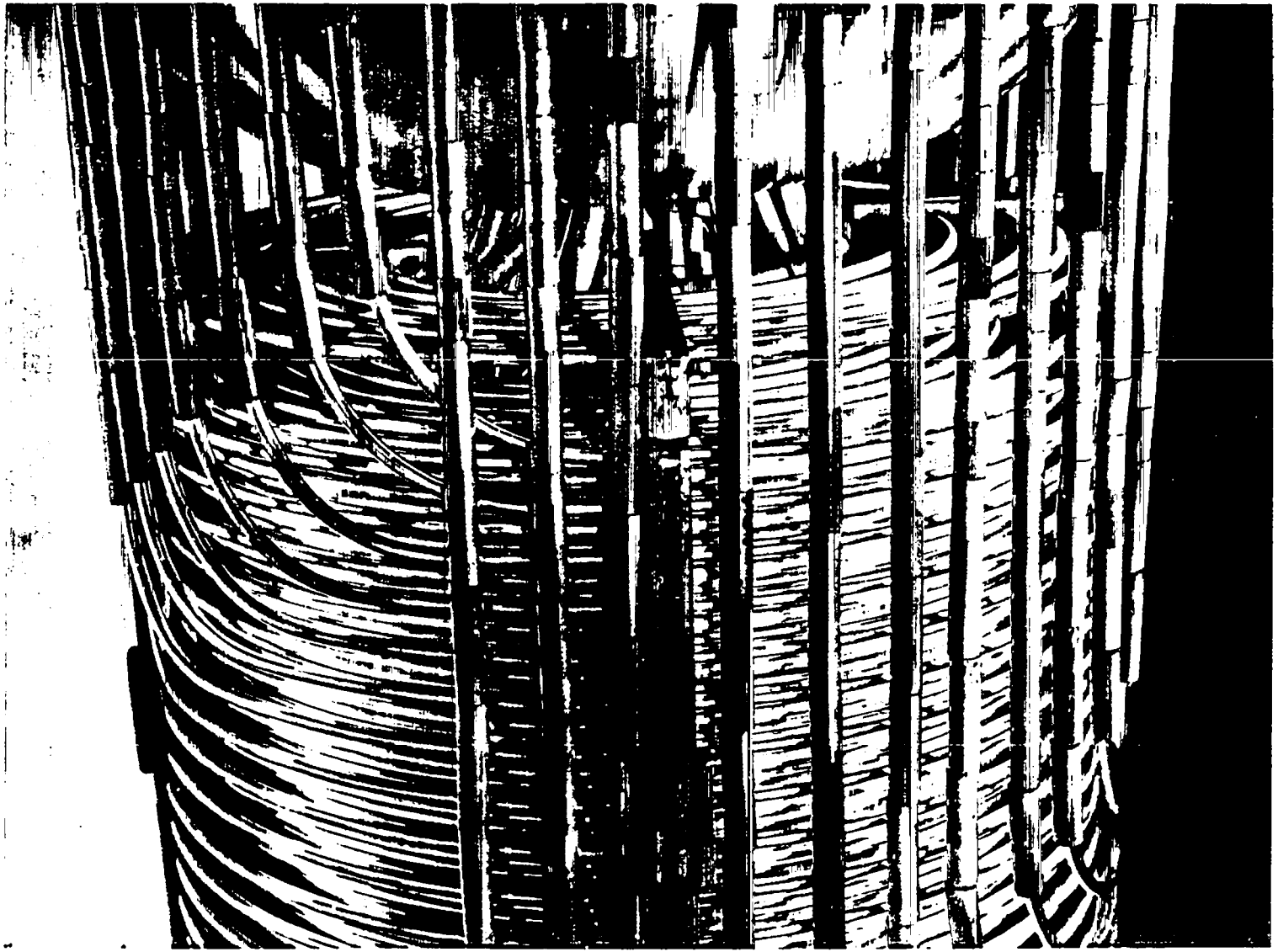

Fig. 3.18 Top View of Heat Exchanger

a. Hydraulic Test. The stainless steel tubing was tested by applying an internal pressure of 10,000 psi (giving a stress ~ 0.8 of yield point). The hydraulic test indicated that the stainless tubing had acceptable mechanical properties and that cladding of the tubing could proceed.

b. Helium Pressure Test. After it was formed into spirals, the gold clad tubing was exposed to an external helium pressure of 1800 psi. During this exposure the interface between the gold cladding and stainless steel was monitored for helium. Although it was determined that a defect in the gold cladding could be detected in ~ 2 hr even when the helium had to travel the full length of a tube, each tube was tested for 20 hr. Forty-four tubes were tested and no discontinuities were found in the cladding.

c. Acid Test. Following the helium test the ends of the tubes were sealed off by driving a taper pin into the tube end and then inert-arc welding the pin into place. After welding the end was dressed, a gold cap was placed over the tube end and soldered with pure silver to the tube cladding. A graphite cap was then placed over the tube end. The 44 tubes were then stacked in a silver clad autoclave, graphite spacers separating the tubes, and were immersed in 85% phosphoric acid. The tubes were held at 660°F in the acid for 8 days. Inspection of the tubing upon removal from the autoclave revealed no corrosion. (Mockup tests, under the above conditions, showed complete penetration of the stainless steel tube in 48 hr through a < 0.005 in. flaw in the gold cladding.)

3.4 Fuel Line

The fuel line connecting the fuel reservoir tank and the reactor vessel was made in two pieces to facilitate its installation. This line was a gold-lined stainless steel tube; the stainless steel outer tube was 5/8 in. o.d. x 0.120 in. wall, and the internal gold cladding was 0.010 in. thick. Before the flanges were installed on the tubes, the gold liner was pickled twice with 6 M HCl at 150°F. After the second pickling operation, no dissolved solids were found in the HCl. It was assumed that this procedure (1) removed any iron inclusions, and (2) indicated by the absence of dissolved iron that no holes existed in the gold liner.

Following the HCl treatment, the end flanges were installed. The connection to the reactor vessel was a conical, compression type tightened with a flange to the bottom of the vessel. The other connections were modified Van Stone type flanges. Details of these connections are shown in Fig. 3.19. The gold cladding on the flange faces was 0.015 in. thick and was welded to the internal cladding by the inert gas arc welding process, using a mechanized, automatic welding device. After installation of the flanges, the lines were further tested by exposure to 95% H_3PO_4 at a temperature of 700°F for 450 hr. After this test the tubes were bent to shape. The portion of the line between the fuel reservoir tank and the safety enclosure vessel was subsequently fitted with a cooling water jacket which was connected in parallel with the cooling water jacket on the fuel reservoir tank.

The fuel transfer line connecting the fuel reservoir tank to the fuel storage system was a stainless steel-copper duplex tube. This tube was 5/8 in. o.d. x 0.120 in. wall stainless, 12 ft long, internally clad with 0.100 in. of copper. Flange construction was similar to that described above for the gold clad fuel line. This tube was helium leak tested by evacuating the space between the copper and the stainless steel while pressurizing the inside of the copper tube to 300 psi with helium. Because of the thickness of the copper, acid testing was not considered to be necessary.

3.5 Safety Enclosure

The safety enclosure contained the reactor vessel, the shim and reflector assembly, and the concrete shielding above the reactor vessel. In addition, it provided containment following a vessel rupture, a leak in fuel line, feedwater line, or steam line. The safety enclosure was installed in an excavation which was then backfilled (Fig. 1.3).

Dimensions of the safety enclosure were: 42 in. i.d., 20 ft inside length, and wall thickness 5/16 in. The bottom end plate was 3 in. thick. It was built of mild steel, with the bottom half internally clad with 1/16 in. of copper.

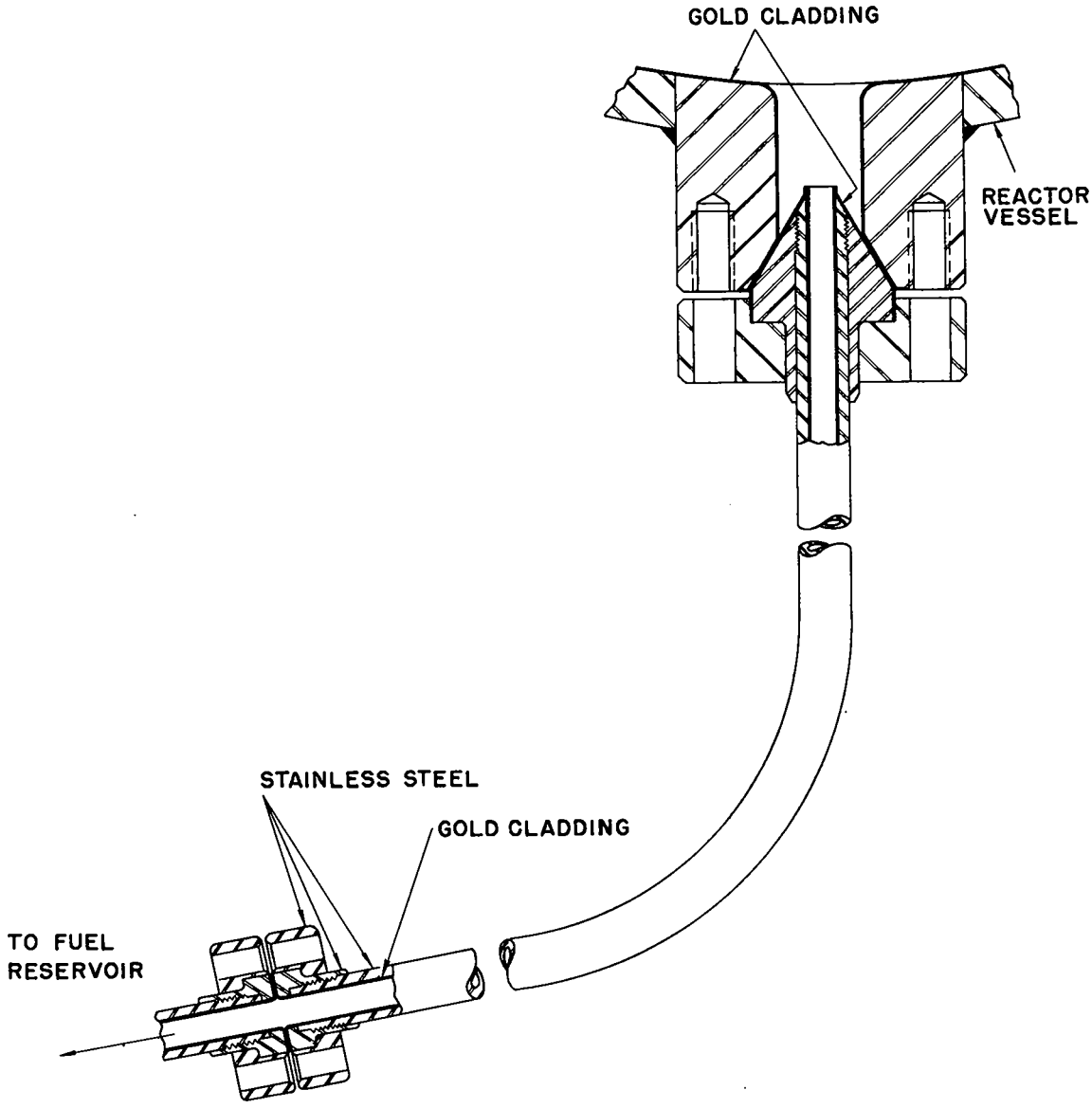

Fig. 3.19 Details of Reactor Fuel Line Connections

The internal copper cladding of the safety enclosure extended through the flange to the sealing face. Details of the access port, mating flange, and associated seals are shown in Fig. 3.20.

Centered 8 ft above the bottom on the east side of the safety enclosure was an 8 in. flanged port which provided access for the feedwater and steam lines, the thermocouple extension lines, the leak detector lines, and a pressure relief valve. The internal copper cladding extended through this port to the sealing face. The thermocouple leads were taken out through the cover plate for the port in 1/4 in. stainless steel tubing. These, and the leak detector lines which were of similar tubing, were sealed to the cover plate by drilled-through Ermeto fittings. The safety valve, water, and steam lines penetrated the cover plate and were seal welded to the plate. Details of the cover plate are shown in Fig. 3.21.

The concrete shielding was divided into two sections or plugs, each 54 in. thick. The lower shield plug was 41 in. o.d., and rested on a support rim 10 ft above the bottom of the vessel. The upper shield plug was an integral part of the top closure flange. The steel closure flange was 3-1/2 in. thick and 50-3/4 in. o.d. to fit the standard 40 in., 125 psi slip-on welding flange which was used at the top of the safety enclosure.

The shield plugs were constructed as steel cans from 1/8 in. steel plate with reinforcing rods on the inside. These cans were filled with concrete after delivery at the reactor site. A hole was provided through the center of each plug for the shim control rod. A chevron packing gland was provided at the top of the upper, or closure, plug to seal the enclosure where the shim control rod entered. The 40 in. flange was sealed to the enclosure flange with a silicone-rubber gasket.

An access port for a neutron source tube was provided on the east side of the enclosure, entering the enclosure 8 ft-6-1/2 in. from the bottom. This tube was constructed of stainless steel and extended from near the top of the safety enclosure on the outside to a position in the graphite reflector on the inside. It entered the enclosure at an angle of 15° from the vertical, so that the neutron source could be lowered into position by gravity. The source was suspended by a small cable fastened to the flange which closed the source tube. Details of this tube are shown in Fig. 3.22.

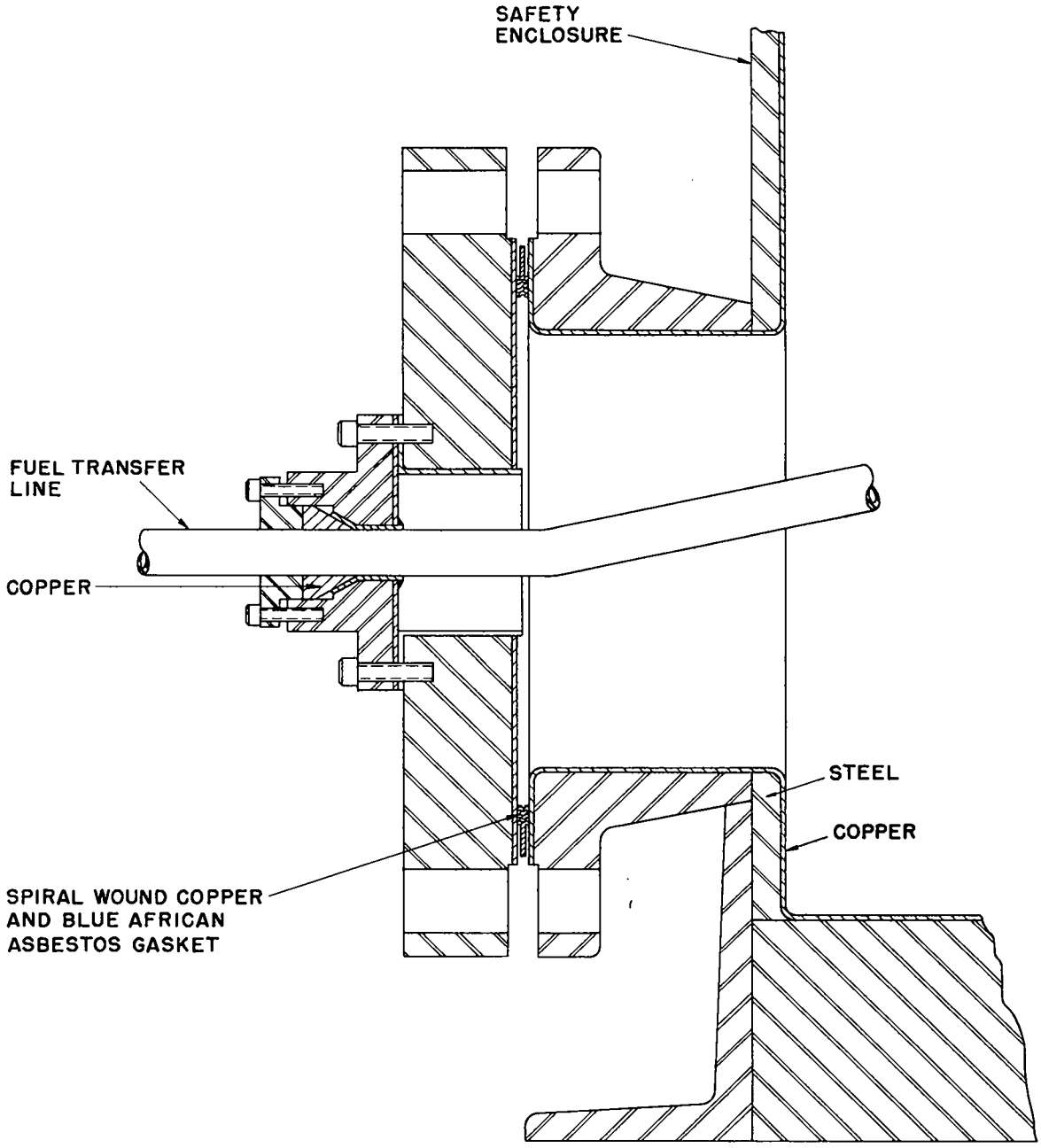

Fig. 3.20 Fuel Line Port in Safety Enclosure

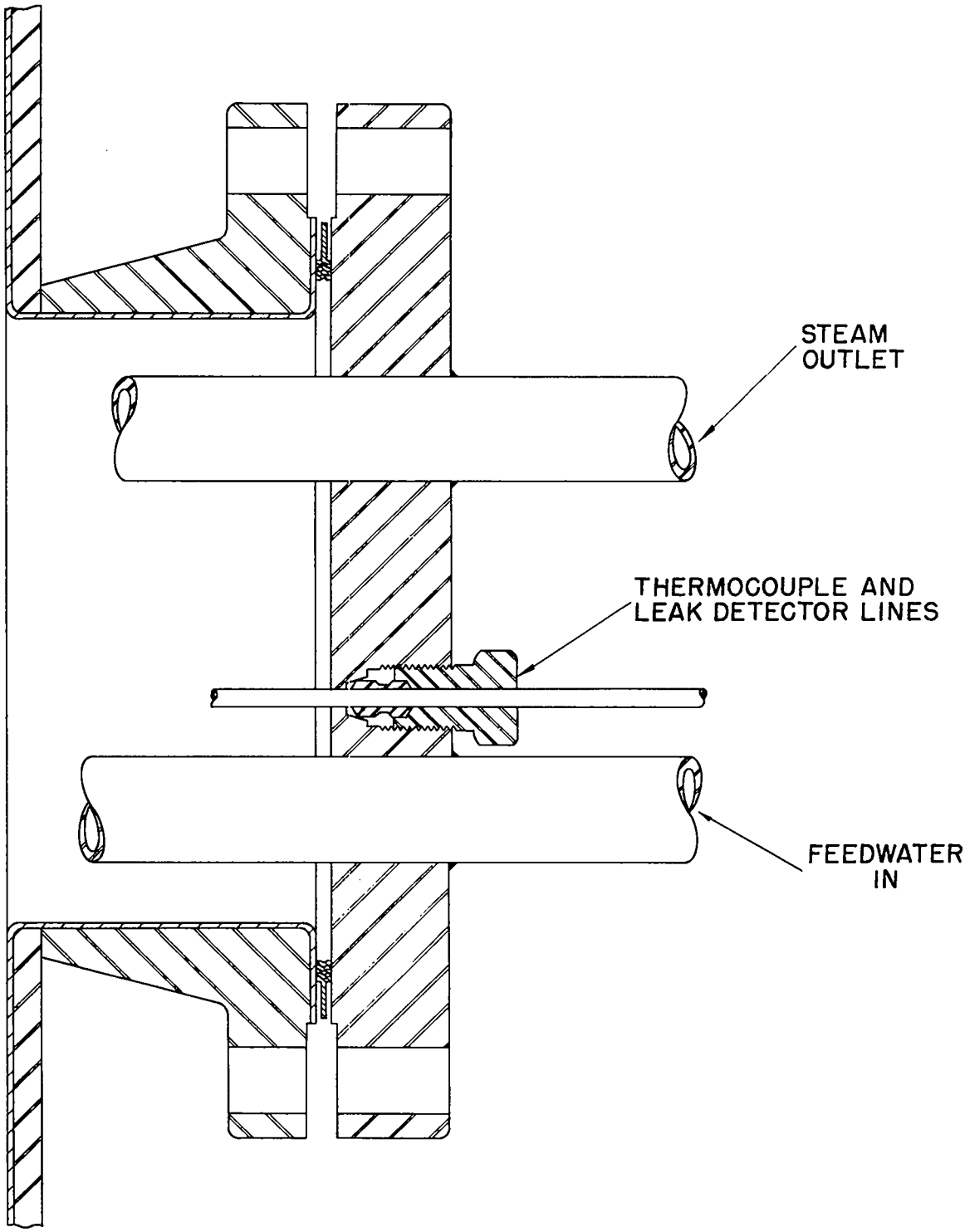

Fig. 3.21 Details of Steam and Feedwater Port in Safety Enclosure

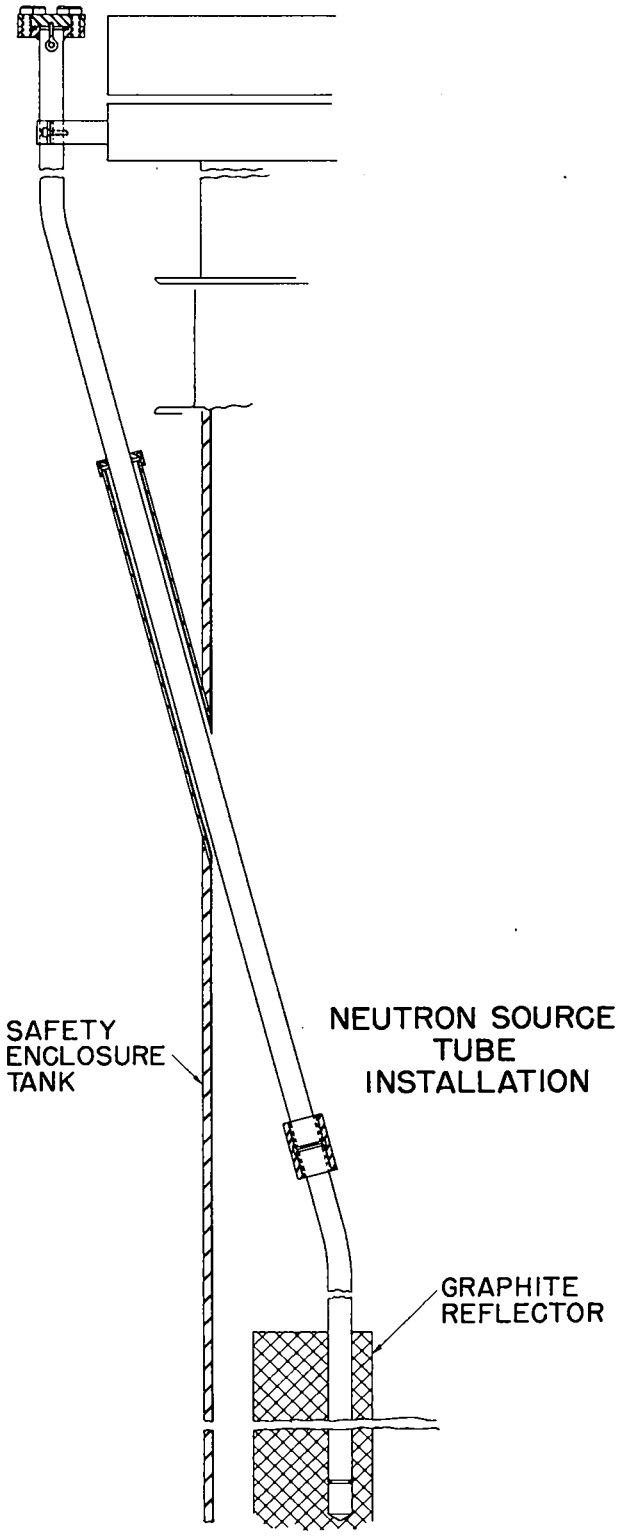

Fig. 3.22 Neutron Source Tube

During operation of the reactor, the enclosure was filled with nitrogen to protect the enclosed components from oxidation.

The enclosure was provided with a pressure relief valve which was set to relieve the internal pressure at 250 psi. This valve discharged into the reactor vent system.

In event of a reactor vessel failure, it was anticipated that the copper cladding in the lower section would contain the fuel solution, at least until the phosphoric acid could be neutralized by the iron in the reactor and reflector mounting assembly.

3.6 Reflector

An external annular reflector was provided in LAPRE II to increase the neutron economy of the system and to provide a means of temperature regulation. The outer section of the reflector was fabricated from graphite (CBB grade, $\rho = 1.64$ g/cc) and was mounted on a fixed support in the reactor pedestal assembly. This stationary section of the reflector was 38-1/2 in. o.d. x 28-1/4 in. i.d. x 48 in. long and was positioned concentrically with respect to the reactor vessel.

The bottom reflector was mounted in the reactor pedestal immediately below the reactor vessel. This fixed reflector was machined from graphite (CS 3-12 grade, $\rho = 1.75$ g/cc) and was 14-3/8 in. o.d. x 1 in. i.d. x 15-1/2 in. long. Six compartments, arranged symmetrically 3 in. from the top of the reflector, contained BeO (3 x 3 x 1-5/16 in.) blocks which were to serve as a neutron source for startups subsequent to the initial one. The central 4 in. sleeve was split to allow assembly of the fuel line to the reactor.

A movable portion of the reflector or shim mounted inside the outer reflector was built with an outer graphite (ATL grade, $\rho = 1.67$ g/cc) section with BeO ($\rho = 2.7$ g/cc) blocks being stacked on the inside to make an annular section 28 in. o.d. x 16-3/8 in. i.d. x 23 in. long, with the inner 3 in. containing the BeO (Fig 3.23). The shim was supported on a steel base suspended from 4-3/8 in. steel rods connected to an X-frame which was supported from

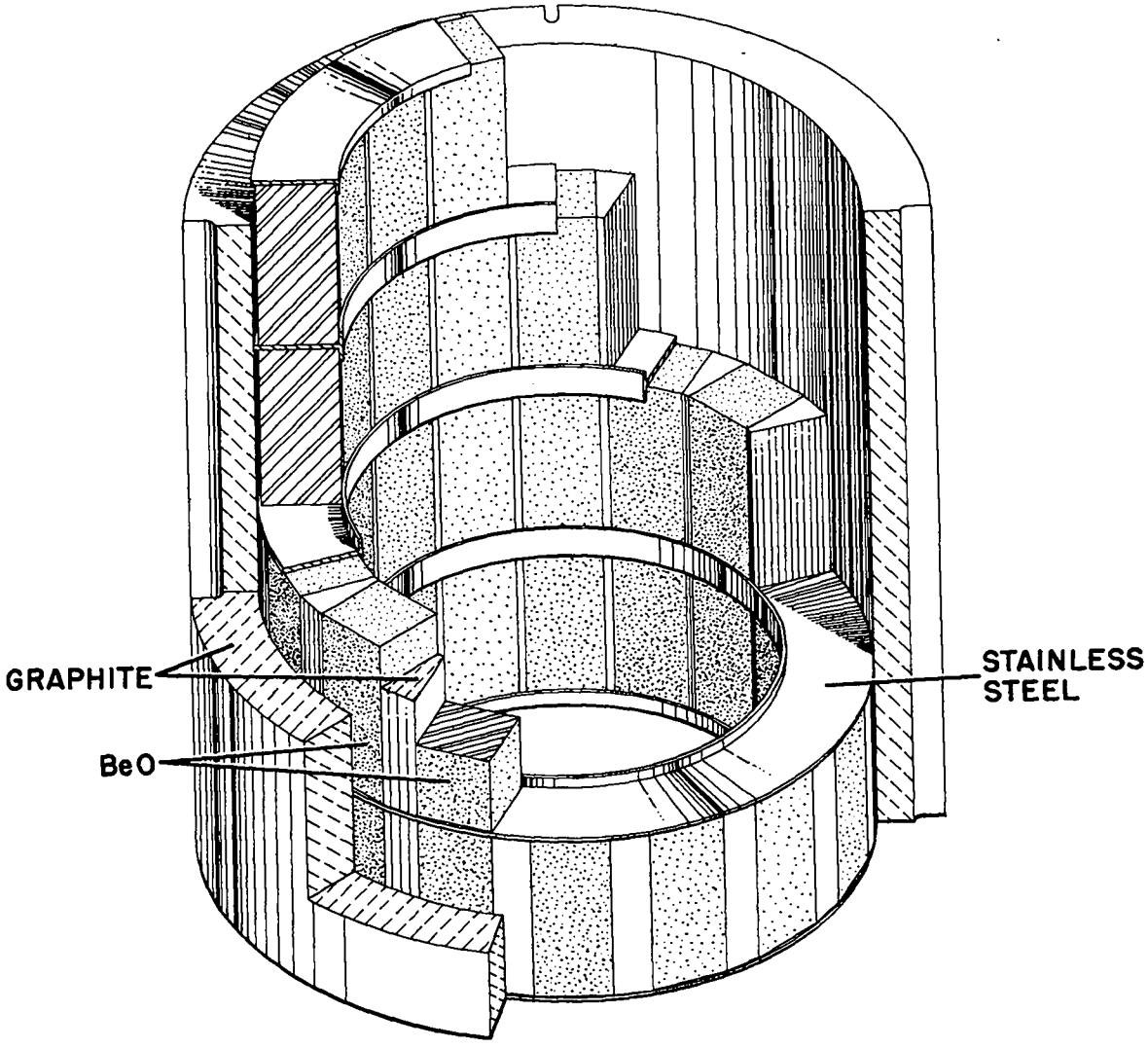

Fig. 3.23 Movable Reflector or Shim

the shim drive rod. The shim drive rod was constructed in two sections, the lower 5-1/2 ft being 1-1/8 in. diam and connecting to the upper stainless steel section 3/4 in. diam and 7-3/4 ft long.

The shim drive mechanism consisted of a three-phase reversible motor driving a 1 in. Acme thread nut. The rotating nut lifted a keyed lead screw which was connected to the shim drive rod. A Selsyn transmitter was geared to the motor drive and actuated a Selsyn receiver with mechanical counter on the control panel. The counter indicated shim position in hundredths of an inch. Shim travel was about 23 in. The gear train on the drive motor limited the shim insertion and withdrawal rate to 1.44 in./min.

Chapter 4

FUEL AND GAS SYSTEM

4.1 Fuel System

The fuel system provided for the storage, transfer into and out of the reactor system, and sampling of the fuel. The reactor fuel system included the fuel reservoir tank, reactor vessel, and the fuel line which connected the reservoir tank to the reactor vessel. Connected to the reactor system was the storage and transfer system and the sampling station. A diagram of the fuel system is shown in Fig. 4.1. All components in the fuel system, except the fuel reservoir tank and two fuel lines, were 18/8 stainless steel. Valves and fittings, except where otherwise described, were Ermeto type, 10,000 psi rating.

The storage and transfer system consisted of two storage tanks, the metering tank, and the associated transfer system. These components were originally installed for use in the LAPRE I fuel system,[5] and except for some simplification in the plumbing, remained essentially unchanged. This system provided a place for fuel storage and for metering the fuel to and from the reservoir tank with an accuracy of 0.01 liter. Transfer of fuel was accomplished by the use of gas (H_2) pressure.

The sampling station had as its primary function the removal of fuel samples from the reactor. Since this required access to a fuel line from the reservoir tank, the fuel transfer line from the metering tank to the reservoir tank was routed through the sampling station, and two of the valves in the

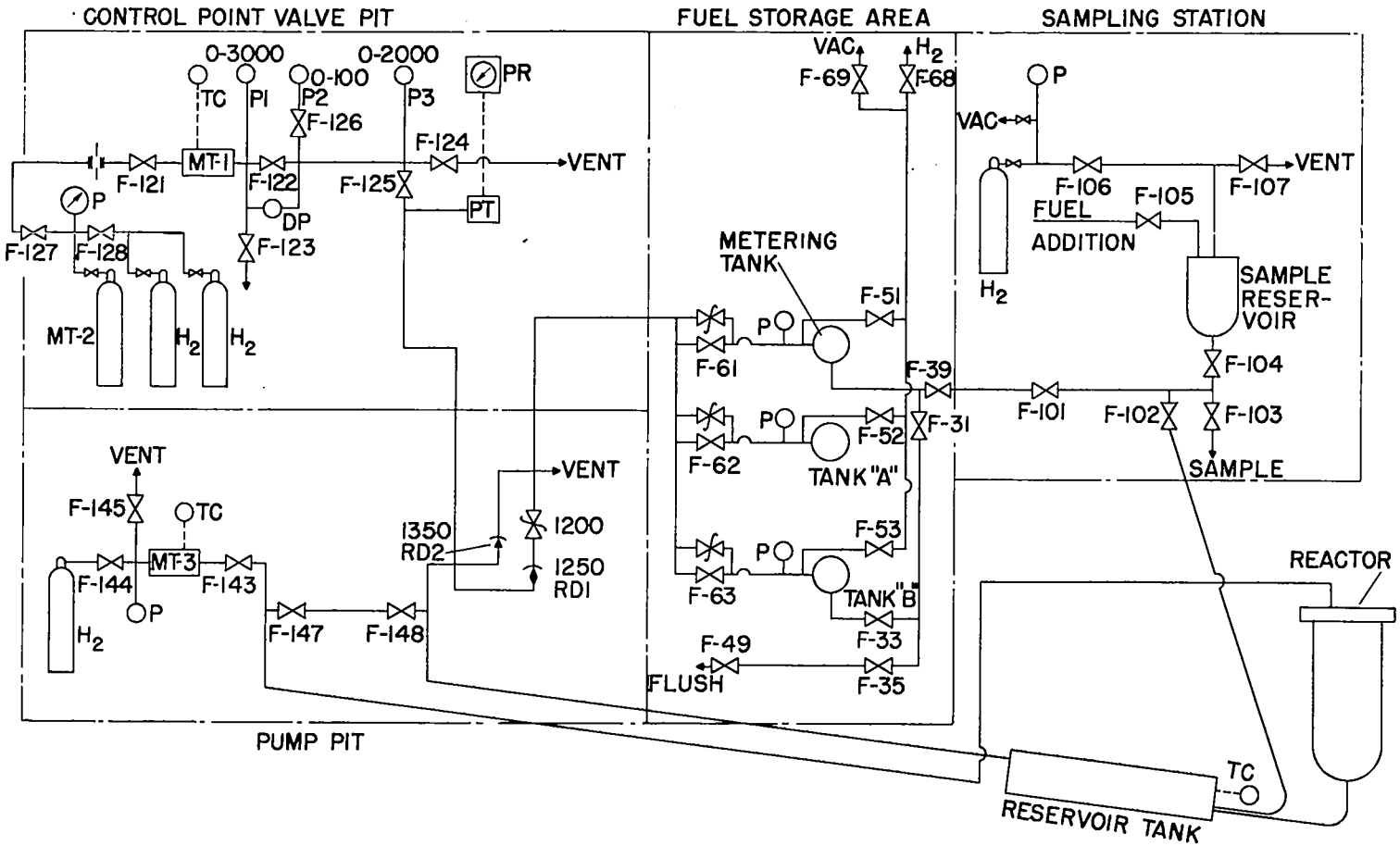

Fig. 4.1 Schematic Diagram of Fuel and Gas System

transfer line were at this location. The central component in the sampling system was the sample reservoir, a stainless steel (Type 347) vessel of about 4 liters capacity which had connections to the fuel system, hydrogen bottle, vacuum system, vent system, pressure gauge, sample discharge line, and a line for the addition of small quantities of fuel or phosphoric acid directly to the sample reservoir. The sample reservoir and the valves were mounted on a concrete pad and were shielded by lead bricks. The sample was discharged into a small (5 cc) conical bottle which was carried in a portable, lead-shielded cart. A mirror was mounted on the cart so that the discharge line and the bottle could be viewed from the valve operating position through a telescope.

Fuel samples were withdrawn from the fuel reservoir by forcing fuel into the sample reservoir until it was about half full, as determined by the pressure increase. Five to 10 cc samples were then discharged into the sample bottles through the delivery tube, a first sample being considered a rinse sample and a second used for chemical analysis.

Materials added to the fuel reservoir tank through the sampling system were drawn into the sample reservoir by vacuum and discharged into the fuel reservoir tank by pressurizing the sample reservoir with hydrogen.

The fuel reservoir tank had an inside diameter of 7.00 in. and an inside length of 180 in., giving it a capacity of about 113.5 liters. It was mounted (Fig. 1.3) on a slope of 0.124 with the lower end toward the reactor. Two connections were made to the lower end of the tank, entering the end flange 1.5 in. above the bottom (Fig. 4.2). One of these connections led to the reactor, and the other to the fuel transfer and storage system. Entering the upper end flange, 1 in. below the top, was a connection to the gas system.

The fuel reservoir tank was fabricated from a low alloy steel tube with a 1/8 in. thick copper liner. Copper was selected for a liner material since it was considered to have adequate corrosion resistance at temperatures up to 100°C and the fuel reservoir tank was kept below that temperature by its external cooling jacket. However, a gold sleeve was inserted in the lower end of the tank, where hot fuel might impinge on the liner as it entered from the reactor vessel. This sleeve was 0.010 in. thick and 1 ft long. It was flared on the lower end to

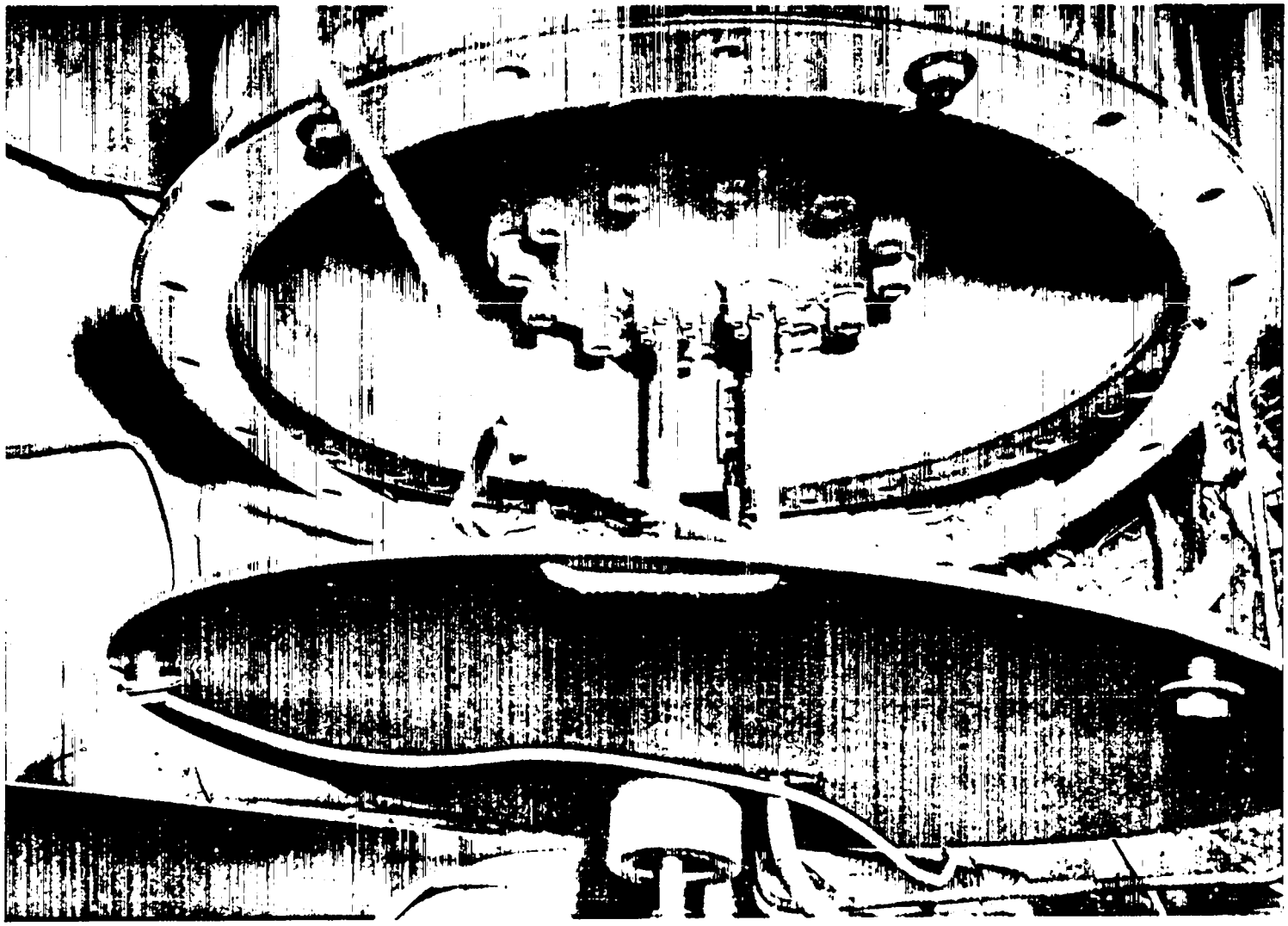

Fig. 4.2 Fuel Line Connections to Fuel Reservoir Tank

cover the sealing face of the flange. The steel tube was of low alloy steel, 8 in. o.d. x 0.375 in. wall x 15.0 ft long with 400 lb slip on flanges welded on the ends. The liner was made of a seamless deoxidized copper tube 7-3/16 in. o.d. x 1/8 in. wall. Before inserting the copper tube into the steel tube it was helium leak tested by evacuating it and flooding the outside of the tube with helium in a plastic envelope. The copper tube was inserted into the steel tube and the ends spun out over the sealing face of the flange. The ends were covered with special blind flanges having O-ring seals and the copper liner was hydraulically expanded to fit the steel tube, using a pressure of 3000 psi. After expansion the liner was again helium leak tested by evacuating the space between the copper and steel through weep holes drilled through the end flanges and the wall of the steel tube at its center. For this second helium leak test the inside of the tube was pressurized with helium to 300 psi. After the test, the weep holes were closed with threaded steel plugs of proper length to fill the hole and support the copper liner.

A stainless steel outer shell was placed around the outside of the steel tube to provide a cooling water jacket. The 9 in. inside diameter of the water jacket allowed a 1/2 in. fluid annulus. Connections to the cooling jacket were 2 in. copper tubing; an expansion bellows was incorporated into the cooling jacket to allow for differential expansion. The 2 in. cooling lines connected to the water circulating pump and the air radiator. The operation of the circulating pump and the air radiator was controlled by a thermocouple mounted in the center of the outside surface of the lower end flange.

The end flanges of the fuel reservoir were 400 psi raised face flanges having the inside face clad with 1/8 in. of deoxidized copper, silver-soldered in place. Over the copper cladding of the lower flange was an additional cladding of 0.010 in. of gold. The copper cladding was extended through the upper flange to the gas connections, and both copper and gold cladding were extended through the lower flange to the fuel line connections. Details of these connections are shown in Fig. 4.3.

The gaskets for the flanges were profile-clad gaskets having a steel core and copper cladding. Over the copper cladding, the gasket for the lower flange had a 0.010 in. gold cladding. On assembly, the flange bolts were torqued to 500 ft-lb.

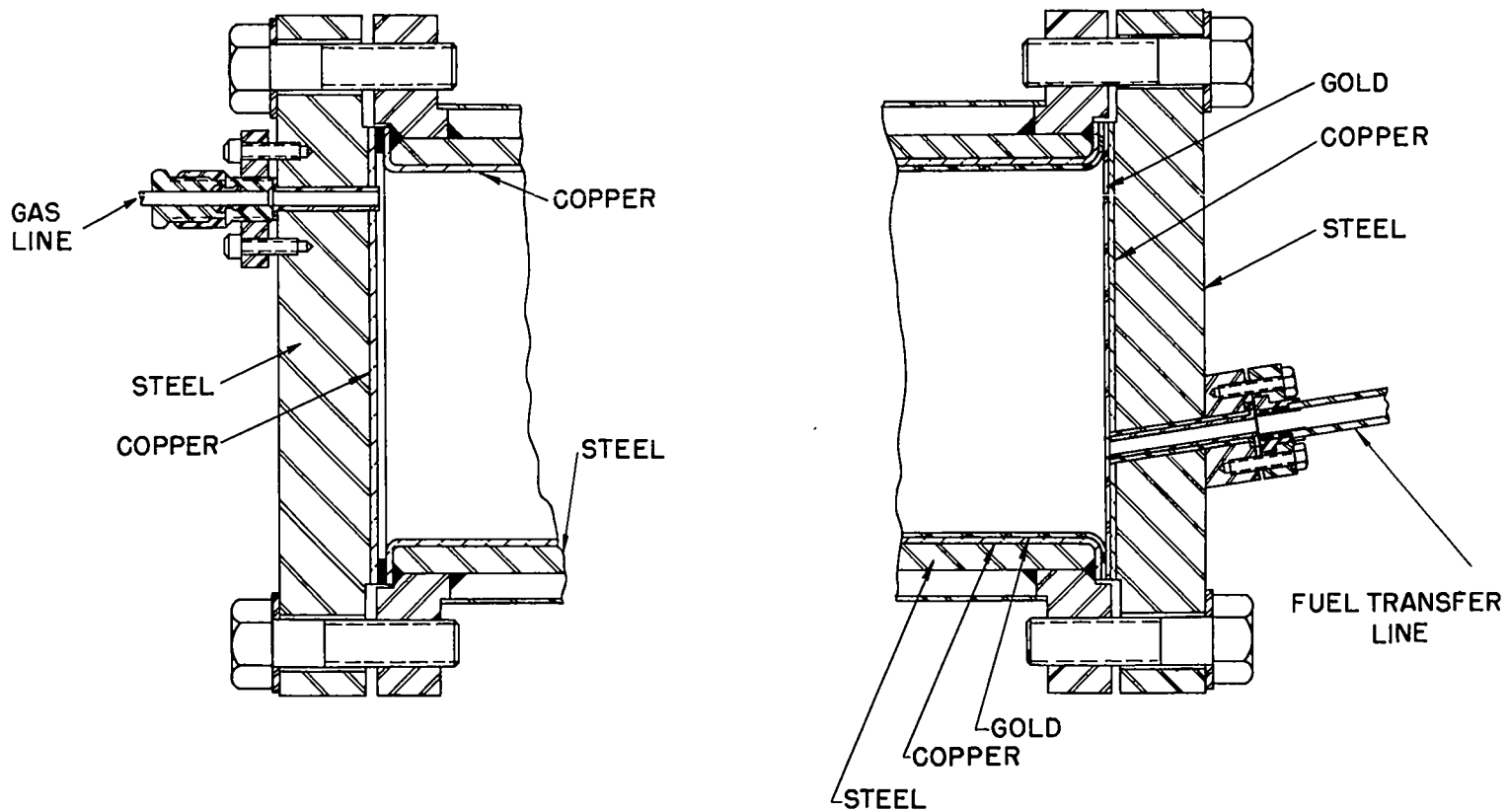

Fig. 4.3 Fuel Reservoir Tank Flange Details

For protection against damage during backfilling, the fuel reservoir tank was housed in a 24 in. o.d. corrugated metal pipe. The reservoir tank was mounted inside the corrugated pipe on a 8 in. x 2 in. steel channel. The cooling water lines entered through the upper end of the corrugated pipe and had bellows expansion joints for protection against differential expansion. The ends of the pipe were closed with 1/4 in. thick flanges. The lower half of this corrugated metal enclosure was lined with copper, and the lower end flange was made of 18/8 stainless steel and was sealed to the copper liner by a gasket of blue African asbestos. From the bottom of the lower end flange, a 1/2 in. copper tube led to a tank in the emergency fuel recovery system.

4.2 Gas System

The gas system provided for the transfer of fuel between the fuel reservoir tank and the reactor vessel. The components in this system, like those in the fuel system, were primarily of 18/8 stainless steel construction with 10,000 psi Ermeto fittings and valves. The principal components of the system were located in the valve pit, adjacent to the control point. The valve handles extended through the wall to the control point, and windows were provided through which the gages were read, using a small, 6-power telescope.

The addition of fuel to the reactor was accomplished by adding gas to the fuel reservoir tank through the control point system. A small metering tube (MT-1, Fig. 4.1) was provided in the valve pit so that measured small increments of gas could be added to the system. For the addition of larger increments, a larger metering tube (MT-2, a D-size H_2 cylinder) was provided. The smaller one was made from a short length of 2 in. pipe. An orifice was placed in the line to control the rate at which gas could be added to the system.

Removal of fuel from the reactor was normally accomplished at the control point by releasing gas from the reservoir tank to the vent system through valve F-124.

Pressure gages mounted in the valve pit indicated metering tube pressure, fuel reservoir tank (reactor) pressure, and differential pressure

between the metering tube and reservoir. The differential pressure gage had a range of 0-20 psi, but was capable of withstanding 2500 psi overpressure in either direction. It was used during startup for the precise measurement of small increments of gas from the metering tubes to the fuel reservoir tank.

The portion of the gas system located at the pump pit (Fig. 4.1) was not intended for use during normal operation of the reactor. The metering tube (MT-3) was provided so that measured increments of gas could be added to the vapor space in the reactor. It was identical in construction to the small metering tube at the control point. The bypass valves (F-147, F-148) were provided so that pressure could be equalized between the reactor vessel and the fuel reservoir tank.

Rupture discs were installed in the gas line in the pump pit to protect the reactor vessel from overpressure. One rupture disc was set to rupture at 1250 psi and was backed up by a 1200 psi safety valve which was intended to stop flow after the overpressure had been reduced. Another rupture disc (1350 psi rating) was placed in parallel with the first, in order to provide additional pressure relief in case the first line lacked sufficient capacity to relieve the overpressure.

The gas line to the fuel reservoir tank was fastened with an Ermeto fitting to the upper end flange as shown in Fig. 4.3. The gas line connection to the reactor vessel was made with a 0.063 in. o.d. x 0.020 in. i.d. platinum capillary connected to the gas port of the derby with a gold swage seal. The capillary was connected to a 1/4 in. o.d. copper-lined stainless steel duplex tube. Outside the safety enclosure, this duplex tube was connected to an ordinary 1/4 in. o.d., 18/8 stainless steel tube. Details of these connections are shown in Fig. 4.4.

No operational difficulties were encountered in the gas system during reactor operation, except that some of the valves developed a slight seat leakage. At that time, valves F-121, -122, -127, and -128 were replaced with O-ring sealed valves manufactured by the Grove Valve and Regulator Company. These valves functioned quite satisfactorily.

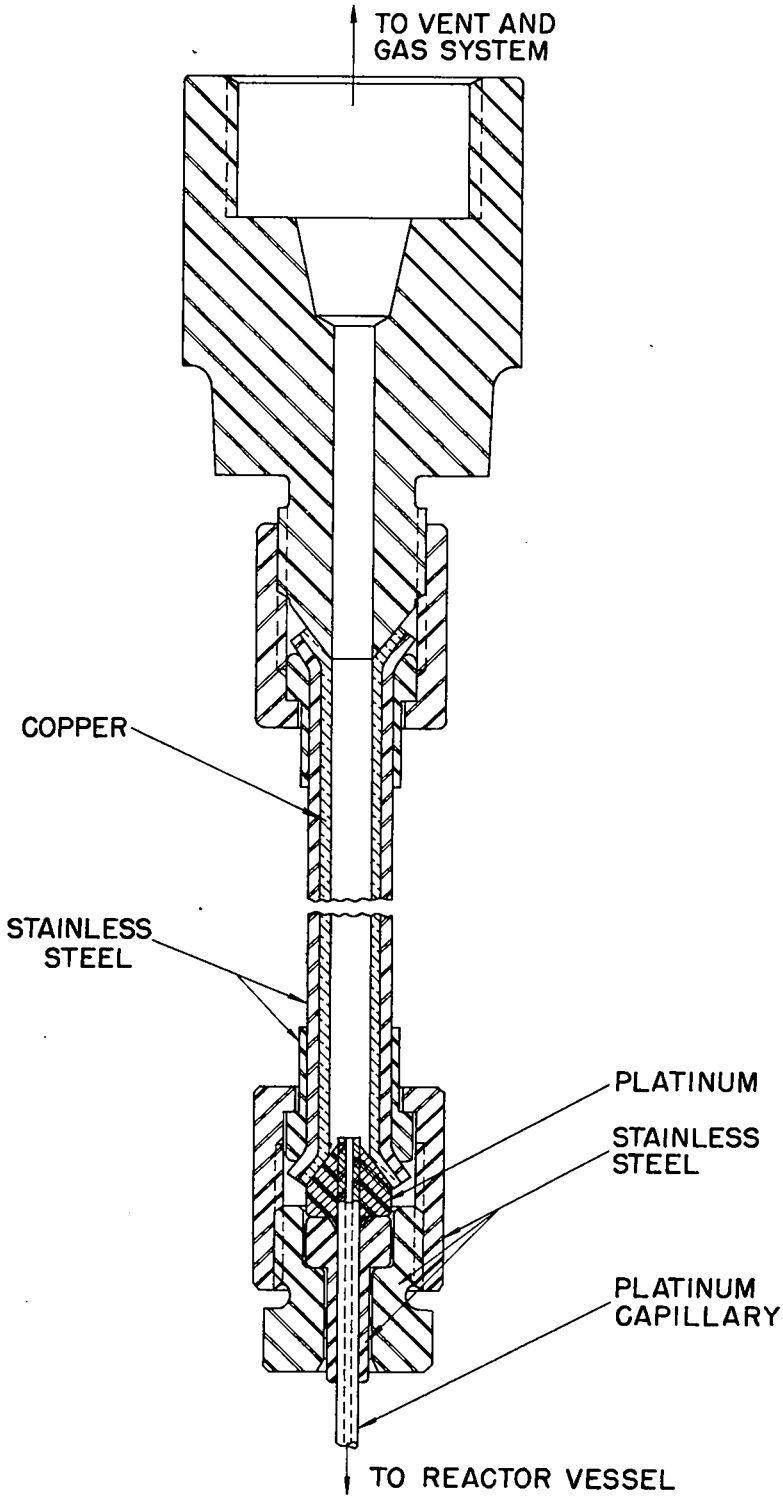

Fig. 4.4 Reactor Vessel Vent Line

4.3 Emergency Fuel Recovery System

The emergency fuel recovery system was installed to facilitate recovery of the fuel in event of a fuel leak in the fuel reservoir tank or in the reactor vessel. For recovery of fuel from the fuel reservoir tank, a copper tank 7-3/16 in. o.d. x 1/8 in. wall x 16 ft long with copper ends was placed parallel to the fuel reservoir tank and 2.5 ft below its corrugated metal enclosure. The delivery line from the fuel reservoir tank enclosure entered the recovery tank through the top at the lower end. A vent line to grade level was connected to the top at the upper end. From the end of the tank on the bottom side a line was connected to the siphon system through which the fuel could be elevated to the surface.

To catch the fuel in event of a reactor vessel leak, the lower half of the safety enclosure tank was lined with copper. A copper siphon tube to the bottom of the tank was brought out through the side of the enclosure tank 10 ft above the bottom.

In event of fuel leakage into either the safety enclosure tank or the tank below the fuel reservoir tank, the fuel was to be elevated to the surface by vacuum. Since the density of the fuel was so high that the fuel could not be lifted to the surface directly, ~ 20 ft, a two-stage lifting system was provided, as shown in Fig. 4.5. Intermediate stainless steel tanks were placed about halfway to the surface with lines connected in such a fashion as to allow lifting the fuel into the intermediate tank in one step, and from the intermediate tank to the surface in the next step.

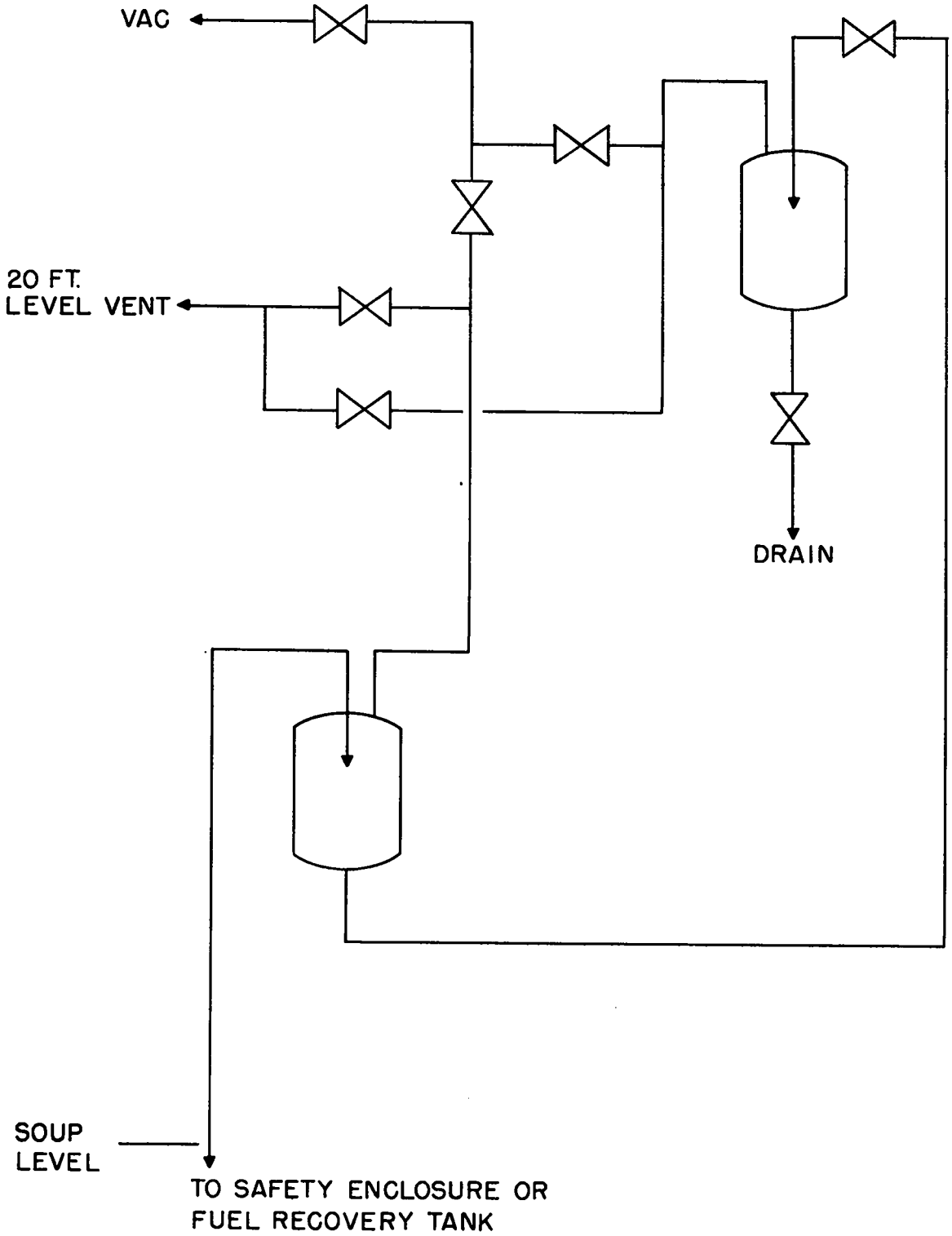

Fig. 4.5 Schematic Diagram of Emergency Fuel Recovery System

Chapter 5

HEAT REMOVAL SYSTEM

A schematic diagram of the 1 Mw heat removal system is shown in Fig. 5.1. The system is divided into two piping loops composed of (1) a closed primary loop for circulating feedwater to the reactor and removing steam from the reactor heat exchanger and (2) a secondary loop arranged to condense the reactor-produced steam and to dissipate the heat to atmosphere through a forced draft air radiator. Operating features of the heat removal system are described below.

5.1 Primary Loop

Superheated steam from the reactor heat exchanger outlet was desuperheated and condensed in the tubes of a shell and tube heat exchanger. Condensate from the steam desuperheater-condenser was then passed through the tubes of a shell and tube drain cooler designed to reduce condensate temperature to a maximum of 250°F as required for satisfactory operation of the reactor feedwater pumps. The shell side coolant in both desuperheater-condenser and the drain cooler was an ethylene glycol solution circulated in the secondary loop. Condensate from the drain cooler was then pumped back to the reactor heat exchanger inlet using canned-motor centrifugal pumps. Two double-stage feed pumps piped in series were required to overcome the piping, feedwater heater, and reactor heat exchanger pressure losses. Also, a second set of feed pumps were arranged in parallel for use as standby service.

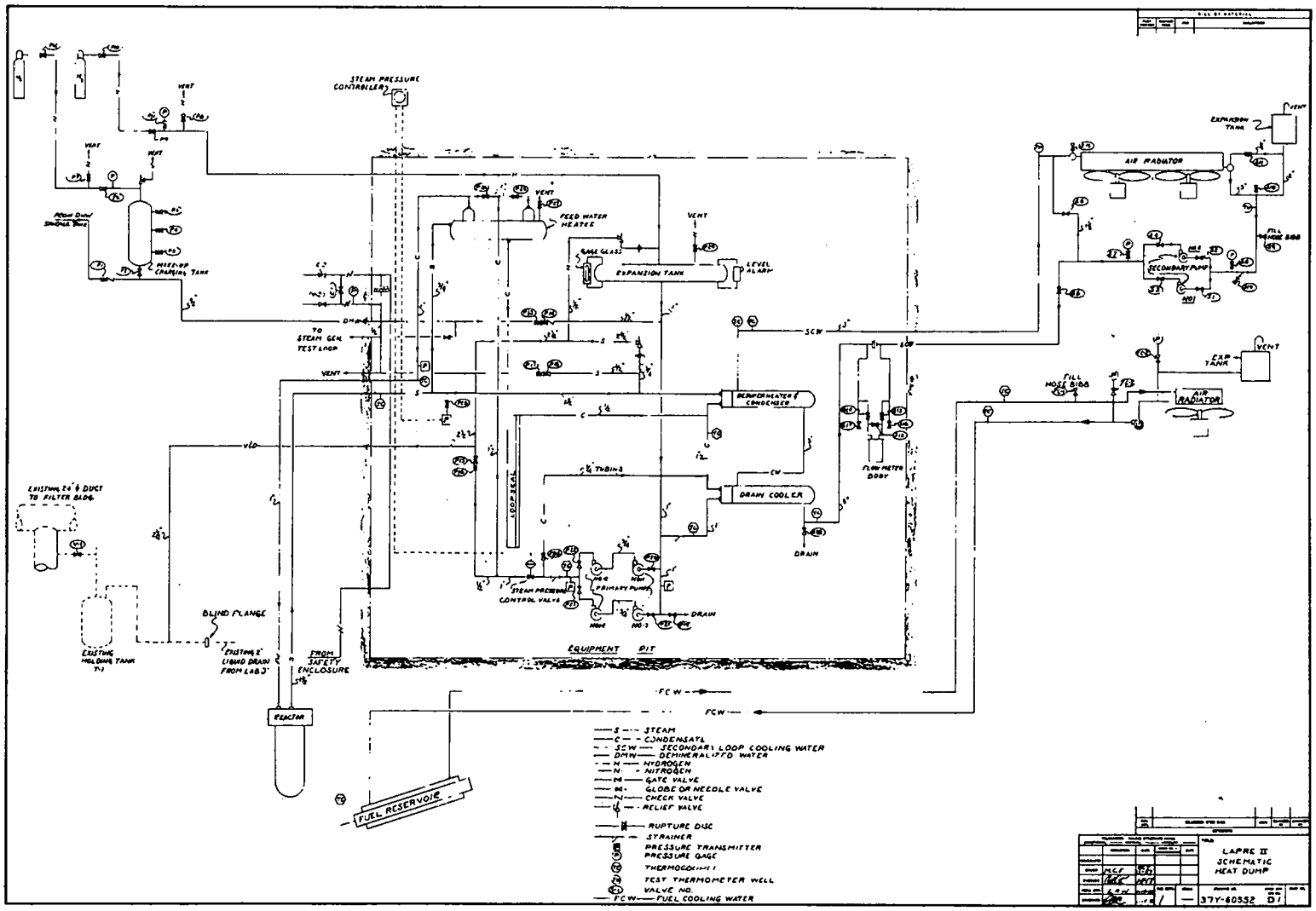

Fig. 5.1 Schematic of Heat Removal System

A shell and tube feedwater heater was installed between the feed pump discharge and the reactor heat exchanger inlet manifold in order to reduce thermal shocks caused by incoming cold feedwater. Steam supplied to the feedwater heater was taken from the reactor superheater steam outlet. Condensate from the feedwater heater shell was drained back to the water system through a loop-seal type of drain trap.

Reactor steaming rate was controlled by an air-operated control valve located at the feed pump discharge and functioning to throttle the quantity of feedwater to the reactor. The control point for the load control valve was located at the reactor control panel.

Primary system operating pressure was controlled through a combination pressurizing and thermal expansion tank physically located at the highest point in the system. Hydrogen gas was admitted to the top of the pressurizing tank as required to adjust to the desired system operating pressure. The pressurizing tank was further designed to provide reserve water storage capacity required by the system. The tank was fitted with both a gage glass and low water level alarm for determining water level. The low level alarm was also arranged to shut down the feed pumps in the event of a dangerously low water level.

The closed features of the primary loop required essentially no feedwater makeup subsequent to the initial water charge. However, a makeup charging tank was provided in which feedwater could be forced into the primary system using a high pressure nitrogen gas as a driving agent. Feedwater used in the primary system was obtained from a deaerated and demineralized water treatment plant producing water having > 0.5 ppm total solids, 0.03 ppm chlorides and 0.03 ppm O_2.

Due to the induced radioactivity in reactor outlet steam, all primary system piping and equipment was located in an underground concrete pit having plan dimensions of 8 ft 0 in. x 12 ft 0 in. and a depth of 21 ft 3 in.

5.2 Secondary Loop

In order to prevent freezing in the outdoor installation, a 30% ethylene glycol solution was used as a secondary loop coolant. The ethylene glycol solution was pumped through the shells of both the primary loop desuperheater-condenser and drain cooler to condense and cool the reactor outlet steam. Heat transferred to the secondary loop coolant was then dissipated to atmospheric air through a forced draft, fin tube heat exchanger. A single stage centrifugal pump was used for circulating the secondary pump coolant. An orifice type flowmeter with metering body arranged for electrical transmission to the reactor control panel was used to meter and continuously record secondary loop flow. The temperature rise of secondary loop coolant across the desuperheater-condenser and drain cooler was also recorded. Reactor power output to the heat removal system was then computed using secondary loop flow and temperature rise considerations.

5.3 Equipment Design Data

The following is a tabulation of pertinent equipment design data:

1. Desuperheater-Condenser

Type	Shell and tube; removable U-tube bundle; single pass on shell side, 2-pass on tube side	
Capacity	2.45×10^6 Btu/hr	
Surface	31 ft^2	
Heat transfer coefficient	390 Btu/hr ft^2 °F	
LMTD	342°F	
Tube size	5/8 in. o.d., No. 18 BWG	
No. tubes	26	
Type tube joint	Tube expanded into tube sheet	
	Tube Data (primary loop)	Shell Data (secondary loop)
Fluid	Steam	Cooling water
Flow rate	3000 lb/hr	78,200 lb/hr
Temperature in	600°F	133.6°F

	Tube Data (primary loop)	Shell Data (secondary loop)
Temperature out	487°F	165°F
Design pressure	1000 psi	150 psi
Pressure drop	Negligible	1.5 psi
Construction material	Type 316 S.S.	Carbon steel

2. Condensate Drain Cooler

Type	Shell and tube; removable U-tube bundle; single pass on shell side, 4-pass on tube side
Capacity	1.063×10^6 Btu/hr
Surface	44 ft^2
Heat transfer coefficient	267 Btu/hr ft^2 °F
LMTD	121°F
Tube size	5/8 in. o.d., No. 18 BWG
No. tubes	24
Type tube joint	Tube expanded into tube sheet

	Tube Data (primary loop)	Shell Data (secondary loop)
Fluid	Condensate	Cooling water
Flow rate	3000 lb/hr	78,200 lb/hr
Temperature in	487°F	120°F
Temperature out	150°F	133.6°F
Design pressure	1000 psi	150 psi
Pressure drop	Negligible	2.5 psi
Construction material	Type 316 S.S.	Carbon steel

3. Feedwater Heater

Type	Shell and tube; serpentine tube bundle; all welded construction.
Capacity	850,000 Btu/hr
Surface	11.0 ft^2
Heat transfer coefficient	480 Btu/hr ft^2 °F
LMTD	161°F
Tube size	1/2 in. o.d., No. 20 BWG
No. tubes	6
Type tube joint	Tube welded in tube sheet

	Tube Data (primary loop)	Shell Data (secondary loop)
Fluid	Feedwater	Steam
Flow rate	3000 lb/hr	1040 lb/hr
Temperature in	150°F	600°F
Temperature out	425°F	487°F
Design pressure	1000 psi	1000 psi
Pressure drop	5 psi	Negligible
Construction material	Type 347 S. S.	Type 347 S. S.

4. Secondary Loop Air Radiator

Type	Horizontal, forced draft, finned tubes
Capacity	3.6×10^6 Btu/hr
Water flow rate	160 gpm
Water temperature in	165°F
Water temperature out	120°F
Air temperature in	85°F
Air temperature out	122°F
Tube surface	710 ft^2
Total finned surface	11,280 ft^2
Number water passes	3
Number tubes	182
Tube length	24 ft
Tube size	5/8 in. o.d., No. 19 BWG
Tube material	Inhibited Admiralty
Fin material	Aluminum
Number fans	2
Total fan capacity	88,800 cfm
Fan speed	600 rpm
Fan motor size (each)	10 hp

5. Primary Loop Pumps

Number	4
Type	Centrifugal, horizontal, double-stage, seal-less with canned motor drives

Rated capacity	8 gpm
Total dynamic head	180 ft water @ 200°F
Pump speed	3450 rpm
Casing design pressure	825 psi
Construction material:	
Shafts, casings, impellers	Stainless steel
Bearings	Graphitar
Motor size	3 hp

NOTE: See Figs. 5.2 and 5.3 for pump test curves.

6. Secondary Loop Pumps

Number	2
Type	Centrifugal, horizontal, close-coupled, single-stage, electric motor driven
Rated capacity	160 gpm
Total dynamic head	56 ft of water
Speed	3450 rpm
Motor size	3 hp
Construction material	Bronze fitted cast iron

7. Primary Loop Pressurizing and Expansion Tank

Total volume	10.3 ft^3
Design pressure	1000 psi
Construction material	Type 347 S.S.

8. Secondary Loop Expansion Tank

Total volume	15 ft^3
Construction material	Carbon steel

9. Feedwater Makeup Charging Tank

Tank size	10 in. diam x 3 ft-10 in. long
Volume	2.1 ft^3
Design pressure	1000 psi
Construction material	Type 347 S.S.

10. Load Control Valve

Type	Air-diaphragm operated with remote control at control panel; parabolic needle type plug

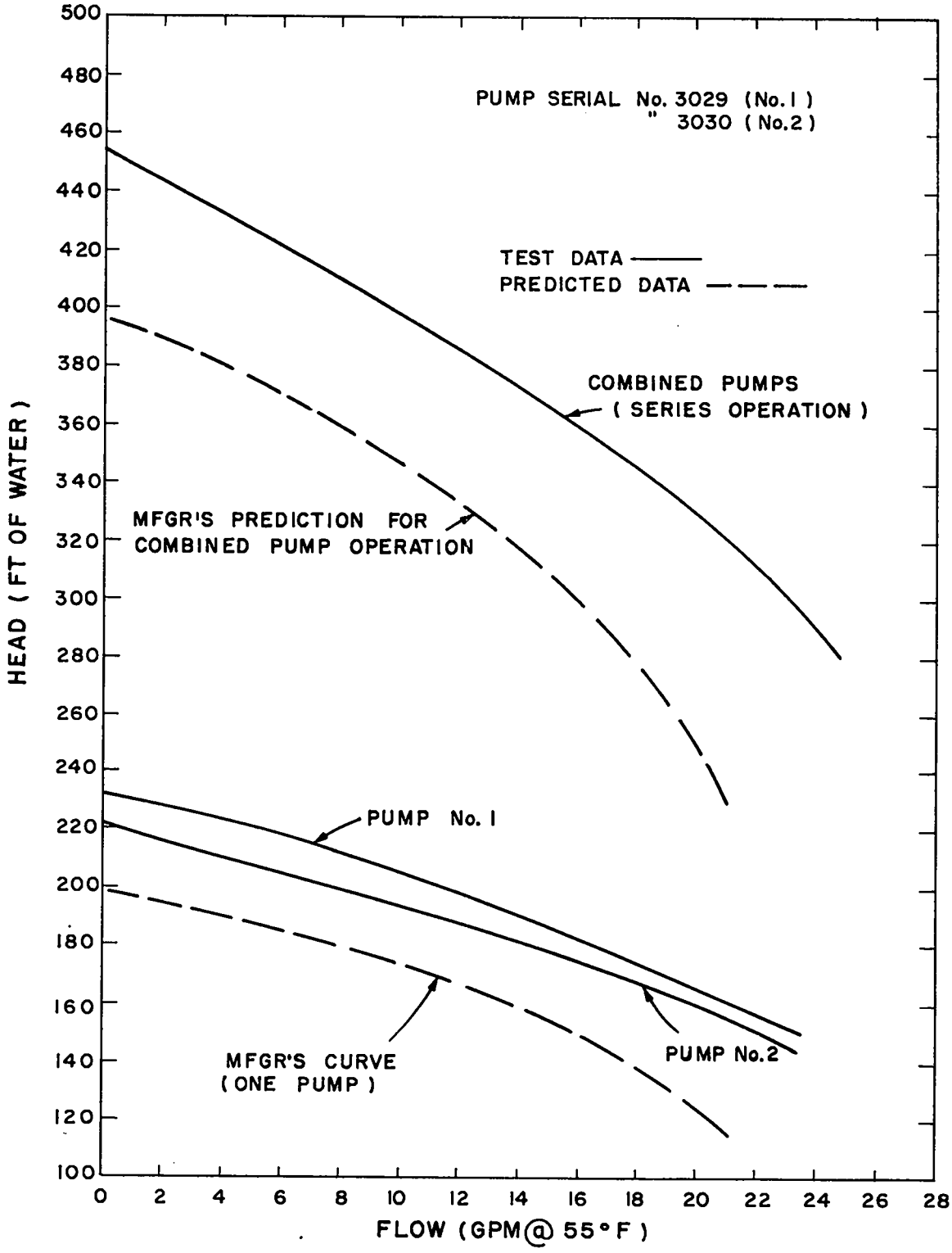

Fig. 5.2 Primary Pumps No. 1 and No. 2 Flow vs Head

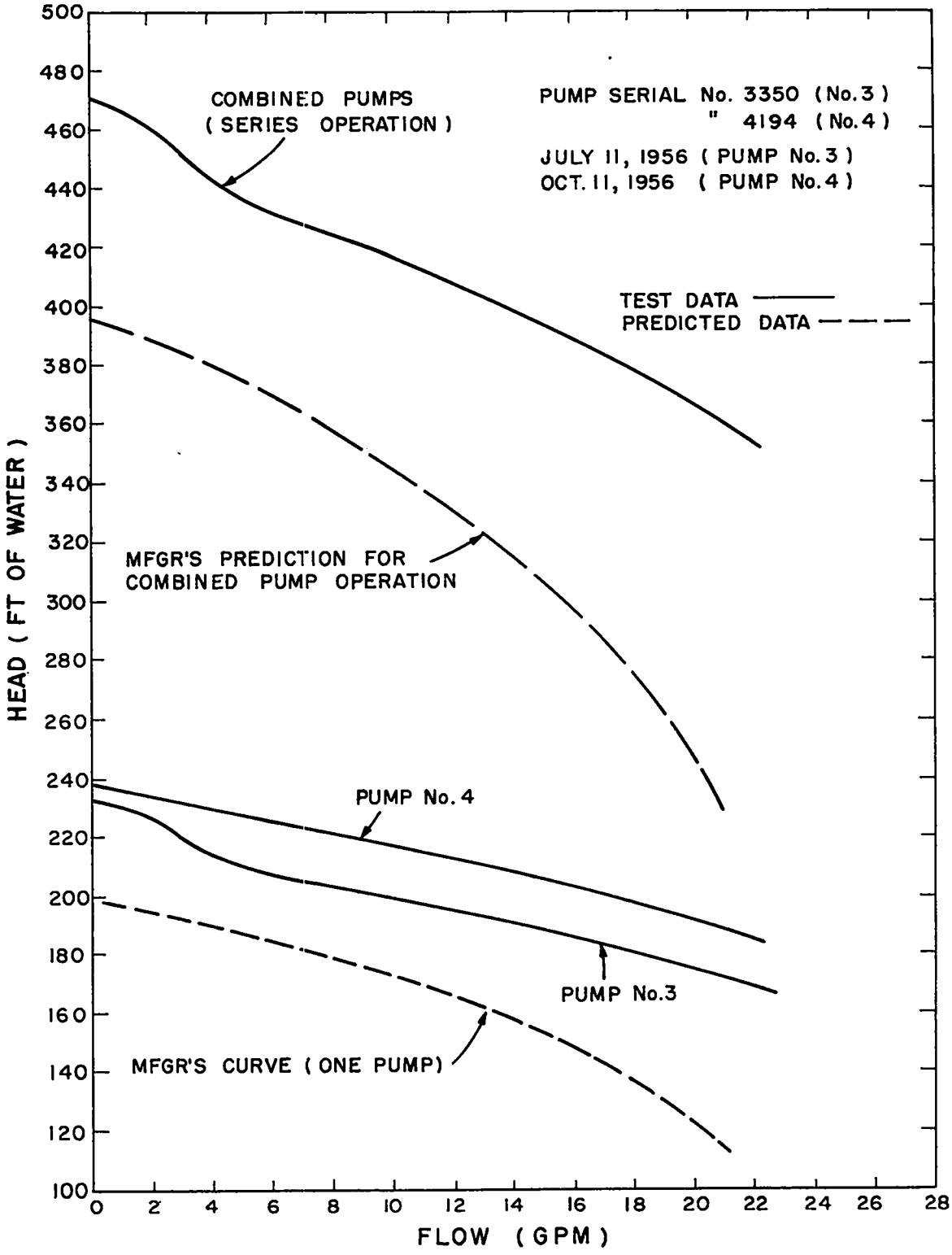

Fig. 5.3 Primary Pumps No. 3 and No. 4 Flow vs Head

Valve size	1 in. body with 3/8 in. internals
Design flow capacity	6 gpm with 22 psi pressure drop; 1.2 gpm with 160 psi pressure drop
Construction material	Stainless steel with teflon packing

NOTE: See Figs. 5.4 and 5.5 for valve flow characteristics.

11. Secondary Loop Water Flowmeter

Type	Orifice plate primary element with Ledoux bell meter body; electric transmission between meter body and panel-mounted recorder
Flow range	0 to 100,000 lb/hr

5.4 Vent Drain System

All vents, drains, rupture discs, and relief valves used during reactor operation discharged into a common waste system. The waste system is shown schematically in Fig. 5.1. Batchwise operation of the system was used, with gaseous wastes in the shielded delay tank (stainless steel, 1000 gal capacity) being discharged to the atmosphere periodically through a two-stage capillary gas washer and stack, while liquid wastes were held for decay and later removal through the top access flange.

The operation of the system was in general satisfactory, but leakage of fission product gases through the discharge valve resulted in temporary high air counts in the control point and laboratory building on two occasions. The activity was sampled and was determined by analyses to be I^{133}, I^{131}, and I^{135}/Xe^{135}. A maximum dose rate of 125 mr/hr was observed at the control point. Future designs should certainly allow more delay capacity and a discharge valve with better shut-off characteristics.

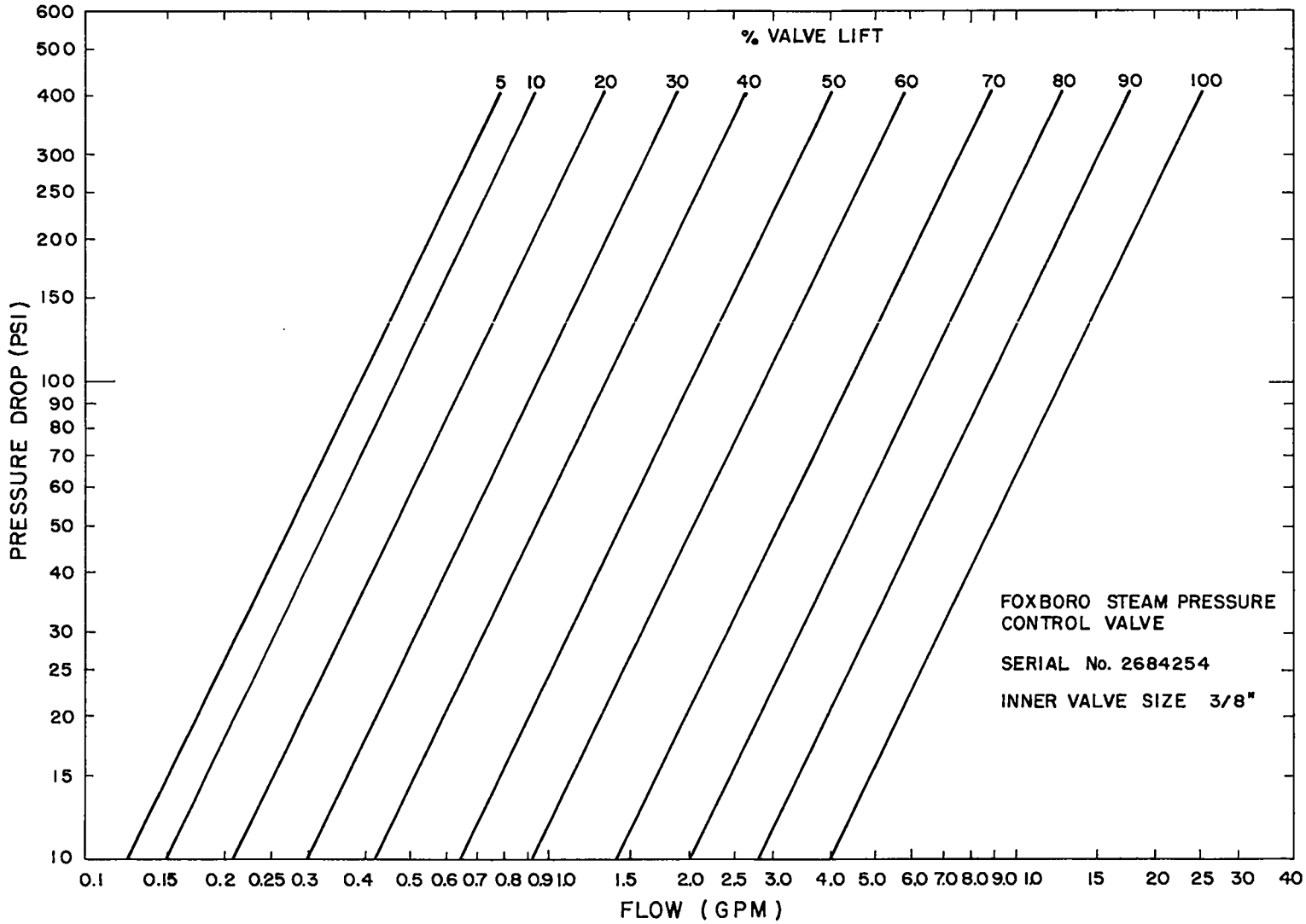

Fig. 5.4 Control Valve Flow vs Head

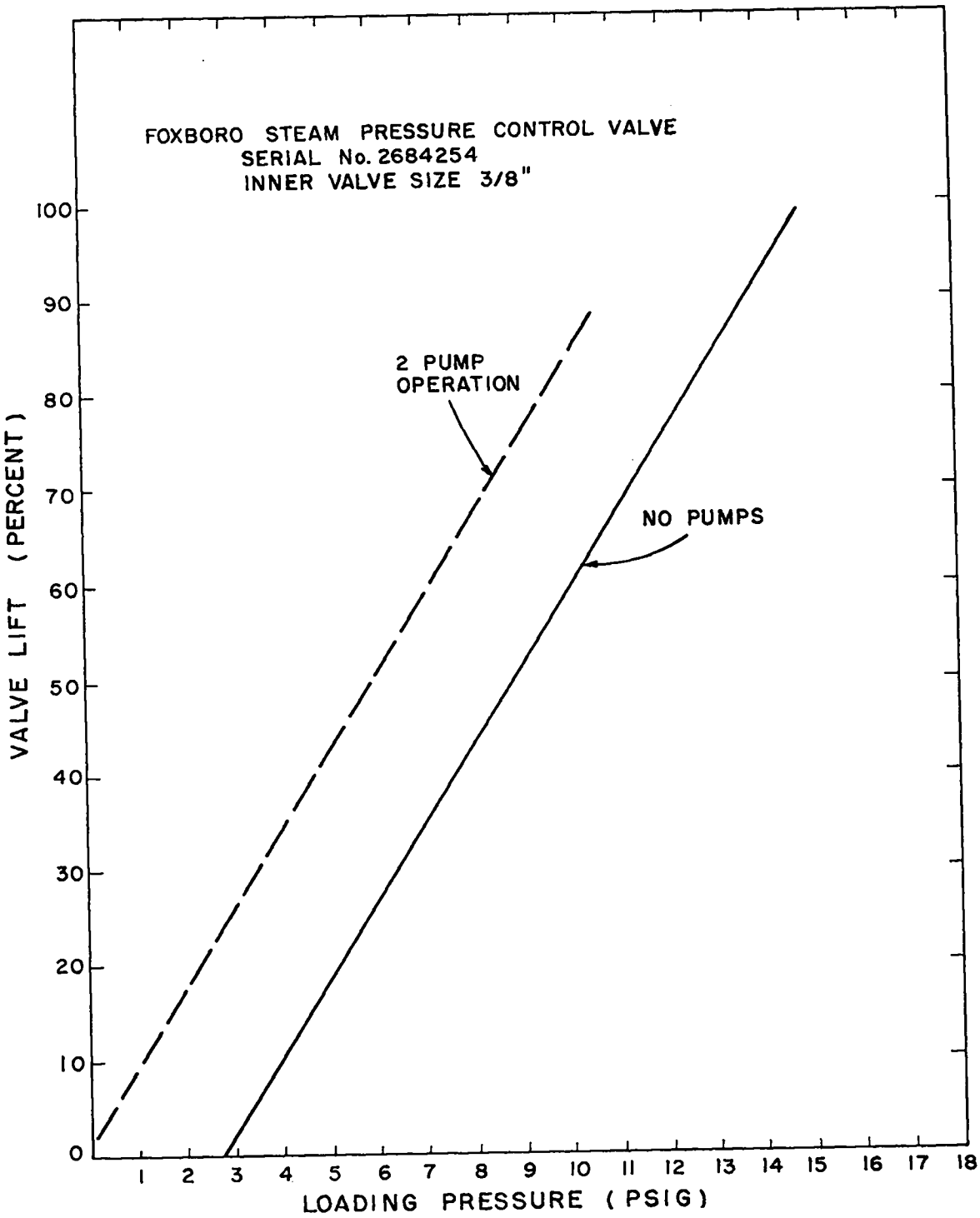

Fig. 5.5 Control Valve Loading Pressure vs Valve Lift

5.5 Operating Experience

A tabulation of heat removal operating data is included in the Appendix.

In general, the heat dump system operated satisfactorily to dissipate reactor-produced heat and to demonstrate the reactor characteristics under investigation.

One inadequate aspect of the system, however, was the instrumentation for determining reactor heat output to the heat removal system. As pointed out, reactor power was computed based on secondary loop flow data and secondary loop temperature rise across the steam condenser and drain cooler. It is believed that possibly these computations were not accurate to better than ± 15% due to (1) inaccuracies in the secondary loop flowmeter, particularly at low flows, and (2) inaccurate temperature data due to the relatively small temperature rise in the secondary loop, and (3) heat loss from primary loop piping and components. It will be noted that a rather poor correlation was obtained between reactor power based on neutron level instrumentation and the heat dump calculations. A steam flowmeter together with pressure and temperature instrumentation in the reactor heat exchanger inlet and outlet would have permitted heat rates to be determined directly from primary loop conditions. The additional complication and expense of such instrumentation would have been justified by this associated improvement in the heat transfer data.

Chapter 6

INSTRUMENTATION

6.1 Control Point

The control point, containing the major portion of the reactor instrumentation, was located in the main laboratory building approximately 50 ft from the reactor exclusion area. The control point was below ground level and was shielded from the exclusion area with a 10 in. concrete wall and earth fill. A plan view of the control point is shown in Fig. 6.1, with the instrument panels, etc., shown in Figs. 6.2, 6.3, and 6.4. Additional instruments were located at the pump pit and fuel system valve manifolds.

6.2 Operational Instruments and Controls

6.2.1 Fuel System

All gages and transmitters associated with the transfer of fuel from the reservoir into the reactor were located in the valve pit immediately adjacent to the south wall of the control point. The gages were viewed through two 4 in. x 8 in. openings in the concrete shield wall. Valve handles extended through the shield wall and were operated from the control point. Additional gages used in transferring fuel from storage to the fuel reservoir and from the fuel reservoir for sampling were located at the valve manifolds. The fuel level in the metering tank was indicated at the control point and also at the valve manifold.

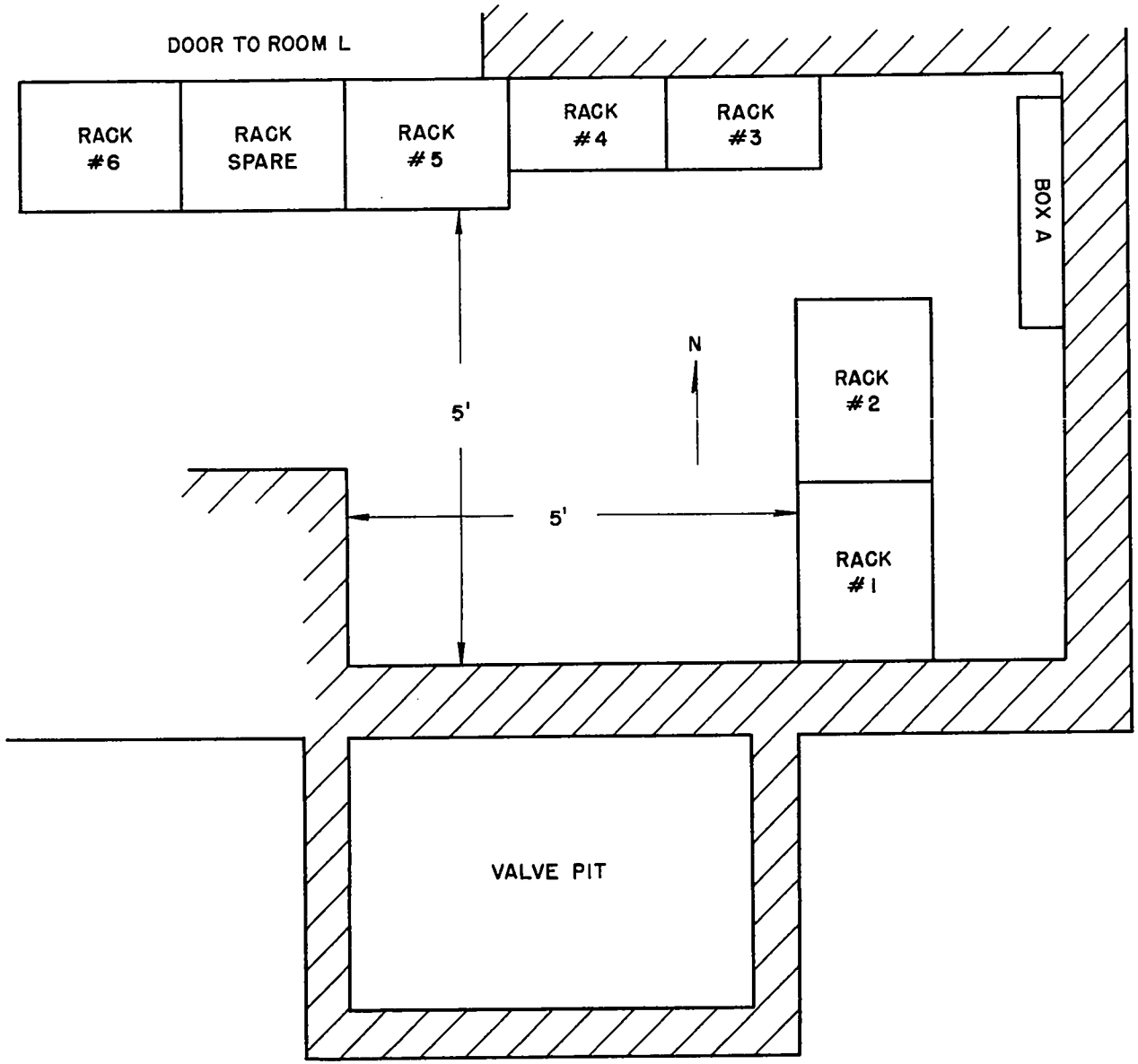

Fig. 6.1 Plan of Control Point

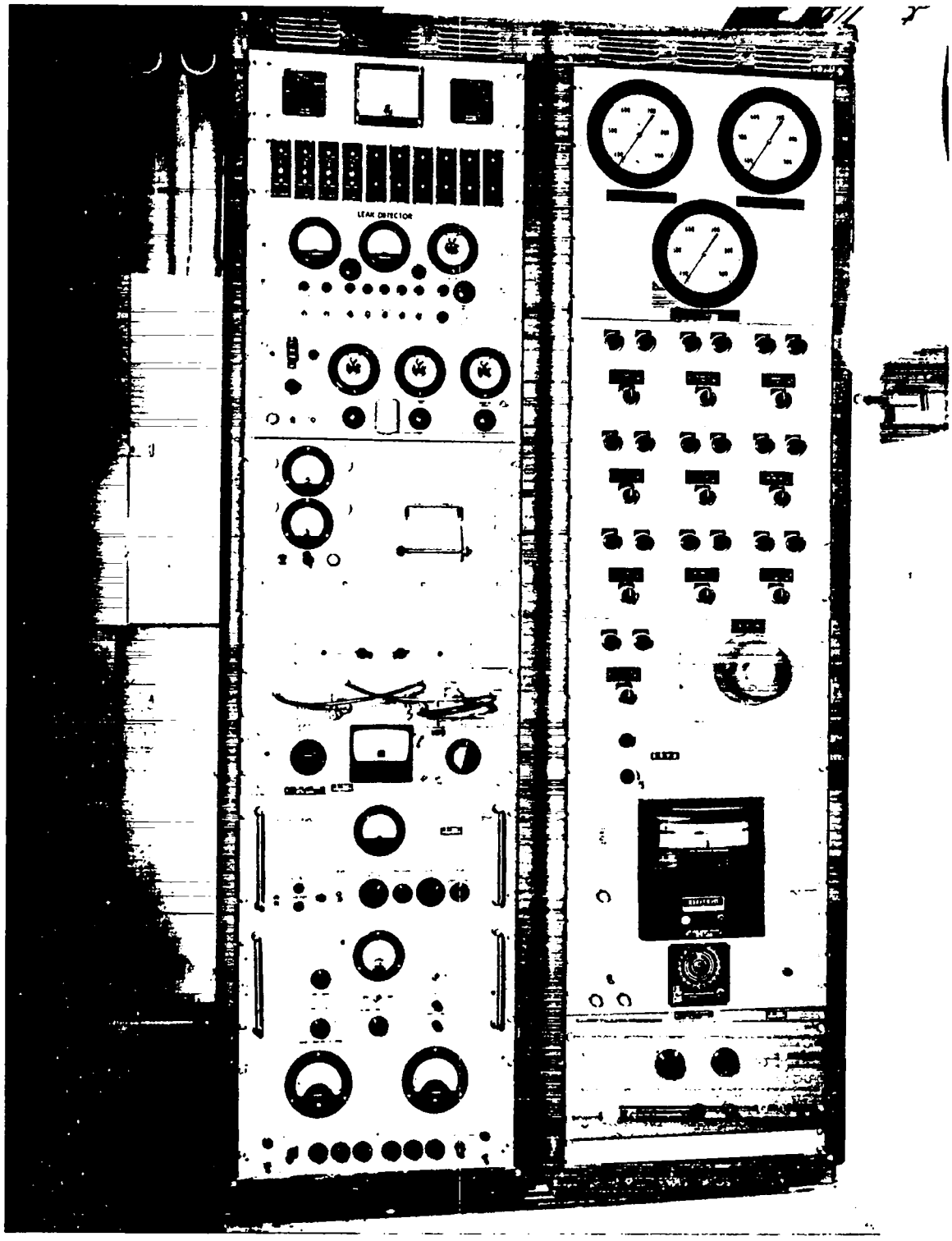

Fig. 6.2 Control Point Instrument Panels

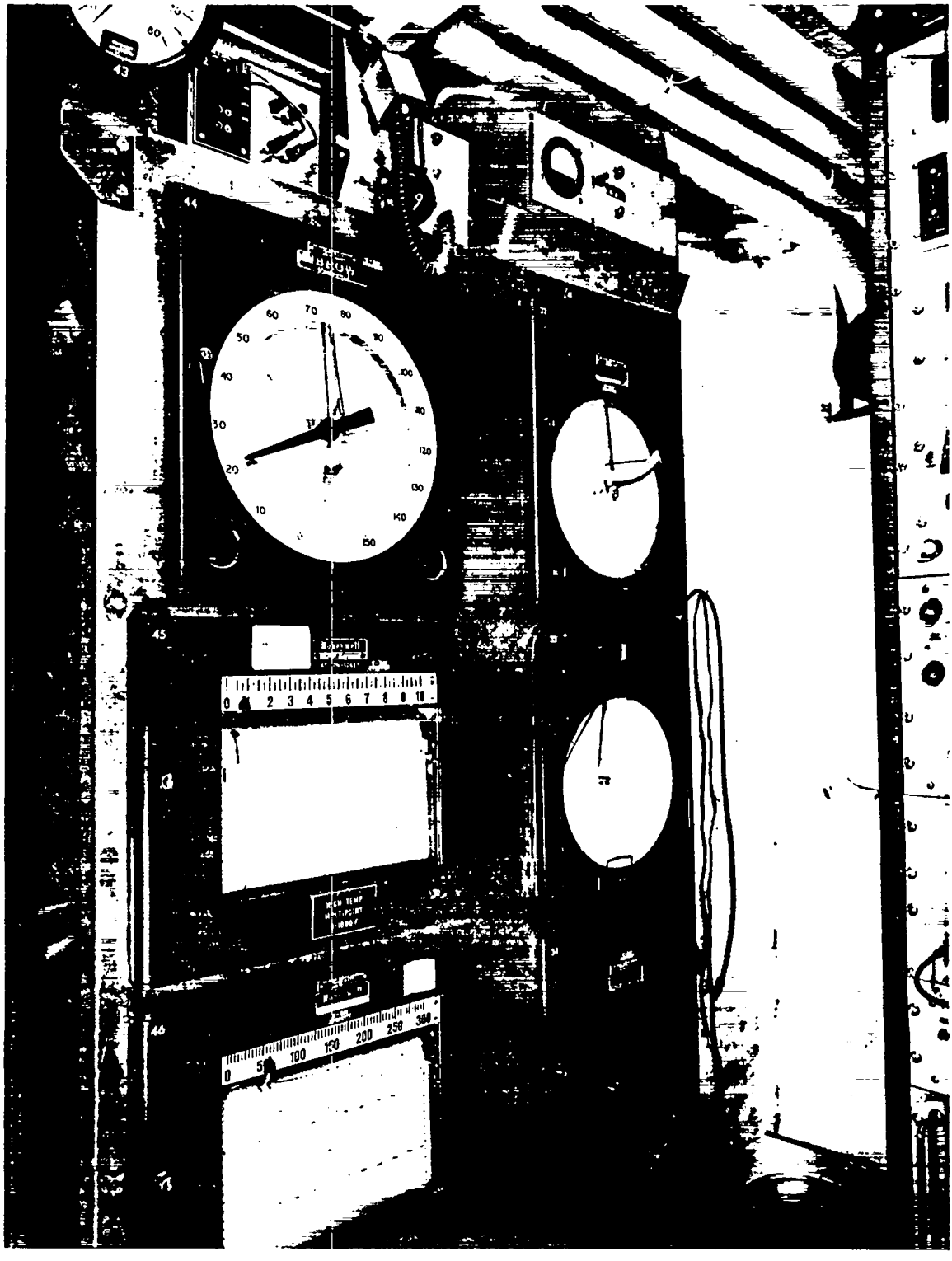

Fig. 6.3 Control Point Instrument Panels

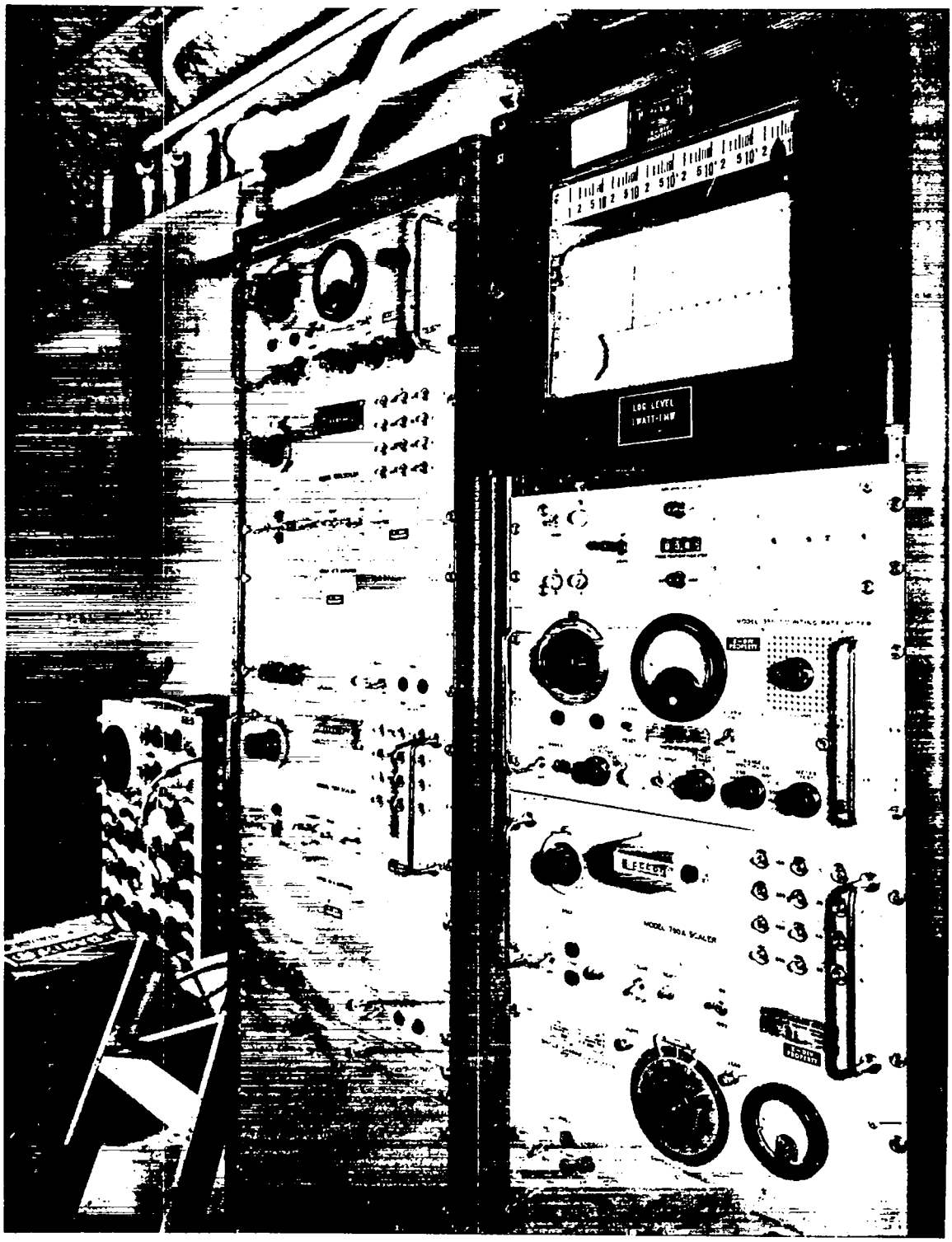

Fig. 6.4 Control Point Instrument Panels

The pressure of the reactor system was monitored with two 10-1/2 in. Heise gages (0-100 psi and 0-2000 psi) and a Barton differential pressure gage (0-20 psi). A pneumatic pressure transmitter and receiver were used to record the pressure. The low range and differential gages were used during the approach to cold critical filling of the reactor and enabled the pressure to be read to 0.1 psi. The differential gage was also useful at full pressure operation for observation of small pressure changes.

Chromel-Alumel thermocouples for monitoring fuel temperature were located (Fig. 3.1) at the bottom of the reactor vessel and at the bottom of the derby. These temperatures were recorded at the control point on a 0-1000°F twelve-point strip chart recorder.

6.2.2 Heat Removal System

Primary Loop. The principal instruments and controls for the primary system were located at the control point; however, a few indicators and transmitters were located in and at the pump pit.

The following loop pressures were indicated at the instrument panel: (1) steam, (2) pump suction, (3) pump discharge, (4) feedwater inlet, and (5) expansion tank. Steam pressure was also recorded on a circular chart recorder.

Chromel-Alumel thermocouples were used on the primary loop to monitor temperature at the (1) desuperheater inlet, (2) condenser outlet, (3) drain cooler outlet, (4) pump outlet, (5) feedwater heater outlet, (6) feedwater manifold, and (7) top heat exchanger coil outlet. These temperatures were recorded at the control point on a 0-1000°F twelve-point strip chart recorder.

On-off controls for the primary pumps, low water level alarm, throttle valve controls, and the hydrogen pressurizing system were also located at the control point.

Secondary Loop. On-off controls for the secondary pumps and the air radiator fans were located at the control point, but all of the valving and pressure gages were located in the exclusion area. Flow in the secondary loop was measured with an orifice and was recorded on a 0-100,000 lb/hr circular chart recorder at the control point. The flow recorder also indicated the integrated flow.

Chromel-Alumel thermocouples were used to measure temperature at the (1) drain cooler shell inlet, and (2) the condenser shell outlet.

The temperature rise measured between these points was recorded on a circular chart recorder at the control point. The temperature of the condenser shell outlet was also displayed on an 8-point, 0-300°F strip chart recorder located at the control point.

6.2.3 Fuel Reservoir Cooling System

A Chromel-Alumel thermocouple mounted on the lower end of the fuel reservoir was used to drive a 0-300°C Pyrovane controller located at the control point. The set point of the controller started the reservoir coolant circulating pump and the air radiator fan. Manual on-off controls for the pump and fan were also provided.

6.3 Radiation Detection

A Jordan remote area gamma monitoring system was located at the control point. Six gamma monitors were provided to indicate radiation levels in (1) the valve pit, (2) pump pit, (3) steam line, (4) top of the safety enclosure, (5) feedwater heater, and (6) control point. Four of the detectors were connected to an audio warning system while all channels were displayed at the instrument panel.

6.4 Neutronics

6.4.1 Startup Counters

Three boron-coated proportional counters were installed in the vertical irradiation tubes for use during critical measurements, the power supply and pre-amp being located at the top of the safety enclosure. The high voltage supply, amplifier, and scalers were located at the control point. During power operation the counters were removed from the irradiation tubes and were used as area monitors.

6.4.2 Neutron Level

The neutron level was indicated and recorded on panel meters and a 0-10 mv strip chart recorder. A boron-lined ionization chamber and a fission chamber were located in the 3 in. and 4 in. vertical irradiation tubes. The output from either chamber could be applied to the input of a linear amplifier or log amplifier. The output from either amplifier could be recorded on the strip chart recorder.

6.4.3 Reactor Period

Two channels for period measurement were provided at the control point. One channel indicated and recorded periods from 25 to 2.5 sec and the other periods from 2.5 to 0.25 sec.

6.4.4 Reactor Fuel Level Detector

The power supplies, position indicator, motor controls and scalers used to detect the fuel level in the reactor were located at the control point. A complete description of the instrument and its operation may be found in a separate report.[18]

Chapter 7

FUEL SOLUTION

7.1 Chemical Properties

The chemical properties of the LAPRE II fuel solution were well known from previous studies.[16,19] The corrosion resistance of gold, platinum, graphite, copper, and stainless steel when in contact with the fuel solution had also received extensive investigation under nonradioactive conditions. Some of the previously observed physical properties are summarized in Table 7.1. Actual fuel behavior during reactor operation was expected to resolve the remaining uncertainties, as follows: Formation and recombination rates for radiolytic gases, over-all fuel stability in the presence of radiation fluxes and fission products, and possible radiation-induced corrosion effects.

7.2 Fuel Preparation

Fuel was prepared from 93.5% enriched UO_2, containing about 3% UO_3. The oxide was dissolved in a weighed quantity of 95% chemically pure phosphoric acid by stirring for 3 hr at 120°C. After cooling, the solution was weighed and restored to correct volume with distilled water. Although the presence of hexavalent uranium was undesirable from the corrosion standpoint, there were no readily available means for its reduction without adding undesirable impurities to the solution. The excess hydrogen present in the reactor when operating was expected to rapidly reduce all the hexavalent uranium as soon as a moderately high temperature was attained. The initial preparation consisted of 66.5 liters

of solution which was 0.343 M in U(IV) + 0.010 M in U(VI). The total phosphate concentration was 17.3 M. Later fuel preparations were made in the same manner except that additional 95% H_3PO_4 was added in some cases.

In order that the liquid level detector could be used to show solution addition to the reactor before criticality was obtained, 150 curies of La^{140} were added in the form of 7 mg of lanthanum dissolved in excess phosphoric acid. Transfer of the fuel from the storage tank to the reactor required provision of heaters for all transfer lines to keep the fuel above its freezing point of 18.5°C.

7.3 Effects of Reactor Operation on the Fuel

7.3.1 Radiolytic Gas

The pressure observations reported in Section 9.5.1 show that adequate recombination rates were obtained at all reactor temperatures above 700°F, although no detailed rate measurements were made. There was no apparent change in behavior with respect to generation or recombination of radiolytic gas over the operating period. The behavior appeared to confirm the laboratory studies which predicted very small radiolytic gas pressure,with the recombination taking place mainly within the liquid phase. The presence of copper in the solution noted below may have assisted in the recombination. There were no observable net changes in the fuel solution attributable to radiolytic gas.

7.3.2 Analysis of Fuel After Operation

The analyses[20,21,22] made in the fuel solution after various periods of reactor operation are listed in Table 7.2. In general these analyses indicated no changes in the fuel resulting from reactor operation except small increases in copper and iron content. Changes in uranium concentration were consistent with those expected from the various dilutions and other manipulations given to the fuel. The copper picked up by the fuel must have come from the copper cladding of the fuel reservoir, possibly by the action of some of the hexavalent uranium initially in the fuel. The source of the iron is undetermined but possible sources are rust initially in the vessels and lines, or iron leached from the graphite components. The hexavalent uranium present in the original fuel was

TABLE 7.1

EXPANSION COEFFICIENTS AND VAPOR PRESSURES OF THE FUEL

Temperature, °C	Expansion coefficient	Vapor pressure, psia
350	1.14	390
400	1.16	660
450	1.18	1060

TABLE 7.2

FUEL ANALYSES

Date sample received	Total U molarity (± 1/2%)	U(VI) molarity (±.003M)	Total phosphate Molarity (± 1%)	Other	Comments
3/15/59	0.354	0.013	17.3	0.005 M Cu	First sample after operation at power
4/27/59	0.322	0.218	18.5	----	Sample had stood in S.S. pot 1 week
4/29/59	0.335	0.032	18.5	----	From fuel reservoir
5/4/59	0.325	0.014	18.3	----	From fuel reservoir 50% H_3PO_4 had been added previously
5/18/59	0.326	0.004	18.0	----	Sample had stood in S.S. pot 1 week
5/18/59	0.327	0.004	18.05	0.021 M Cu 0.015 M Fe Undetectable Au or Pt	From fuel reservoir

reduced significantly by reactor operation although not to zero as expected. Interference in the analysis by the iron present and various sampling uncertainties may account for the small hexavalent content observed.

No detectable gold or platinum was dissolved in the fuel and no effects on fuel stability were observed from reactor operation or the presence of fission products.

Chapter 8

REACTOR PHYSICS

8.1 Calculational Method

Criticality calculations for LAPRE II were made using Carlson's S_n method for solving the neutron transport problem.[23] This choice was based on the following considerations. First, the S_n code was available at Los Alamos for solving reactor problems at the time the LAPRE II design was started, and a set of eight-group cross sections for thermal systems had been developed by means of which it was possible to compute critical radii to ± 2% for hydrogen-moderated reactors with a variety of reflector materials and H/U ratios. The availability of a tested set of multigroup cross sections was a contributing factor in the choice of the S_n method, and this method proved preferable to diffusion theory for handling the strongly absorbing gold-clad stainless steel wall of the reactor vessel.

8.2 System Geometry

For calculational purposes, the following configuration was assumed for the LAPRE II reactor.

Inner radius of vessel: 18.69 cm

Vessel wall (15-mil Au liner plus 5/8 in. stainless steel): 1.63 cm

Shim thickness (3 in. BeO plus 2.8 in. graphite): 14.76 cm

Stationary graphite (radial): 13.02 cm

Bottom graphite: 38.1 cm

The dimensions of the reactor as built (Fig. 3.1) differed, in some cases, from those used in the calculations. The differences, however, were small enough so that no significant error was introduced in applying the calculated results to the actual system.

In the calculations, the gold liner and stainless steel were homogenized and treated as one region. This was done because of the difficulty of treating the gold liner as a single region; however, the procedure adopted should give conservative results, i.e. an overestimate for the critical mass. Since the bottom of the vessel was not a simple shape, it was convenient to interpret the calculational results in terms of volume of fuel required for criticality. In this connection, the assumption was made that the critical volumes for the LAPRE II reactor and a flat-bottomed cylinder of the same radius were equal. This assumption was not based on theoretical considerations but was simply postulated as being a reasonable one. The validity of this assumption should be better for the hot critical than for the cold critical case, because of greater fuel heights.

8.3 Fuel Solution Data

The fuel solution composition at room temperature was inferred from the measured density of the solution. A tabulation of the constituent molarities for the fuel solution - 0.35 M UO_2 in 17.5 M H_3PO_4 - used in the calculations is given below.

Temperature	H	O	P	U(93.5% U^{235})
21°C	61.8 M	75.5 M	17.5 M	0.35 M
430°C	51.3 M	62.8 M	14.6 M	0.292 M

The hydrogen and oxygen molarities at 430°C reflect, in addition to the density change, a small correction for the loss of water to the vapor space at elevated temperatures.

The expansion ratio of the fuel, over the temperature range from room temperature to 450 °C (see Chapter 7), had been measured as 1.18. However, in order to allow for uncertainties in the measurements, and in order to be conservative in estimating criticality, the fuel density at 430 °C was assumed to be 1/1.20 times the room temperature value of 1.906 g/cc. It should be pointed out that the expansion of the fuel was measured in closed vessels and, for a given fuel, was a function of the relative volume occupied by the liquid at room temperature. In view of the interconnection between core and reservoir in this reactor (see Fig. 4.1), it was not possible to define an equivalent "closed" system for the core. The expansion ratio of 1.18 was appropriate to an 80-85% initial filling of the reactor; this initial filling would expand to the desired volume at operating temperature if the reactor were a closed vessel.

8.4 Calculations

At the time the calculations were initiated, it was realized that detailed criticality data could not be obtained in this experiment. At best, one could only count on obtaining reliable experimental data at room temperature for the shim in and shim out cases. The simplicity of the internal reactor instrumentation, coupled with uncertainties in the calculational input data, would make it difficult to compare realistically the calculated and experimental results at higher temperatures. The main purpose of the calculations was therefore to specify a system which would, with a fair degree of certainty, be critical at the design temperature and power with approximately half the shim inserted. It was quite important, for example, that operation at 430 °C be achieved in order to demonstrate successful recombination of radiolytic gas and the production of high quality steam. With this in mind, very conservative assumptions were made in the calculations. In what follows, a rather detailed outline of the calculational methods employed will be given. Insofar as possible, the calculations are corrected to conditions which were obtained during the experiment. Thus, the figures quoted will be slightly different from those reported prior to the complete analysis of the experimental data.[24]

As mentioned earlier, calculations were made using the S_n method ($n = 4$), and eight-group cross sections formulated by G. I. Bell. Calculations were made for spherical systems, and the results were extended to cylindrical systems by conversion procedures based on the equality of bucklings (B^2) for the two geometries. In making this conversion, the question always arises as to what values are to be used for the total extrapolation length δ, defined as the bare extrapolation length plus reflector savings. There is no satisfactory method of calculating δ for arbitrary reflector configurations and it would be useful if one could employ the S_4 results to obtain values for this parameter. With this in mind, the following scheme was adopted. Calculations were first made to determine the critical radii of spherical cores with no reflector, and then for cores with reflectors corresponding to the LAPRE II shim in and shim out configurations. For each case, the calculated thermal flux as a function of radius was fitted to a ($\sin Br/r$) variation in the region from $r = 0$ to r equal to approximately half the core radius. This was done for uniform fuel solution temperatures of 20°C and 430°C. A value for the critical buckling was thus obtained; the critical buckling and the critical radius were then used to obtain a value for the total extrapolation length. These figures were then used to compute the shim in and shim out bucklings for the cylindrical reactor.

In order to check the accuracy of the above conversion scheme, a comparison with experiment was made for a few selected cylindrical systems.[25,26] The results of this comparison are shown in Table 8.1. Admittedly, the number of systems for which the comparison was made was small; however, except for system No. 6 the method yields fair agreement with experiment. For a clean geometry, the method might reasonably be expected to yield ± 10% estimates for the critical heights.

As applied to spherical models of LAPRE II cores, this calculational method yielded critical bucklings of 0.1205 and 0.1025 cm^{-1} at 20°C and 430°C, respectively. The values for δ, the total extrapolation length, obtained from the calculated bucklings are tabulated in Table 8.2.

TABLE 8.1

CALCULATED AND EXPERIMENTAL DATA FOR CYLINDRICAL ASSEMBLIES

System No.	D, in.	h, cm	Reflector	H/U^{235}	g U^{235}/ g solution	Accuracy of measured h	Δ, %
5^{25}	8	19.5	Water	52.9	0.293	± 5%	- 8.7
6^{25}	8	23.8	Water	86.4	0.213	± 5%	-16.3
7^{25}	10	20.0	Water	226	0.0995	± 5%	- 5.6
8^{25}	12	26.3	Water	499	0.0488	± 5%	1.5
11^{26}	12.4	16.4	3 in. Fe	212	0.112	± 1.2%	- 1.7

D = cylinder diameter

h = experimental critical height

$$\Delta = \frac{\text{(Calculated critical volume - Experimental critical volume)}}{\text{(Experimental critical volume)}}$$

Systems 5 to 8 consisted of aqueous solutions of UO_3-H_2F_2. The container wall thickness was 1/16 in. Container material for System 5 was Type 3-S Al; Type 347 S.S. was used for Systems 6, 7 and 8. The U^{235} content of the U was 93.4%. System 11 consisted of an aqueous solution of UO_3-H_3PO_4. The container wall thickness was 0.1 cm stainless steel. The U^{235} content of the U was 93.5%.

TABLE 8.2

CALCULATED TOTAL EXTRAPOLATION LENGTHS

Reflector	δ (20°C)	δ (430°C)
None	2.54 cm	2.16 cm
Shim out	5.85	6.31
Shim in	9.20	10.07
Bottom graphite	8.71	9.57

From the calculated bucklings and the above values of δ, the critical core volume for the cylindrical reactor was computed. The results obtained, for the room temperature and for the operating temperature cases, are given as a function of shim position in Table 8.3.

TABLE 8.3

CALCULATED CRITICAL CORE VOLUMES FOR CYLINDRICAL REACTOR

Reflector	Critical core volume (20°C)	Critical core volume (430°C)
Shim out	37.0 liters	84.5 liters
Shim in	28.6	45.3

Figures shown are for an unreflected top and without the Pt baffle. Volume of LAPRE II core at 430°C = 63.4 liters. The room temperature volume of the core region of the reactor vessel (that region below the bottom of the heat exchanger) was 62.2 liters. At 430°C, expansion of the vessel would increase this volume to 63.4 liters. Thus, from Table 8.3, it is clear that the calculations predict full core criticality at the desired temperature with a partial insertion of the shim.

Values given in Table 8.3 should however be refined to take into account (1) the poisoning effect of the Pt baffle which directed fuel circulation through the core and (2) the effect of the heat exchanger complex on criticality. In the case of the Pt baffle, one-group perturbation theory was used to estimate the reactivity worth; the results indicated that at 20°C, $\Delta k/k$ contributed by the presence of the baffle was - 0.003. At 430°C, with the core completely filled with fuel solution, the corresponding value was - 0.005 $\Delta k/k$.

The reactivity worth of the heat exchanger region was calculated using a two-dimensional diffusion code, Nick II,[27] at 430°C. With a shim in configuration, and with the heat exchanger region filled with fuel, a reactivity worth of + 0.024 $\Delta k/k$ was obtained. At 430°C, the net reactivity worth of the baffle and heat exchanger was therefore + 0.019 $\Delta k/k$.

In order to apply directly these corrections to the 20°C data of Table 8.3, it was necessary to calculate the reactivity worth of the fuel solution per unit volume for the specified temperatures and reactor configurations. One-group calculations yielded fuel worths of 0.014 and 0.0083 $\Delta k/k$ per liter of solution for the shim in and shim out configuration, respectively.* Application of these

*The one-group parameters used in this estimate were chosen to be consistent with the S_4 critical bucklings. For example, k_∞ and the square of the thermal diffusion length, L^2, may be computed from the thermal cross sections. These values, in conjunction with the critical bucklings, yield the Fermi age, τ; at 20°C and 430°C, τ was found to be 42 and 58 cm^2, respectively.

corrections does not alter the shim worth indicated in Table 8.3, but the predicted critical volumes are slightly different (Table 8.4).

It is more convenient to express shim worth for the 430°C, full core case by a comparison of k_{eff} for the shim in and shim out configuration, rather than in terms of an equivalent fuel volume. This was done using the one-group treatment described previously to calculate k_{eff} for the geometric bucklings appropriate to the specified conditions. (The validity of this method was checked by comparing it to S_4 estimates of the Δk_{eff} resulting from an increase in the core radius of a critical, reflected system.)

Final results of these calculations are summarized in Table 8.4, which gives the estimated shim worths, corrected for the reactivity effect of the platinum baffle and the heat exchanger, at room temperature and at 430°C.

TABLE 8.4

CALCULATED CRITICAL CORE VOLUME AND k_{eff} FOR CYLINDRICAL REACTOR

Reflector	Critical core volume (20°C)	k_{eff} for full core at 430°C
Shim in	28.8 liters	1.093 + 0.019 = 1.112
Shim out	37.4	0.954 + 0.019 = 0.973

8.5 Cold Critical Experimental Data

Data were obtained at ~ 20°C to determine the critical volumes with the shim in and shim out. For these measurements, a fuel level detector external to the reactor was designed,[18] consisting of a scintillation counter encased in a lead pig with a slit collimator system on the side closest to the reactor. This scintillation probe was moved vertically by remotely controlled equipment. The height of the counter slit was measured with reference to a fiducial radioactive source, located near the bottom of the vessel. For a solution containing a gamma-ray source the liquid level can be inferred by observing the change in counting rate as the probe moves past the

liquid-gas interface. For the fuel level measurements during initial filling of the reactor, the solution was spiked with La^{140} and accurate level data were obtained during this phase of the operation. However, after operation at a few milliwatts of power, the activation of the sodium iodide crystal in the scintillation probe made it difficult to obtain accurate level data. Details of the experience with the fuel level detector during the LAPRE II experiment are discussed in Ref. 18.

It was necessary to find some other method for determining the fuel volume at cold critical. One of the methods used was based on the fact that, for a given fuel level in the reactor, the gas pressure in the reservoir must equal the gas pressure in the reactor plus the hydrostatic head produced by the fuel. This required a knowledge of (1) the total reactor and reservoir volumes, (2) the relative location in the vertical plane of reactor and reservoir, (3) the total fuel volume in the system, (4) the liquid volume vs height in reactor and reservoir, and (5) the initial hydrogen pressure in the system with the gas regions in reactor and reservoir interconnected. Prior to filling the reactor, the pressures in the reactor and reservoir were always equalized to $\sim$ 11.5 psia, after which the gas space in the reactor was isolated from the external system. The gas in the reactor was assumed to obey Boyle's law. A second method which was used to infer the critical volume was based on metering known gas increments into the reservoir after the initial equalization of pressures in the reservoir and reactor. Thus, at the start of filling the reactor, the gas pressures and volumes in reactor and reservoir were known. After isolating the reactor gas space from the reservoir, the metering tube (see Fig. 4.1), located between valves F-121 and F-122, was pressurized to a predetermined value P. The metering tube was then opened to the reservoir and the pressure allowed to reach an equilibrium value P_r. From the observed values of P and P_r, together with the metering tube volume and the initial gas volume in the reservoir, the amount of fuel transferred to the reactor was computed. This procedure was repeated many times in the actual filling of the reactor and a cumulative record of the fuel transferred to the reactor obtained.

It should be pointed out that the first of the two methods discussed above is not valid if there is a vapor pressure contribution to the pressure in the reactor. On the other hand, the second method is independent of vapor pressure in the reactor and gives the total volume of cold fuel transferred to the reactor . To obtain the height of the fuel in the reactor an estimate of the average temperature, and hence the expansion coefficient, of the fuel in the reactor was required. The second method was normalized to a measurement with the level detector, at 27.75 liters, by correcting the metering tube volume so as to make the two values agree. For this filling, the first method gave a value of 29.0 liters, the discrepancy between the two methods becoming less for the higher fillings. For the shim in critical case, the first and second methods yielded values of 29.6 and 28.6 liters, respectively; for the shim out case the corresponding figures were 33.9 and 34.1 liters. Since the pressure measurements were accurate to ± 0.1 psig, corresponding to ± 0.3 liter in terms of fuel volume, the accuracy of the quoted volumes is no better than ± 0.5 liter at best. Assigning equal weights to the values obtained by the two methods, the critical volumes are:

Shim in	29.1 liters
Shim out	34.0 liters

A correction should be applied to the calculated cold critical volumes (Table 8.4) since the data were obtained for a 0.354 M UO_2 in 17.3 M H_3PO_4 fuel solution (see Table 7.2), whereas the calculations were made for a 0.35 M UO_2 in 17.5 M H_3PO_4 fuel. The accuracy quoted for the chemical analysis of the fuel used was ± 0.5% for the uranium molarity and ± 1% for the phosphate molarity. Hence, a correction was only made for the change in uranium concentration. From S_4 calculations, it was estimated that a change in uranium molarity from 0.35 to 0.354 was worth + 2.8 x 10^{-3} in $\Delta k/k$. This was converted to equivalent volume of fuel using the previously calculated values of $\Delta k/k$ per liter of fuel (Section 8.4). The final comparison between calculation and experiment is shown below.

Reflector	Calculated critical volume	Observed critical volume
Shim out	37.1 liters	34.0 ± 0.5 liters
Shim in	28.6	29.1 ± 0.5

The calculated and experimental results shown above are rather difficult to evaluate. The calculations were made for a cylinder of uniform cross section; the reactor vessel was constructed of a cylindrical section with a semi-elliptical cap. It is quite possible that the assumption made in the calculations represented an over simplification of the facts. Furthermore, in view of the rather indirect method volume measurement, the accuracy of the experimental observations leaves much to be desired. Thus, no detailed comparison between theory and experiment can be made at this point. On the basis of the data shown above, the calculated and observed critical volumes for the shim in case are in good agreement; for the shim out case, the calculated critical volume was 9% higher than that observed.

8.6 Hot Critical Experimental Data

Before discussing the experimental results, it will be necessary to take account of the fact that the fuel solution for which calculations were made differed from that for which data were obtained. The fuel solution composition (at 21 °C) assumed in the calculations was 0.35 M UO_2 in 17.5 M H_3PO_4. Chemical analysis of the fuel after the experiment indicated a composition of 0.326 M UO_2 in 18.0 M H_3PO_4 (see Table 7.2).* Compared to the fuel used in the calculations, this represented a decrease of 6.9% and 2.6% in the uranium and hydrogen concentrations, respectively. From S_4 calculations it was found that these changes corresponded to a decrease of 2.1% in k_{eff}, the contribution due to the change in uranium and hydrogen concentrations being about equal. Applying this correction to the k_{eff} values for a full core at 430 °C (Table 8.4) the following are obtained:

Shim in k_{eff} = 1.091

Shim out k_{eff} = 0.952

*The difference between the fuel composition (at 21 °C) for the cold critical and hot critical data was due, in part, to the loss of water from the solution during the experiment. In order to maintain the desired total volume of fuel, phosphoric acid was added to the reservoir prior to the time at which the hot critical data were obtained.

The calculations thus imply a total shim worth of 13.9% in k_{eff} and a shim insertion equivalent to about one-third of the total worth required to attain design temperature. The observed shim insertion required to achieve design temperature and power was approximately two-thirds of the total shim travel. Since it was not possible to measure the shim worth in terms of $\Delta k/k$, a direct comparison of the results cannot be made. However, the data do indicate that the calculated k_{eff} is 4 to 5% higher than that observed. For the fuel used, a 1% increase in k_{eff} requires a 7% increase in uranium molarity, all other constituents remaining unchanged. It should be emphasized that in all comparisons made at temperature, the effect on k_{eff} of the nonuniform core temperature and uncertainties in fuel density have not been included. Note that a 1% increase in fuel density corresponds to approximately a 1% increase in k_{eff}.

Data were also obtained for the temperature worth of the shim for shim positions from 10 to 16 in. Figure 8.1 shows the temperature as read by thermocouple No. 8, located on the vessel closure, vs shim position at three power levels. Reference is made to Fig. 3.1 for location of thermocouples and internal components of the reactor vessel. For the 16 in. shim position, at a power of 800 kw, thermocouple No. 8 read 826°F. Thermocouple No. 9, located at the bottom of the reactor vessel, read 785°F under the same conditions. As indicated in Fig. 8.1, the shim worth in the 10 to 16 in. range was 20°F/in. If the 20°F/in. figure is applicable over the entire 23 in. travel of the shim, the shim would be worth 460°F or 255°C. The latter figure can be taken as an upper limit for the temperature worth of the shim. It is estimated that a lower limit for the shim worth is 180°C, corresponding to a 20°F/in. worth in the 4 to 20 in. range. Actually, the total shim worth was taken to be 210°C, based on the following considerations. Since the top of the shim, when fully inserted, was slightly below the bottom of the tube bundle (see Fig. 3.1), the 20°F/in. worth might be expected to hold from the 16 to the 23 in. position. At the shim out position, the top of the shim was at the same level as the bottom of the reactor vessel. Taking account of the semi-elliptical cap at the bottom of the vessel, it seemed conservative to assign the 20°F/in. worth starting with the 4 in. position. If this linearity from 4 to 23 in. applies, the shim worth turns out to

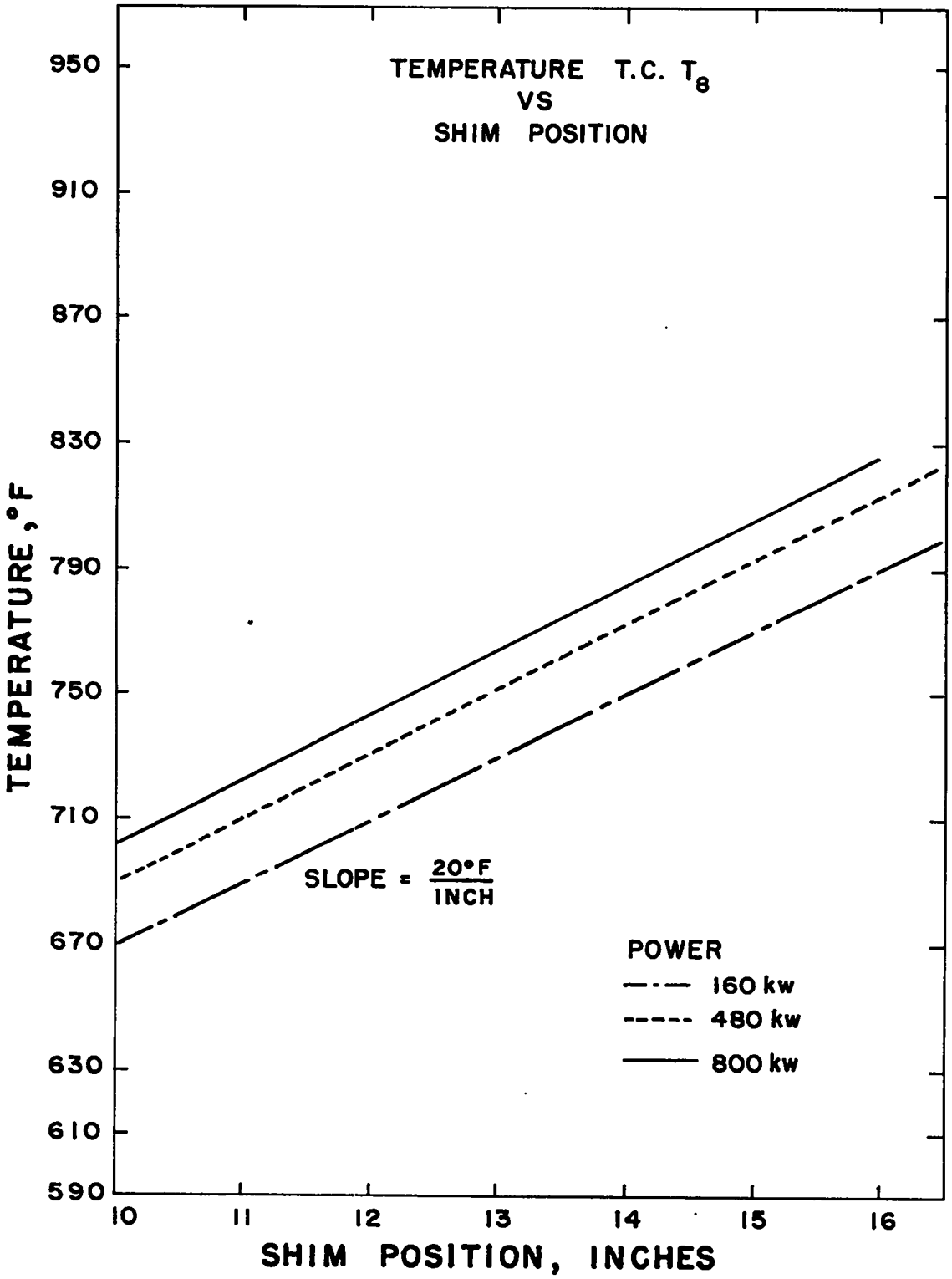

Fig. 8.1 Shim Position vs Fuel Temperature

be 210°C. Combining the 210°C figure with the calculated 13.9% k_{eff} worth for the shim, one obtains 6.6×10^{-4} $\Delta k/k/°C$ for the negative temperature coefficient in the temperature range corresponding to the shim in and shim out positions. One-group calculations for the negative temperature coefficient gave 6.4×10^{-4} and 5.1×10^{-4} at 430°C and 20°C, respectively.

8.7 Nuclear Behavior of the System

The nuclear behavior of the system is best shown by the neutron level record obtained during the final startup and operation of the reactor. A portion of this record, together with the temperatures recorded by thermocouples No. 7 and No. 9 (see Fig. 3.1), is shown in Figs. 8.2, 8.3 and 8.4. In view of its proximity to the fuel inlet to the reactor, thermocouple No. 9 was a very sensitive indicator of the direction of fuel flow between core and reservoir. The introduction of cold fuel from reservoir to reactor always resulted in a marked decrease in the temperature recorded by thermocouple No. 9; for the reverse flow, the hot fuel leaving the reactor resulted in a rise in the indicated temperature since the temperature of the vessel in the neighborhood of the thermocouple was lower than the peak core temperature. Similarly, thermocouple No. 7, measuring steam discharge temperature of the heat exchanger, showed a marked increase in the indicated temperature when the fuel solution level reached the top tube. The same was true for thermocouple No. 8 which was located at the bottom surface of the derby.

In order to examine the self-regulating characteristics of the system, the startup for the final reactor run was made in the following manner. In accordance with the procedure adopted, the pressures in the reservoir and reactor were first equalized and the valves, F-147 and F-148, between the top of the reactor and reservoir then closed. Reference is made to Fig. 4.1 for location of valves in the fuel and gas system. The metering tube, denoted by MT-1 and located between valves F-121 and F-122, was then pressurized to a predetermined filling such that the injection of a quantity of fuel substantially greater than the cold critical volume could be achieved in one continuous phase.

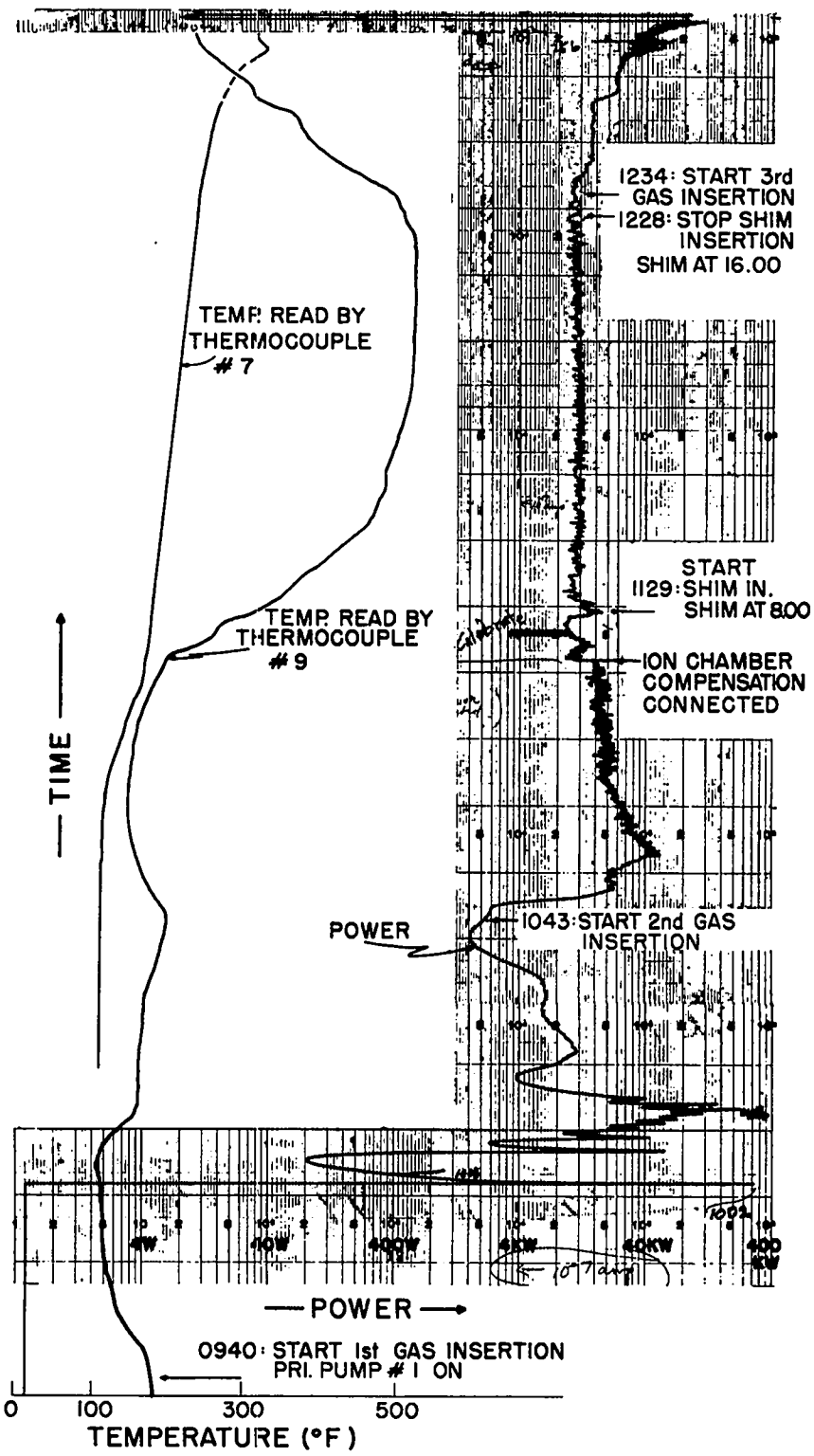

Fig. 8.2 Reactor Startup - Neutron Level and Reactor Temperature vs Time - Phase 1

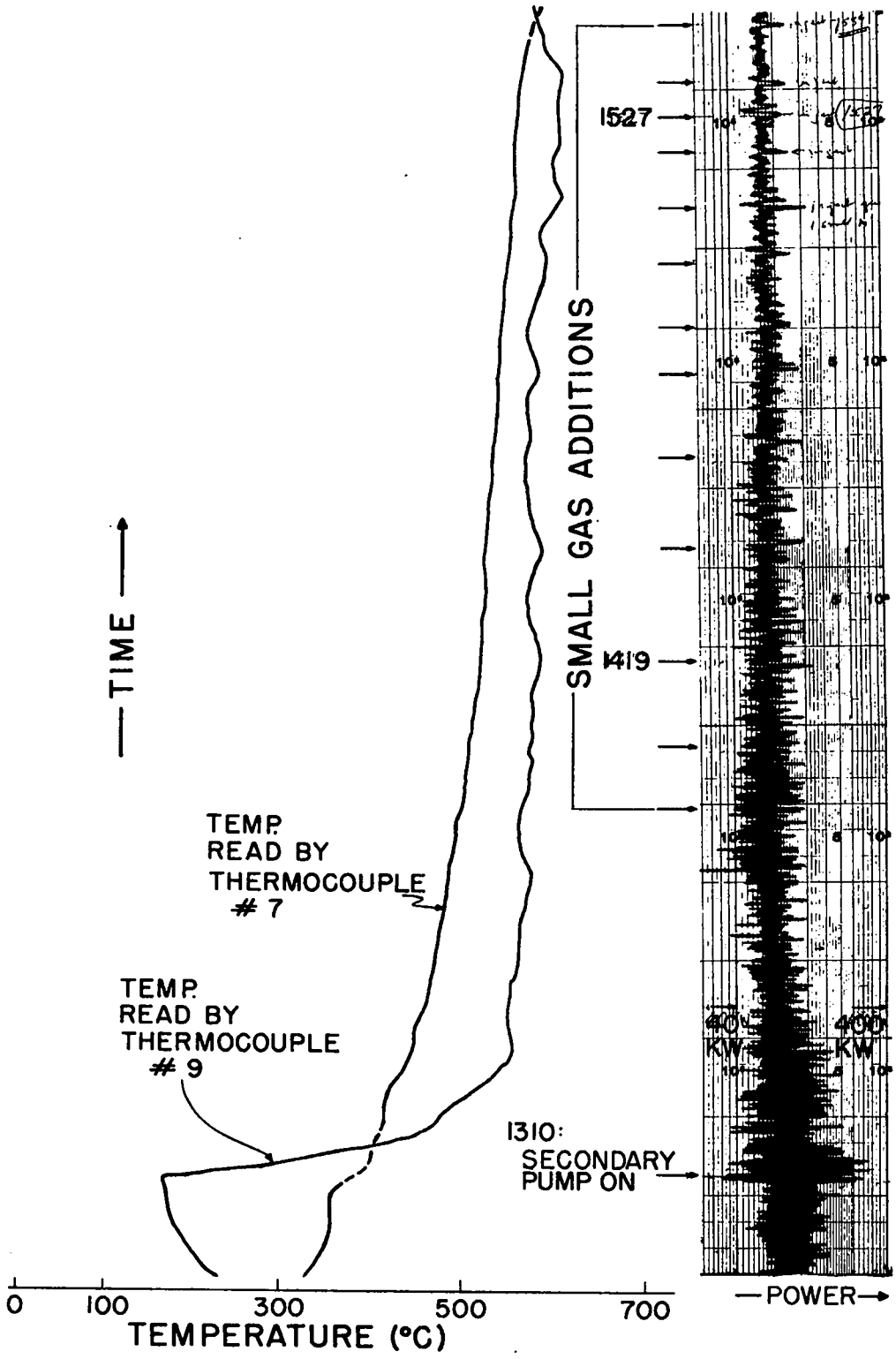

Fig. 8.3 Reactor Startup - Neutron Level and Reactor Temperature vs Time - Phase 2

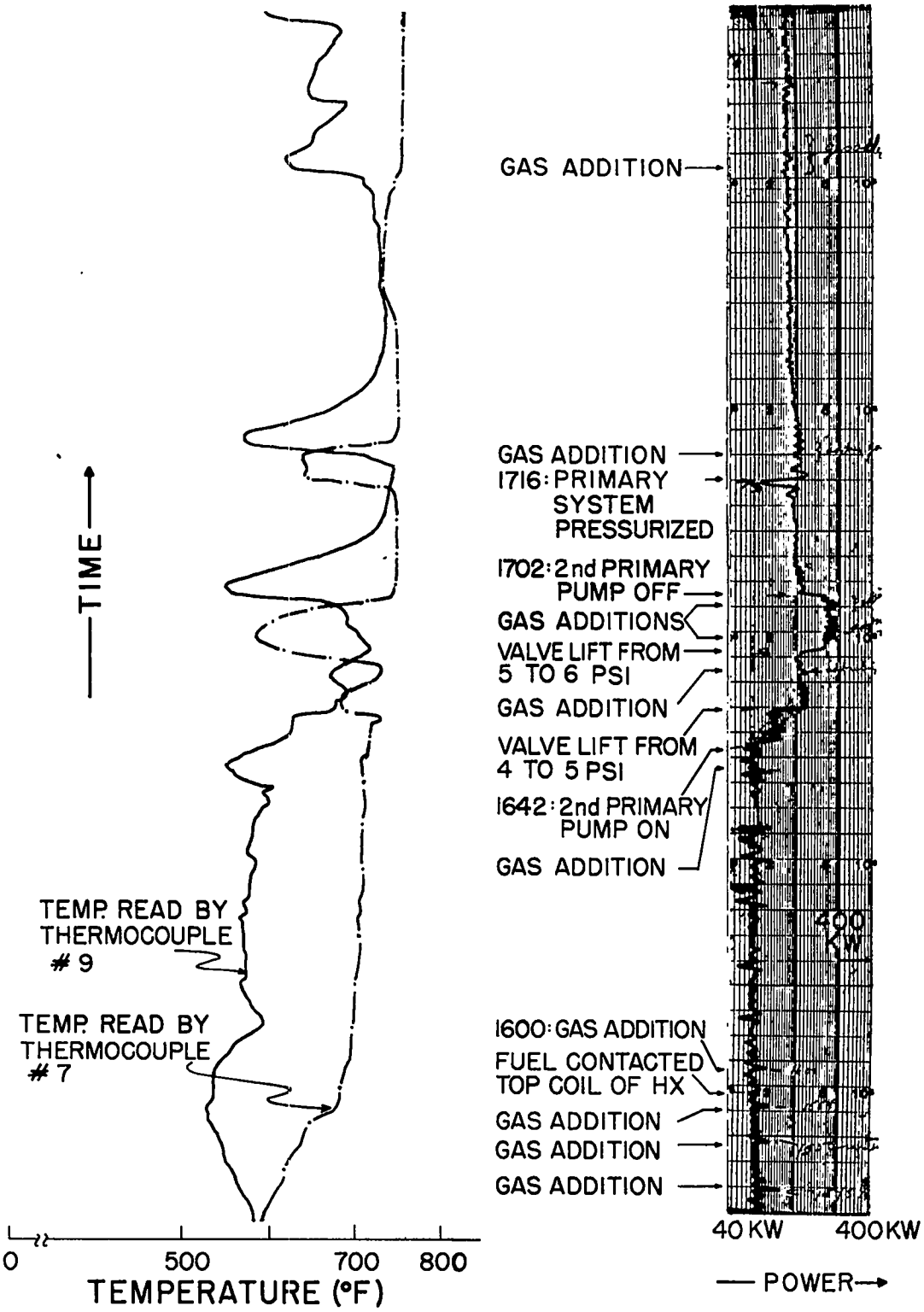

Fig. 8.4 Reactor Startup - Neutron Level and Reactor Temperature vs Time - Phase 3

At this time, primary pump No. 1 was turned on. Valves F-122 and F-125 were then opened and fuel allowed to flow into the reactor in a continuous manner. It should be noted that the impedance of the fuel injection line connecting the reservoir with the bottom of the reactor was designed to limit the reactivity insertion rate to no more than 10¢/sec.

The result of the continuous fuel insertion is shown beginning at the bottom of Fig. 8.2. The power level rose from a few milliwatts to 300 kw in a time interval of 10 sec; the period meter indicated a period of less than 1/4 sec. As expected, the negative temperature coefficient was very effective in terminating this rapid power rise. A short time after the initial power pulse, fuel was ejected into the reservoir; the evidence of this was the rise in temperature recorded by thermocouple No. 9 (Fig. 8.2). The energy deposited in the fuel during the period of the initial power pulse caused a rise in fuel temperature; this rise in temperature is accompanied by an increase in vapor pressure which, in turn, resulted in fuel flow from reactor to reservoir. The immediate effects of this transfer of fuel from reactor to reservoir were (1) an increase in the reservoir pressure due to the reduction in the reservoir gas volume and (2) a decrease in the reactor fuel volume, and hence a decrease in the partial pressure of the hydrogen gas in the reactor. As a result, a point was reached at which fuel flowed from reservoir to reactor. Also contributing to this flow reversal was the fact that the k_{eff} of the system, and hence the temperature at which the system is critical, is decreased as the fuel height in the reactor is lowered. In a similar manner, it can be shown that the flow of fuel from reservoir to reactor will result in a condition which will tend to reverse the direction of fuel flow. One would therefore expect several reversals in fuel flow direction before the system achieves an equilibrium condition. The observed fluctuations in neutron level, following the initial power pulse, can be understood in light of the preceding remarks.

At approximately an hour after the first fuel injection, the metering tube was repressurized and the gas subsequently admitted to the reservoir. The second fuel injection was started at 1043; it was estimated that the fuel level rose to a height slightly below the bottom of the heat exchanger as a result of this

operation. As shown in Fig. 8.2, from 1129 to 1228 the shim was moved, in small steps, from the initial 8 in. setting to 16 in. During this period, fuel was expelled from the reactor due to the increase in vapor pressure with temperature. This illustrated an interesting characteristic of the shim, namely that the immediate effect of shim insertion was to remove fuel from the reactor. Thus, to effect a temperature increase by shim motion required, in addition, the injection of fuel into the reactor.

To continue with the discussion of Fig. 8.2, at 1234 the third fuel injection into the reactor was begun. The increase in amplitude of the fluctuations in power level, recorded near the top of the figure, was an indication that the fuel solution had made contact with the bottom of the heat exchanger; the rise in temperature of thermocouple No. 7 should also be noted. The large negative spike at the top of the figure was a current calibration of the ion chamber circuitry.

Figure 8.3 is a continuation of the record; rather large amplitude oscillations may be noted at the start of the record. These oscillations can be explained as follows. For fuel levels below the top of the Pt baffle, the convection flow was not well defined and local convection paths were set up which resulted in the observed behavior. The effect of this local convection was especially noticeable after the solution contacted the bottom of the heat exchanger. At 1310, the secondary pump was turned on. Following this, fuel was added in several steps and the fuel level rose above the top of the Pt baffle and a well-defined fuel circulation path could be established. A reduction in the amplitude of the power oscillations was subsequently observed (see top of Fig. 8.3).

Figure 8.4 shows the final approach to steaming conditions. At ~ 1555, the fuel solution came in contact with the top tube of the heat exchanger. Following this, the second primary pump was turned on and the power was increased in two steps. These power demands caused the fuel level to fall below the top tube of the heat exchanger, and fuel was added to the reactor to compensate for this drop in height. It appeared desirable at this point to turn off the second primary pump, thus reducing the power demand, to bring the fuel level above the top tube of the heat exchanger. After this was done, the pressure in the primary loop was increased from 250 psig to 400 psig by increasing the hydrogen overpressure in

the loop. This resulting improvement in heat transfer produced a drop in fuel level, as shown by thermocouple No. 7, and gas was added to the reservoir to bring the fuel level above the bottom of the derby; the volume of fuel required to fill the space between the top tube of the heat exchanger and the bottom of the derby was about 3 cold liters. The fuel solution finally contacted the derby at a time later than that corresponding to the end of Fig. 8.4. After this, three additional liters of cold fuel were added, and the power demand experiments described in Section 9.5 were performed.

In conclusion, it is of interest to discuss the observed behavior of the reactor following a malfunction of the reactor gas handling system. As mentioned before, the vapor space in the reactor was isolated (by a valve) from the external gas system during operation. However, in the process of shutting down the reactor it was found convenient to reconnect the top of the reactor to the reservoir gas space. Unfortunately, during one of the shutdowns of the reactor it was discovered that the line from the top of the reactor was plugged, and at a point close to the reactor. However, fuel could still be removed from the reactor by venting the reservoir. In the course of this venting procedure, a point was reached at which the reservoir pressure was about 5 psig; this meant that the pressure in the reactor was in the neighborhood of 3 psig. It was decided to terminate the venting of the reservoir in view of the stipulation that the reactor pressure be kept above atmospheric. At this point, it was estimated that 30 to 40 liters of fuel was still in the reactor; the fuel temperature was still high enough so that the reactor was subcritical. It was expected that as the fuel cooled and the criticality of the system was correspondingly increased, the reactor would attain some lower temperature and operate at heat leak power. However, ~ 20 hr after shutdown it was observed that the reactor preferred to deliver its power in pulses. A few of these pulses are shown in Fig. 8.5. The reactor operated in this manner for almost a month, going through about 500 oscillating power cycles. During this time an unsuccessful attempt was made to dissolve the plug by admitting phosphoric acid, from the external gas system, into the line. The reactor was eventually started up with the line still plugged, but after a few hours operation at temperature the line opened up.

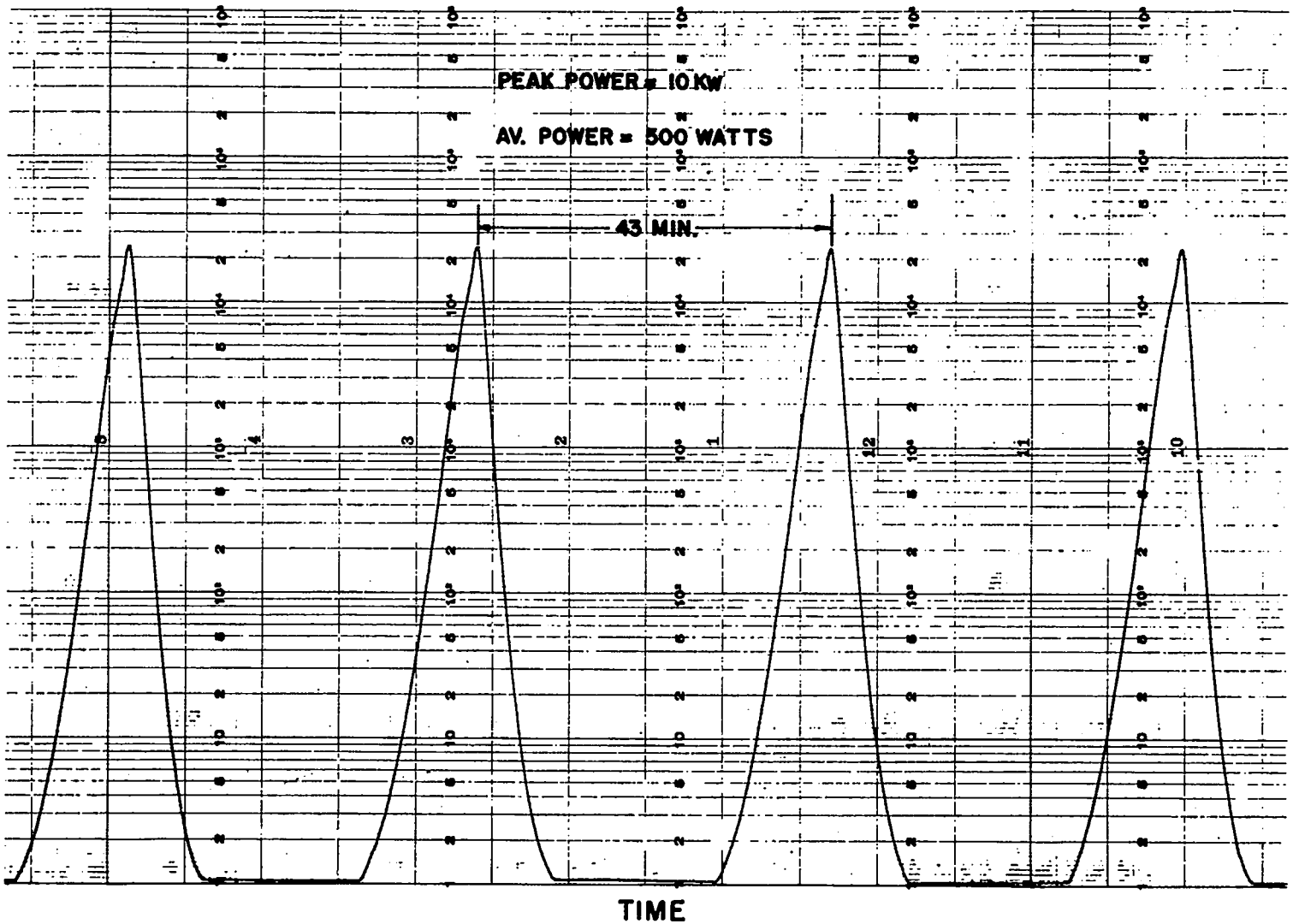

Fig. 8.5 Neutron Level vs Time - Pulse Operation

The pulsed or push-pull behavior of the reactor can be explained qualitatively by the following mechanism. Prior to the start of the pulse, the reactor is in a subcritical configuration and is cooling down due to heat leakage. As it cools, the system gains reactivity for two reasons. One is the negative temperature coefficient of reactivity. The second is that as the temperature decreases so does the vapor pressure, and this causes fuel to flow into the reactor. The end result of this gain in reactivity with time is a continuous rise in the power level (Fig. 8.5). During this power rise, the energy, equal to the integrated power at any given time, deposited in the fuel causes the fuel temperature to rise. Because of the decrease in reactivity with increasing temperature, the rise in power is terminated at some point and the power level of the reactor starts to decrease; however, the fuel temperature continues to rise during this period. The reactor again approaches a subcritical state, the fuel temperature decreases, and the cycle is repeated. Obviously, the preceding explanation is oversimplified; a rigorous analysis would require a detailed consideration of the nuclear, thermodynamic and hydrodynamic aspects of the over-all system.

An indication of the changes in temperature and pressure required to maintain the observed cyclic operation can be obtained from the following considerations. At 100°C, the average temperature during the period of pulsed operation, the vapor pressure of 95% phosphoric acid changes by about 0.02 psi/°C. The pressure due to a 1 cm head of fuel solution at this temperature is 0.025 psi, and a change of 1 cm in fuel height is estimated to be worth 0.6% in $\Delta k/k$ for a 40 liter filling at 100°C. It therefore requires only a small change in temperature, and hence in vapor pressure, to account for this pulsed behavior. Calculations previously made to investigate the feasibility of a reactor system based on this principle indicated that, given the proper conditions, such a cyclic behavior could be maintained.[28] Although these calculations were made for a system consisting of two reactors connected through a heat exchanger, the pulsed operation observed in this experiment is in qualitative agreement with the theoretical results.

Chapter 9

REACTOR OPERATION

Operation of LAPRE II was begun in February, 1959, and the experiment continued into May of 1959. The fuel solution was contained in the reactor at temperature above 200°F for 46 days, reaching a maximum measured fuel temperature of 826°F.

9.1 Fuel Volume

At the start of operation, 82.78 liters of fuel was charged into the fuel reservoir. It was estimated that this volume of fuel would fill the reactor vessel to the bottom of the derby at operating conditions (800°F). There were, however, several errors in this estimate.

1. At a uniform vessel temperature of 800°F the volume of the vessel up to the bottom of the derby would be 96.9 liters.

2. Fuel expansion estimates were based on the assumption of isothermal conditions. Substantial deviations from isothermal conditions occurred when power was extracted from the reactor, and over-all fuel expansion was less due to the temperature distribution in the fuel.

3. The amount of fuel held up as a "heel" in the fuel reservoir tank was larger than the amount calculated from the reservoir geometry. Consequently, the amount of fuel which could be charged to the reactor vessel was less than anticipated.

These errors became evident when it was impossible to charge sufficient fuel to the reactor vessel to cover the top heat exchanger coil. In order to overcome this difficulty, 8 liters of 95% H_3PO_4 were added to the fuel reservoir tank, increasing the fuel volume to 90.78 liters (17.3 M phosphate - 0.32 M UO_2).

The fuel volume problem reoccurred following the push-pull experience (see Section 8.7). When analyzed after this pulsed operation the fuel was 18.5 M phosphate - 0.335 M UO_2, which corresponded to a fuel volume of 83 to 85 liters. This loss in fuel volume (seemingly H_2O) was concurrent with the collection of an appreciable amount of liquid in the weep hole vacuum manifold. While a significant amount of β-γ activity was observed in this liquid, no α contamination (U^{235}) was detected.

An addition of dilute fuel solution was made to the reservoir tank to correct for the loss observed above. The total volume transferred into the reservoir after this addition was 96.76 liters. Analysis of the fuel after this addition was 18.3 M phosphate and 0.325 M UO_2.

At the conclusion of the experiment 88.95 liters (18.05 M phosphate - 0.327 M UO_2) were transferred from the fuel reservoir into the metering tank. This represented a total fuel volume loss of 7.81 liters. During the operation of the reactor, however, the U^{235} inventory showed essentially no loss.

9.2 Shutdown

The platinum capillary connected to the reactor vapor space was intended as a convenient means for equalizing the pressure in the reservoir and reactor. In a normal shutdown procedure the reservoir was vented to a pressure of ~ 200 psi and then hydrogen was inserted into the reactor vapor space. The reactor vapor space and fuel reservoir were then interconnected, which allowed the reactor to cool down with the fuel secured in the reservoir and a positive pressure on the reactor vessel liner. A similar procedure was used to transfer fuel from the reservoir to the storage tanks.

In two instances a stoppage in the capillary resulted in complications in reactor shutdown and fuel transfer procedures. The first stoppage resulted

in the so-called push-pull operation of the reactor (described in Section 8.7) wherein the fuel was held in the lower section of the reactor for ~ 30 days and periodically would reach criticality. This stoppage was removed when the reactor was brought up to temperature again. The second stoppage occurred during the final operation of the reactor and made it mandatory to transfer the fuel in the reactor directly to the metering tank. The fuel transfer under these conditions was tedious but not particularly difficult.

9.3 Radiation

All primary loop components were located below ground level to provide shielding in the event of induced or leakage type radioactivity being found in the loop. Some fission product activity was observed in the primary loop. Analysis revealed that I^{133}, I^{131} and I^{135}/Xe^{135} were present. There was no alpha activity detected in samples from the primary loop. The collection of these gaseous fission products in the feedwater heater was an annoyance but did not prevent reactor operation. The dose rate adjacent to the feedwater heater was several thousand R/hr during the operation of the reactor at full power. Since no alpha activity was found in the primary coolant, all leakage must have occurred in the vapor space of the reactor. The precise manner in which fission products escaped into the steam system was not determined. It was suspected, however, that leakage occurred either through holes in the gold cladding on the tube sheets, or through the heat exchanger tube seals in the tube sheets.

9.4 Full Power Operation

In the first attempt to achieve full power operation a 500 kw level at steam conditions of 749°F, 600 psi, was achieved. The limiting factor in this attempt was the capacity of the feedwater pumps. During the approach to full power the No. 1 feedwater pump suffered a serious reduction in discharge head (47 psi instead of the normal 90 psi). This reduced the combined feedwater head from 180 psi to ~ 145 psi. Subsequent examination of the pump disclosed a failure in the pump shaft which left only one of two impellers operable and explained the loss in head.

Full power operation was achieved on April 22, 1959. The maximum extracted power was 745 kw with steam conditions of 745°F at 670 psi. This power level was easily maintained for 12 hr with the reactor and its auxiliaries functioning very satisfactorily. The maximum power extracted from the reactor was limited by the primary loop pump capacity and not by the nuclear or heat transfer characteristics of the reactor.

9.5 Power Demand Experiment

9.5.1 Recombination

The radiolytic decomposition of water into hydrogen and oxygen is a problem common to all reactors using aqueous fuel solutions. It was calculated that the recombination rate in LAPRE II was adequate to prevent an accumulation of these gases. Although it was not possible to obtain quantitative data on the rate of recombination in LAPRE II, it was shown that internal recombination did take place.

The criteria established for determining recombination rates were as follows. Any change in reactor pressure while reactor temperatures and power remained constant was interpreted as being due to changes in the amount of radiolytic gas in the reactor. The temperature, as read at the thermocouple No. 8 on the derby, was assumed to be the temperature of the fuel in the reactor, and it was necessary to keep solution level above this point during observations.

It was felt that pressure changes which were due to leakage or corrosion could be differentiated from recombination effects by making the observations over a relatively long period before changing operating conditions.

At a reactor temperature of 600°F it was observed that for reactor powers greater than 200 kw there was a steady increase in the reactor pressure which ejected fuel from the reactor so that the fuel level fell below the top heat exchanger coil. When the reactor temperature was increased to 700°F the recombination rate was adequate for operation to 750 kw, no time dependent increase in pressure being observed. Even when rapid power changes were made (120 kw to 750 kw in less than 5 sec) no pressure increase attributable to radiolytic gas was found.

9.5.2 Fuel Solution Temperature

The temperature of the reactor fuel solution was monitored at two positions (at the base of the reactor vessel and at the bottom of the derby, Fig. 3.1). It was thought that thermocouple No. 8 would indicate the temperature of the solution being discharged from the core, while thermocouple No. 9 would read an average fuel temperature. It was found, however, that thermocouple No. 9 was very sensitive to the movement of fuel into and out of the reactor vessel. The movement of fuel into the reactor produced a drop in indicated temperature while the movement of fuel out of the reactor caused an increase in the temperature, indicated by thermocouple No. 9. This made thermocouple No. 9 useful for observing fuel transfer, but unsatisfactory for observing solution temperature except during constant power operation when there was essentially no fuel transfer. Thermocouple No. 8 was not sensitive to fuel transfer but it gave no direct indication of fuel level until the fuel level in the reactor was well up above the bottom of the derby.

The effect of power demand on the fuel temperature as measured at thermocouple No. 8 is shown in Fig. 9.1. An increase of $\sim 32°F$ was demonstrated for a power increase of 600 kw.

9.5.3 Reactor Pressure

All pressure measurements were made in the gas space of the fuel reservoir tank. As measured at this position the pressure represented (1) the vapor pressure of the fuel solution, (2) the pressure due to gases in the reactor vapor space, and (3) the hydraulic head. The vapor pressure varied with the temperature of the surface of the reactor fuel; the gas pressure varied with reactor filling, reactor temperature, recombination of radiolytic gases, the gas solubilities, and the initial gas overpressure in the reactor; the hydraulic head was dependent upon the density (temperature) and liquid level of the fuel in the reactor. The total effect of power changes on the pressure in the reactor can vary greatly depending upon the interaction of all the factors mentioned above.

For example, in Fig. 9.2 the reactor pressure is shown at three different shim settings (16 in., 13 in. and 10 in.) which also represent three different liquid levels. In all three cases the fuel level was above thermocouple No. 8.

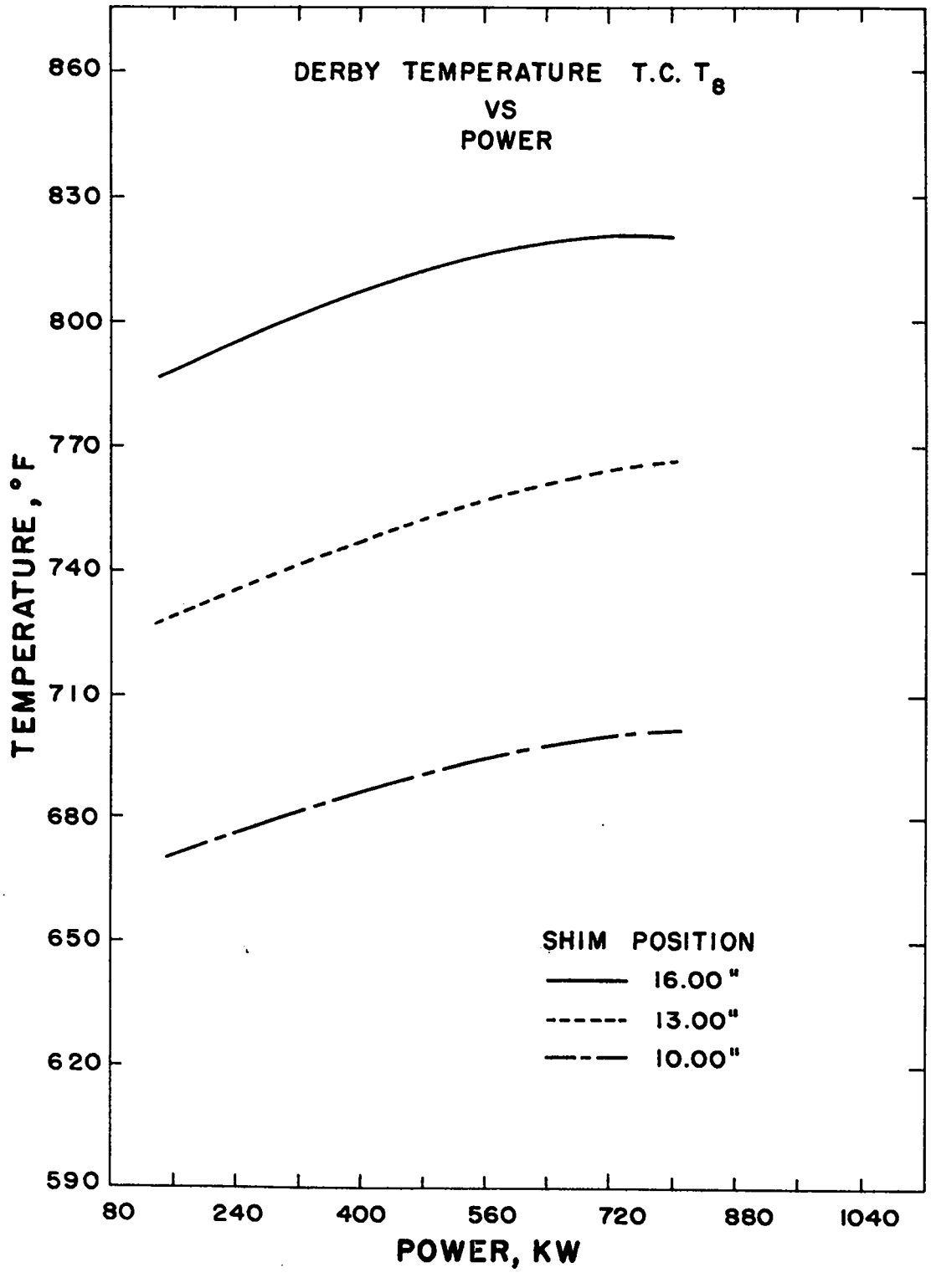

Fig. 9.1 Fuel Temperature vs Reactor Power

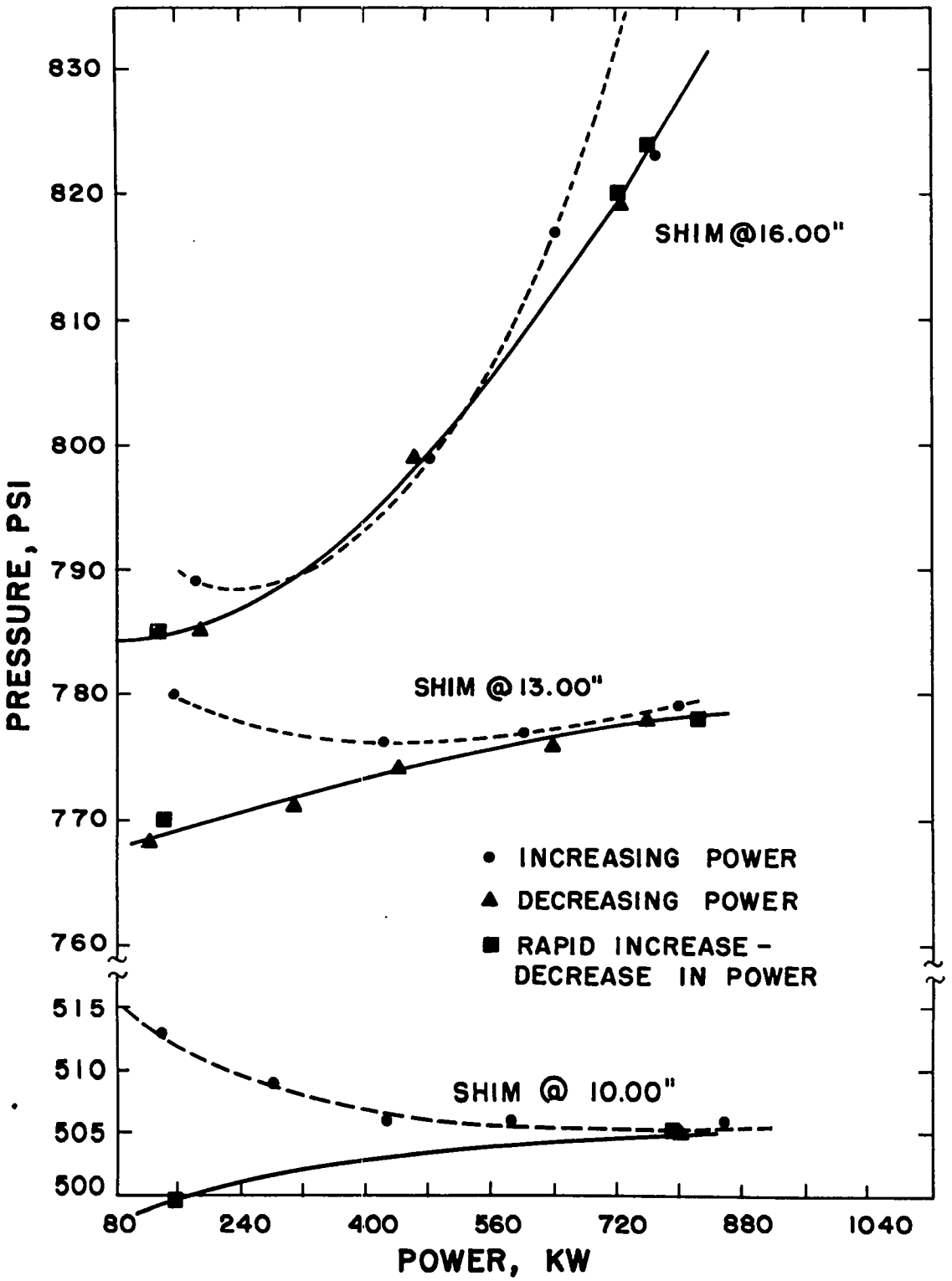

Fig. 9.2 Reactor Pressure vs Reactor Power

When power demand was increased at the 16 in. shim setting, an increase of 40 psi was observed, while at the lower settings it appears that the pressure actually decreased. It appears reasonable, however, that the solid line actually represents the pressure after all components have come to equilibrium and that an increase of 9 and 5 psi represents the change in the pressure.

This observed dependence of reactor pressure on shim setting may be explained in the following way. The initial filling of the reactor vessel to a level above the bottom of the derby was made with the shim at 16 in. Subsequently, as the shim was lowered, the decrease in reactor fuel temperature and pressure allowed more fuel to flow from the reservoir into the reactor vessel. This addition of fuel caused the fuel level to rise up into the narrow annular space between the derby and vessel wall. The 44 heat exchanger tubes pass through this region as they connect to the steam manifold. Therefore, when the fuel level is up in the annular space, the fuel surface temperature is greatly influenced by the steam temperature in the heat exchanger tubes. The average steam temperature varied from 50°F less than the fuel temperature indicated by thermocouple No. 8 (shim at 16 in.) to 100°F less than No. 8 (shim at 10 in.). Thus, the fuel surface temperature, at the lower shim settings, was isolated more strongly from temperature changes in the core following changes in power demand. Consequently, the lower the shim setting the smaller the observed pressure increase accompanying a power demand increase.

An interesting transient in the pressure was observed during the rapid power change experiments. The sudden decrease in fuel volume (fuel contraction) in the heat exchanger regions caused by a rapid increase in power demand was observed as a momentary decrease in pressure followed by the usual increase in pressure with increased power demand. The opposite effect was observed for a rapid reduction in power demand, the expansion of fuel in the heat exchanger region being observed as a momentary increase in pressure followed by the usual reduction in pressure with reduced power demand.

9.5.4 Rapid Power Changes

Possibly the outstanding characteristic of LAPRE II was observed in the rapid power change experiments. In Fig. 9.3, a composite plot of neutron

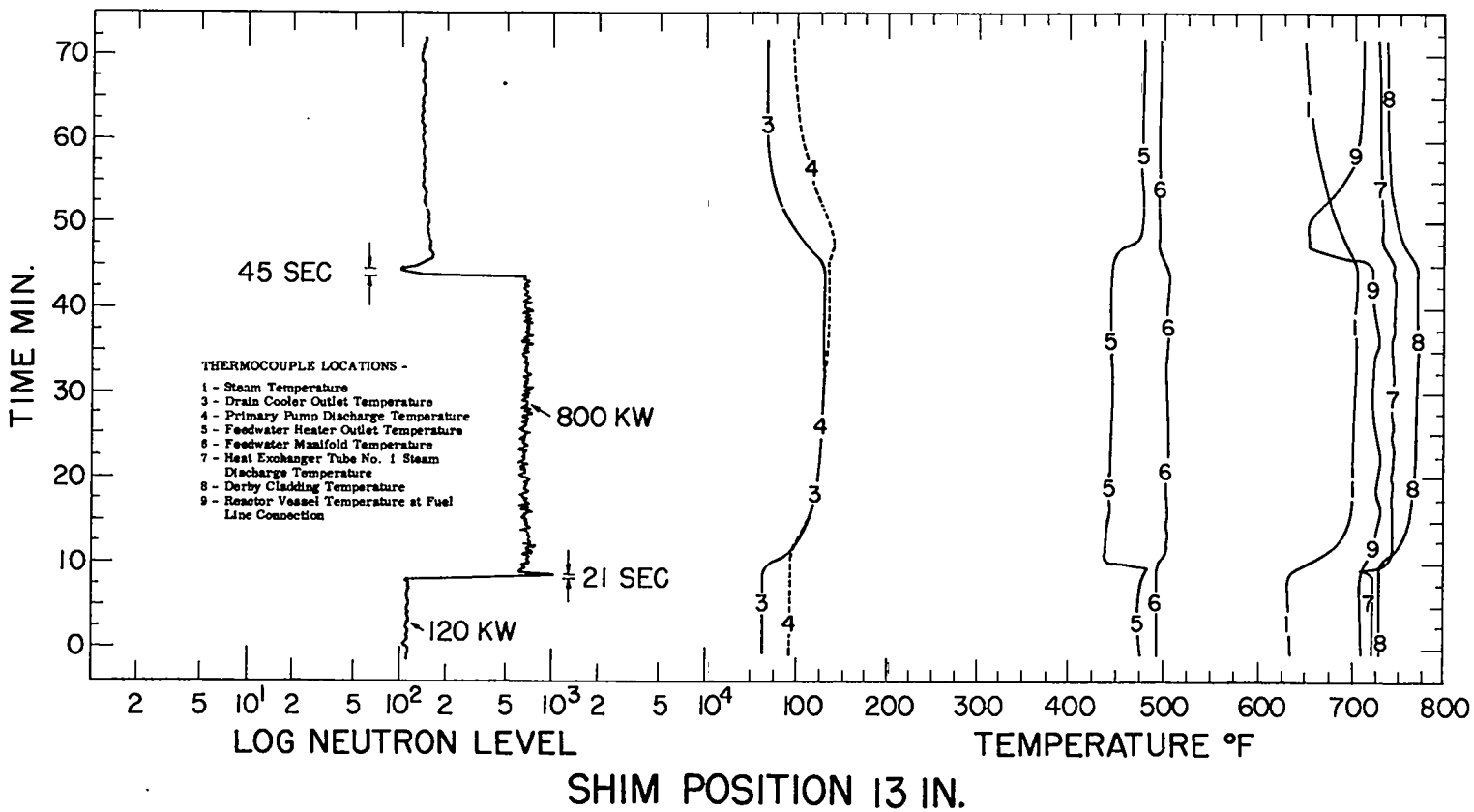

Fig. 9.3 Neutron Level and Reactor System Temperatures vs Time

level and reactor system temperatures vs time, the ability of the reactor to automatically and rapidly adjust to power demand changes is shown. In this example a change in power level from 120 kw to 800 kw was made in ~ 21 sec, with the reactor system adjusting to the new operating condition and leveling off to a constant power output. The system achieved thermal equilibrium in ~ 5 min. Pressure changes (Fig. 9.2) closely followed the increase in temperature. A subsequent power decrease from 800 kw to 120 kw was accomplished in 45 sec with a similar time required for thermal equilibrium. It should be emphasized that the reactor system adjusted to these power variations without movement of the shim.

9.5.5 Steam Temperature

The steam discharge temperature was measured at the outlet of the top heat exchanger tube in the steam manifold (thermocouple No. 7, Fig. 3.1) and at the inlet to the desuperheater-condenser (thermocouple No. 1). The changes in steam temperature with reactor power and shim position (fuel temperature) are shown in Figs. 9.4 and 9.5.

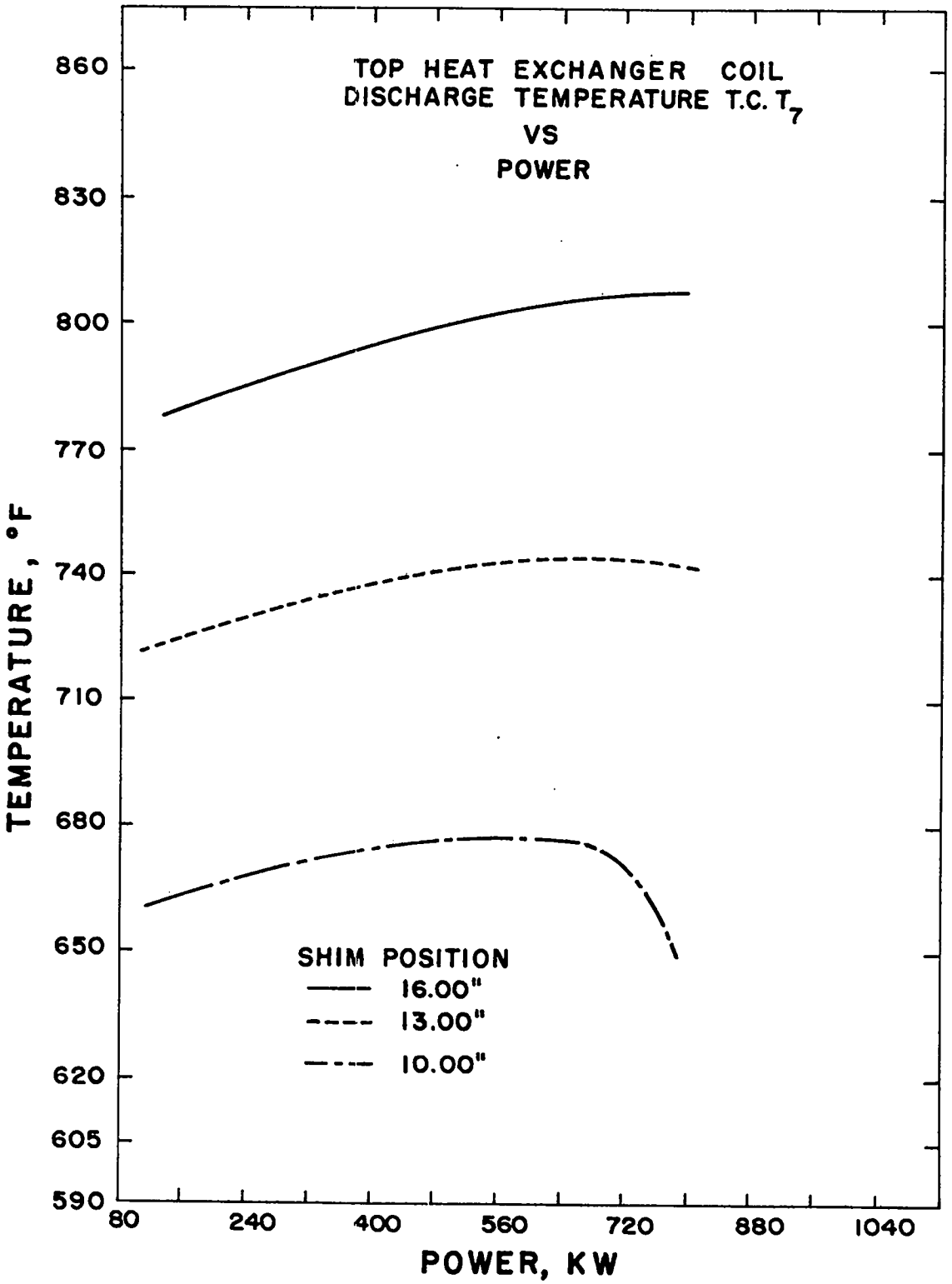

Fig. 9.4 Steam Discharge Temperature from the Top Heat Exchanger Coil vs Reactor Power

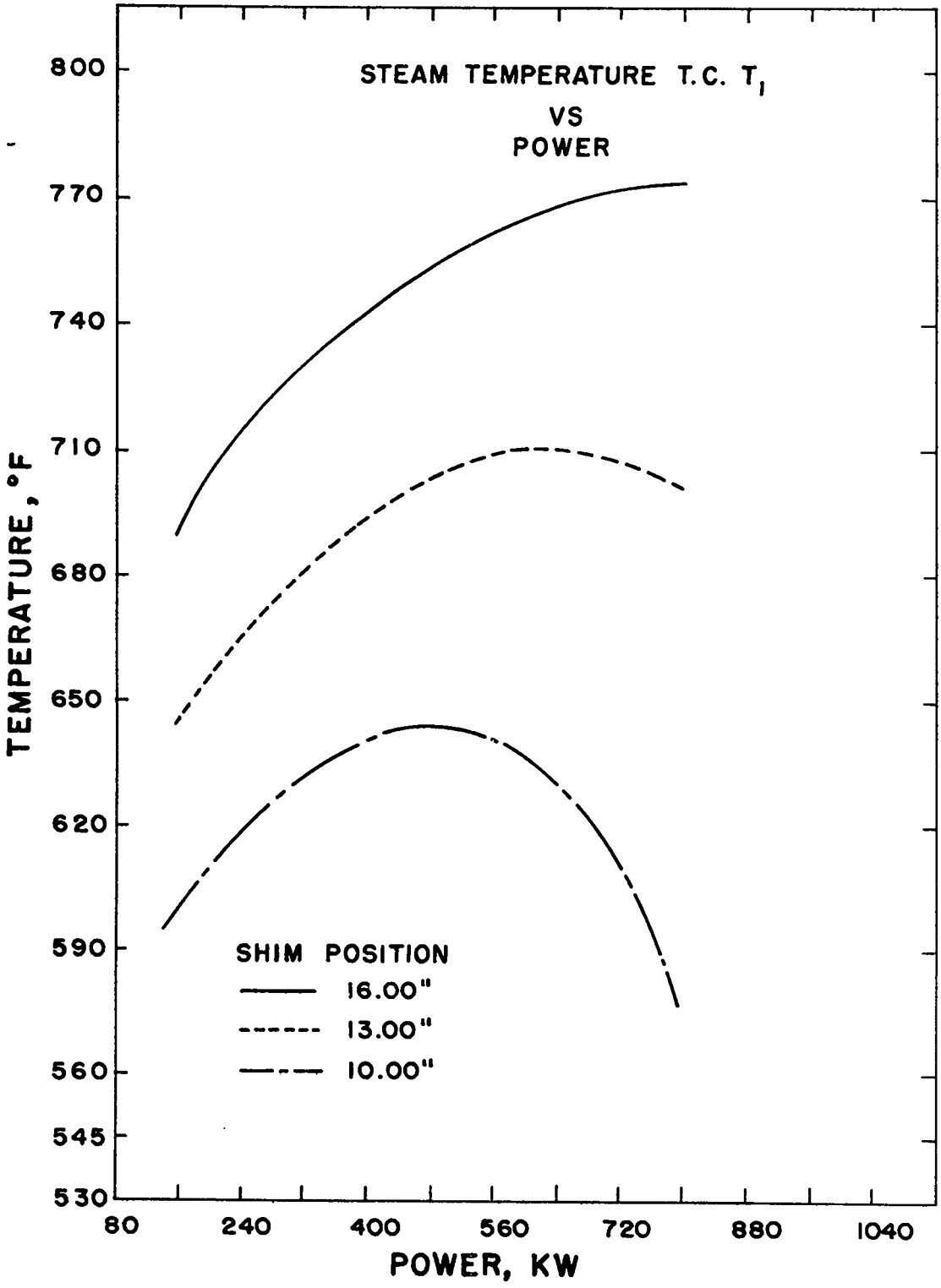

Fig. 9.5 Steam Temperature vs Reactor Power

Chapter 10

POST MORTEM

10.1 Fuel Solution

Dismantling of the experiment was begun on May 8, 1959, when the fuel solution was transferred back into the storage tanks. In general appearance the fuel solution was unchanged, having the same dark green color and being a clear, viscous liquid. Analysis of the fuel is shown in Table 10.1

TABLE 10.1

FUEL ANALYSIS

	U	U^{+4}	PO_4	Cu	Fe	Au	Pt
Feb. 1959	0.354 M	0.341 M	17.3 M	0.005 M	----	*	*
May 8, 1959	0.327 M	0.323 M	18.05 M	0.021 M	0.015 M	*	*

* Not detectable

A radiochemical determination of the number of fissions using Sr^{89}, Cs^{136}, Cs^{137}, and Ce^{144} gave a value corresponding to an integrated power of 2.02 Mwd^{29} (integration of the neutron level data yielded 2.2 Mwd). The beta-gamma activity level was ~ 30 curies per liter when the fuel was transferred to storage.

10.2 Vessel and Steam Generator

The safety enclosure tank was opened and the shield plugs were removed on August 28, 1959. Figure 10.1 shows the appearance of the reactor at this stage of the disassembly. Water shielding was used during the remote removal of the feedwater and steam piping, the thermocouple lines, and the bolt ring. The vessel seal weld was ground off by personnel standing on a lead shield erected on the top of the reactor vessel. Some difficulty was experienced in separating the vessel flanges, and some damage to the gold cladding occurred in the flange region during this operation. The gold cladding on the vessel and on the derby was otherwise apparently undamaged, but its appearance had undergone a color change from the characteristic yellow gold to a copper color. An analysis of a sample taken from the surface of the gold was made using x-ray diffraction techniques. The reported major constituent was gold with an appreciable amount of a solid solution of gold with some element of smaller atomic size. A trace of the compound Au_3Hg was observed.[30]

Gamma ray spectroscopy indicated that 0.51, 0.62, 0.875, 1.05, 1.53 and 1.72 Mev gamma rays were given off by the gold cladding. This gamma ray spectra was attributed to Ru^{106} and its daughter Rh^{106}.[31]

The platinum parts in the assembly were also intact and also showed a change in apparent color, the characteristic silvery platinum surfaces having changed to a dull gray. An examination of a sample, taken from the surface of the platinum, revealed the major constituent to be platinum metal; there was also evidence of a solid solution of platinum with the transition element Cr through Ni.[30]

The gamma ray spectra of the platinum sample included 0.33, 0.62, 0.875, 1.05, 1.53 and 1.72 Mev energies. Cr^{51}, Ru^{106} and Rh^{106} were identified from this spectra.[31]

The heat exchanger assembly is shown in Fig. 10.2 as it appeared before insertion in the reactor vessel, and as it appeared after disassembly. Visual inspection of this unit has disclosed no damage. All of the coils were intact and the graphite parts were undamaged.

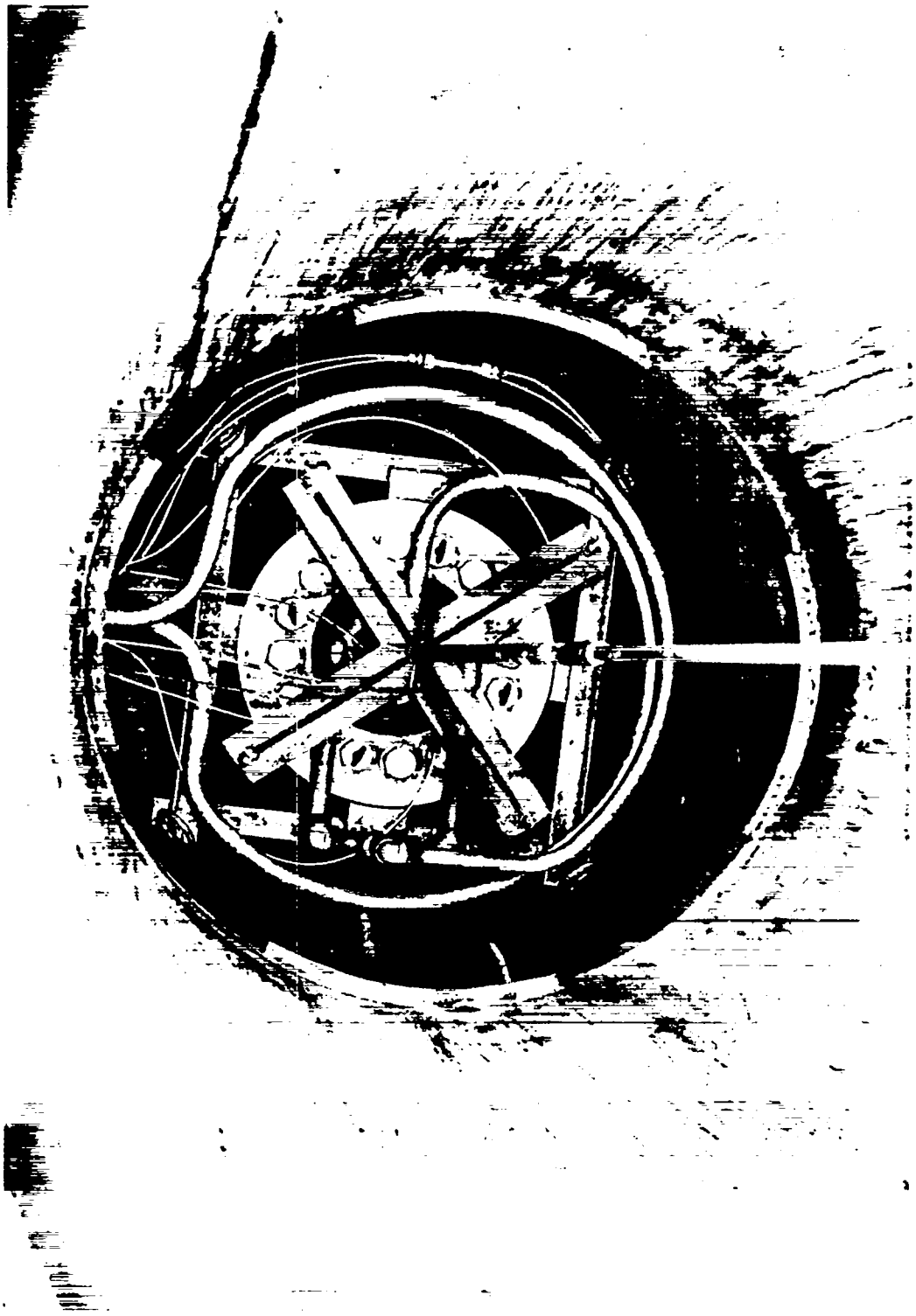

Fig. 10.1 Reactor Assembly in Safety Enclosure at Start of Post Mortem

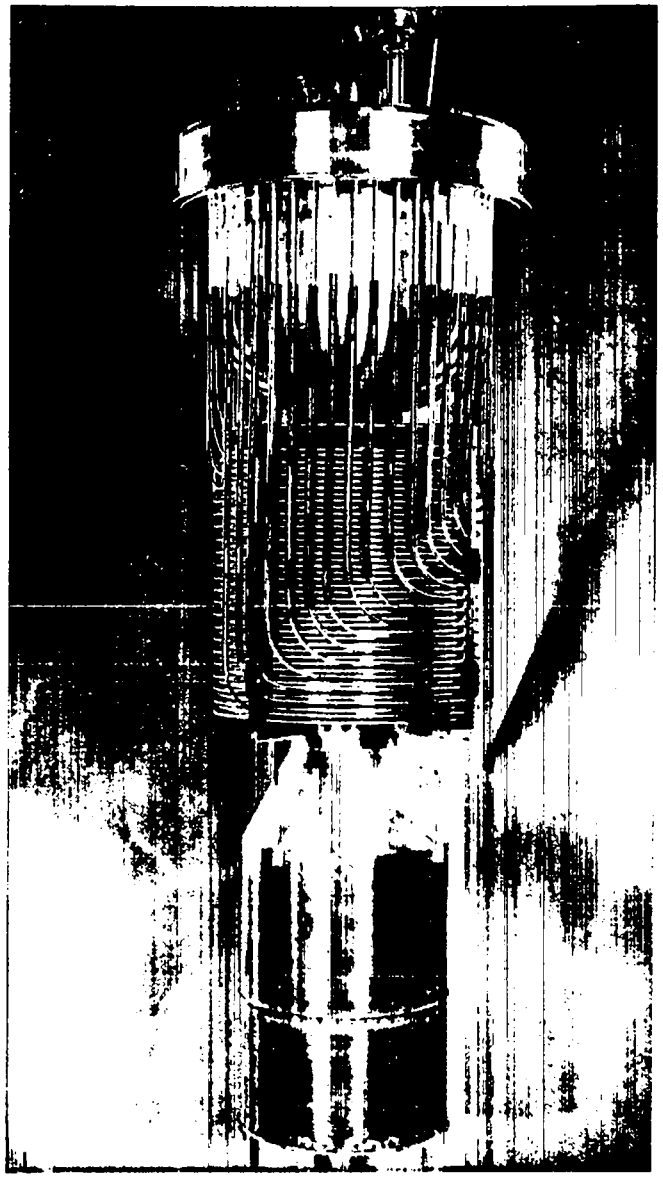

Fig. 10.2 Reactor Heat Exchanger, Derby, and Flow Baffle before Installation in Reactor Vessel

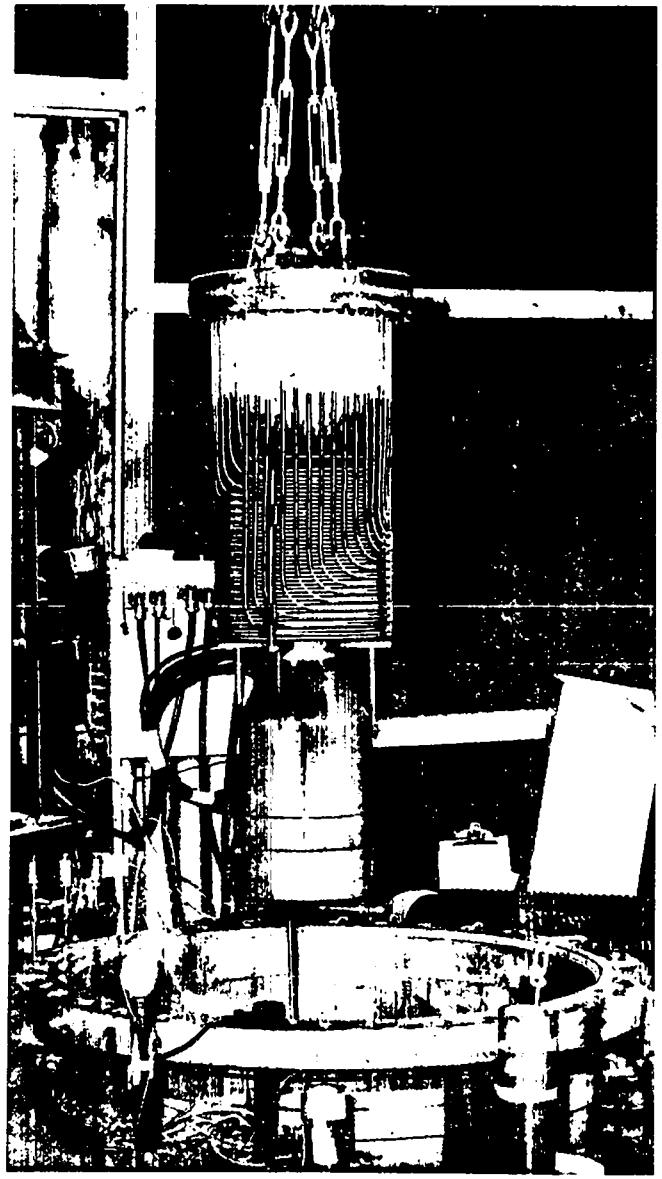

Reactor Heat Exchanger, Derby, and Flow Baffle after Reactor Operation

APPENDIX

A simplified schematic of the LAPRE II heat disposal system is presented in Fig. A. 1. The temperatures and pressures displayed in Fig. A. 1 are identified below.

TABLE A. 1

TEMPERATURE-PRESSURE IDENTIFICATION

Loop	Symbol	Description
Primary	T_1	Steam temperature
Primary	T_2	Condenser outlet temperature
Primary	T_3	Drain cooler outlet temperature
Primary	T_4	Feedwater heater inlet temperature
Primary	T_5	Feedwater heater outlet temperature
Primary	T_6	Feedwater inlet manifold temperature
Reactor	T_8	Fuel temperature at derby
Reactor	T_9	Fuel temperature at bottom of vessel
Secondary	t_1	Condenser outlet
Secondary	t_2	Drain cooler inlet
Primary	P_1	Pump suction pressure
Primary	P_2	Pump discharge pressure
Reactor	P_3	Pressure (measured at reservoir)
Primary	P_4	Feedwater inlet pressure
Primary	P_5	Expansion tank pressure

Typical pressure, temperature, and flow rate data obtained during reactor operation are shown in Table A. 2.

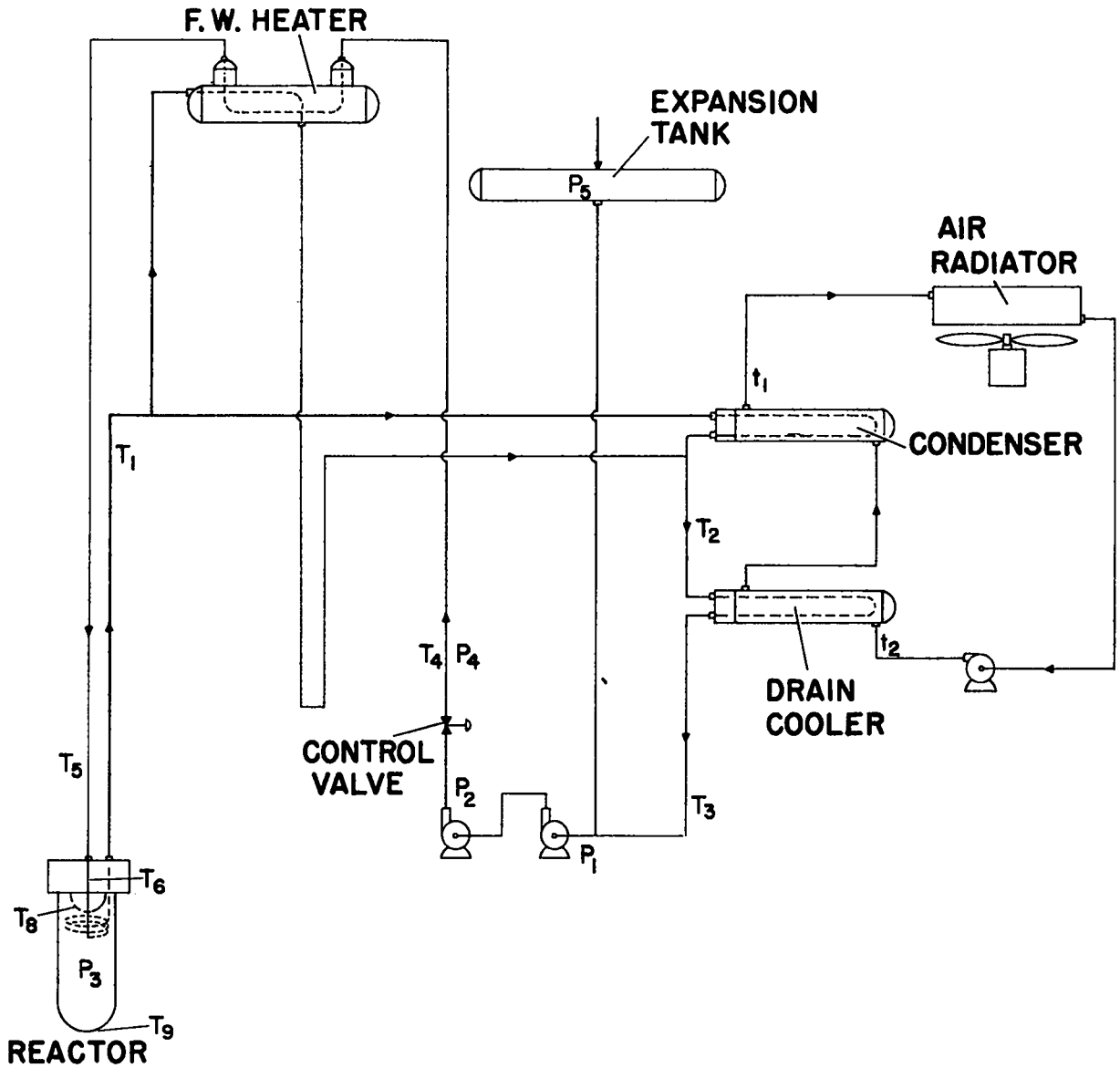

Fig. A. 1 Schematic Diagram of LAPRE II Heat Disposal System

TABLE A. 2

REACTOR OPERATION DATA

Time 5/7/59	Power, kw	Shim, in.	T_1, °F	T_2, °F	T_3, °F	T_4, °F	T_5, °F	T_6, °F	T_8, °F	T_9, °F	t_1, °F	t_2, °F	Sec. loop flow rate, lb/hr	P_1, psi	P_2, psi	P_3, psi	P_4, psi	P_5, psi
2000	800	13	702	--	128	132	446	503	767	721	159	114	54,500	645	835	775	780	628
2130	148	13	640	250	65	90	475	492	703	675	70	63	54,500	650	850	555	655	632
0245	720	16	770	330	132	137	448	508	825	783	167	124	55,000	670	860	822	815	650
0615	140	16	685	205	60	90	474	492	785	725	72	63	55,000	670	875	798	685	652

REFERENCES

1. Clark, R. A. and King, L. D. P., "The Los Alamos Power Reactor Experiment No. II, Description and Test Operation," Trans. Am. Nuclear Soc., 2, No. 2, 109 (1959).

2. King, L. D. P., "A Brief Description of a One Megawatt Convection Cooled Homogeneous Reactor LAPRE II," Los Alamos Scientific Laboratory Report LA-1942, April 13, 1955.

3. Froman, D. K., Hammond, R. P., and King, L. D. P., "Los Alamos Power Reactor Experiments," Proceedings of the International Conference on the Peaceful Uses of Atomic Energy, 1955, Vol. 3, p. 283, P/500, United Nations, New York, 1955.

4. King, L. D. P., "Los Alamos Power Reactor Experiment and Its Associated Hazards," Los Alamos Scientific Laboratory Report LAMS-1611 (Del.), December 2, 1953.

5. Peterson, R. E. and K-Division Staff, "Los Alamos Power Reactor Experiment Number One, LAPRE I," Los Alamos Scientific Laboratory Report LA-2292, January 1959.

6. Lane, J. A., MacPherson, H. G., and Maslan, F., "Fluid Fuel Reactors," Addison Wesley Publishing Co., Reading, Mass., 1958.

7. Baker, R. D., Baxman, H. R., and Maraman, W. J., U.S. Patent No. 2,885,260, May 5, 1959.

8. Baxman, H. R., "The Extraction of Uranium from Phosphate Solutions," AECD-3746, May 1956.

9. Flanary, J. R., "Uranium Recovery from LAPRE-II Fuel Solution by TBP Extraction," Oak Ridge National Laboratory Report CF-60-6-84, June 1960.

10. King, L. D. P. and Hammond, R. P., "Proposed Specifications for a LAPRE II Type Reactor for DEW NET Applications," Los Alamos Scientific Laboratory Internal Report K-1-824, June 1955.

11. Sandia Corporation Engineering Research, "Design Study for Homogeneous Phosphoric Acid Reactor (H PAR)," Sandia Corporation Report SC-4459(RR), August 1960.

12. Code for Unfired Pressure Vessels, Section VIII, 1952 Edition, American Society of Mechanical Engineers, New York, June 1953.

13. Waters, E. O. et al., "Development of General Formulas for Bolted Flanges," Taylor Forge and Pipe Works, Chicago, Ill., 1949.

14. Allegheny-Ludlum Blue Sheets, Allegheny Steel Corp., Pittsburgh 22, Pa.

15. Faupel, J. H., "Yield and Bursting Characteristics of Heavy-Wall Cylinders," Trans. ASME, 78, 1031 (1956).

16. Thamer, B. J., "The Properties of Phosphoric Acid Solutions of Uranium as Fuels for Homogeneous Reactors," Los Alamos Scientific Laboratory Report LA-2043, March 6, 1956.

17. Keil, R. W., Hanks, G. S., and Taub, J. M., "The Rolling of Gold Sheet for the LAPRE II Pressure Liner," Los Alamos Scientific Laboratory Report LAMS-2268, July 1958.

18. Holm, D. M., "A Gamma Ray Sensitive Fuel Level Detector for a Homogeneous Reactor," Los Alamos Scientific Laboratory Report LA-2458, September 1960.

19. Thamer, B. J., "The Fuel System UO_2-H_3PO_4-H_2O and Los Alamos Power Reactor Experiment II," Proceedings of the Second United Nations International Conference on the Peaceful Uses of Atomic Energy, Geneva, 1958, Vol. 7, p. 54, P/925, United Nations, New York, 1958.

20. Hansen, M., "Constitution of Binary Alloys," 2nd Ed., pp. 222 and 1085-6, McGraw-Hill Book Company, Inc., New York, 1958.

21. Schreyer, J. M. and Baes, C. F., Jr., "Volumetric Determination of Uranium (VI) in Phosphate Solutions," Anal. Chem., 25, 644 (1953).

22. Barton, C. J., "Photometric Analysis of Phosphate Rock," Anal. Chem., 20, 1068 (1948).

23. Carlson, B. G. and Bell, G. I., "Solution of the Transport Equation by the S_n Method," Proceedings of the Second United Nations International Conference on the Peaceful Uses of Atomic Energy, Geneva, 1958, Vol. 16, p. 535, P/2386, United Nations, New York, 1958.

24. Battat, M. E. and Carmichael, B. M., "The Los Alamos Power Reactor Experiment No. II, Criticality," Trans. Am. Nuclear Soc., 2, No. 2, 110 (1959).

25. Beck, C. K., Callihan, A. D., Morfitt, J. W., and Murray, R. L., "Critical Mass Studies. Part III," Union Carbide Nuclear Corporation Report K-343, April 19, 1949.

26. Allred, J. C., Bendt, P. J., Peterson, R. E., "Critical Measurements on UO_3-H_3PO_4 Solutions," Nuclear Sci. and Eng., 4, 498 (1958).

27. Stone, P. M., "A Two Dimensional Multi-Group Neutron Diffusion Code for Cylindrical Geometries," Session 10, Paper 5, Second Winter Meeting of the American Nuclear Society, 1957.

28. Battat, M. E. and Tsingou, M., "Calculations for a Push-Pull Reactor System," Abstracts of the Second Annual Meeting of the American Nuclear Society, June 1956.

29. Sattizahn, J. E., Los Alamos Scientific Laboratory Private Communication.

30. Ellinger, F. H., Los Alamos Scientific Laboratory Private Communication.

31. Holm, D. M. and Backus, C. E., Los Alamos Scientific Laboratory Private Communication.